Methods[1]

R.D. Norris, P.A. Wilson, P. Blum, A. Fehr, C. Agnini, A. Bornemann, S. Boulila, P.R. Bown, C. Cournede, O. Friedrich, A.K. Ghosh, C.J. Hollis, P.M. Hull, K. Jo, C.K. Junium, M. Kaneko, D. Liebrand, P.C. Lippert, Z. Liu, H. Matsui, K. Moriya, H. Nishi, B.N. Opdyke, D. Penman, B. Romans, H.D. Scher, P. Sexton, H. Takagi, S.K. Turner, J.H. Whiteside, T. Yamaguchi, and Y. Yamamoto[2]

Chapter contents

[1]Norris, R.D., Wilson, P.A., Blum, P., Fehr, A., Agnini, C., Bornemann, A., Boulila, S., Bown, P.R., Cournede, C., Friedrich, O., Ghosh, A.K., Hollis, C.J., Hull, P.M., Jo, K., Junium, C.K., Kaneko, M., Liebrand, D., Lippert, P.C., Liu, Z., Matsui, H., Moriya, K., Nishi, H., Opdyke, B.N., Penman, D., Romans, B., Scher, H.D., Sexton, P., Takagi, H., Turner, S.K., Whiteside, J.H., Yamaguchi, T., and Yamamoto, Y., 2014. Methods. *In* Norris, R.D., Wilson, P.A., Blum, P., and the Expedition 342 Scientists, *Proc. IODP,* 342: College Station, TX (Integrated Ocean Drilling Program). doi:10.2204/iodp.proc.342.102.2014
[2]**Expedition 342 Scientists' addresses.**

Introduction

This chapter documents the procedures and methods employed in the various shipboard laboratories of the R/V *JOIDES Resolution* during Integrated Ocean Drilling Program (IODP) Expedition 342. This information applies only to shipboard work described in the *Expedition Reports* of the Expedition 342 *Proceedings of the Integrated Ocean Drilling Program* volume. Methods for shore-based analyses of Expedition 342 samples and data will be described in individual scientific contributions to be published in the open literature or in the Expedition Research Results section of this volume.

Authorship of site chapters

All shipboard scientists contributed to this volume. However, certain sections were written by discipline-based groups of scientists as listed alphabetically below.

Newfoundland Ridge sections

Background and objectives: R.D. Norris, P.A. Wilson
Operations: P. Blum, S. Midgley, R.D. Norris, P.A. Wilson
Paleontology: C. Agnini, P.R. Bown, O. Friedrich, C.J. Hollis, K. Moriya, H. Nishi, P. Sexton
Core description: A. Borneman, S. Boulila, A.K. Ghosh, P.M. Hull, C.K. Junium, H. Matsui, B.N. Opdyke, D. Penman, B. Romans, H. Takagi
Geochemistry: K. Jo, M. Kaneko, Z. Liu, H.D. Scher, J.H. Whiteside
Paleomagnetism: P.C. Lippert, Y. Yamamoto
Physical properties: P. Blum, C. Cournede, T. Yamaguchi
Stratigraphic correlation: D. Liebrand, S. Kirtland Turner
Downhole logging: A. Fehr

Motion Decoupled Hydraulic Delivery System sections

P.B. Flemings, T.L. Pettigrew, P.J. Polito

Operations

Site locations

GPS coordinates from precruise site surveys were used to position the vessel at all Expedition 342 sites. A SyQuest Bathy 2010 CHIRP subbottom profiler was used to monitor the seafloor depth

doi:10.2204/iodp.proc.342.102.2014

on the approach to each site to reconfirm the depth profiles from precruise surveys. Once the vessel was positioned at a site, the thrusters were lowered and a positioning beacon was dropped to the seafloor. The dynamic positioning control of the vessel used navigational input from the GPS and triangulation to the seafloor beacon, weighted by the estimated positional accuracy. The final hole position was the mean position calculated from the GPS data collected over a significant portion of the time the hole was occupied.

Coring and drilling operations

The coring strategy for Expedition 342 consisted of advanced piston corer (APC) and extended core barrel (XCB) coring to total depths of ~200–400 meters below seafloor (mbsf), depending on stratigraphic targets recovered. Two or three holes were drilled at each site to build a composite depth scale and a stratigraphic splice for continuous subsampling after the cruise (see **"Sample depth calculation"** and **"Stratigraphic correlation"**).

The APC cuts soft sediment cores with minimal coring disturbance relative to other IODP coring systems and is suitable for the upper portion of each hole. After the APC core barrel is lowered through the drill pipe and lands near the bit, the drill pipe is pressured up until one or two shear pins that hold the inner barrel attached to the outer barrel fail. The inner barrel then advances into the formation at high speed and cuts the core. The driller can detect a successful cut, or "full stroke," from the pressure gauge on the rig floor.

The depth limit of the APC, often referred to as APC refusal, is indicated in two ways: (1) the piston fails to achieve a complete stroke (as determined from the pump pressure reading) because the formation is too hard or (2) excessive force (>60,000 lb; ~267 kN) is required to pull the core barrel out of the formation. When a full stroke could not be achieved, one or two additional attempts were typically made and each time the bit was advanced by the length of recovered core. Note that this resulted in a nominal recovery of ~100% based on the assumption that the barrel penetrated the formation by the length of core recovered. When a full or partial stroke was achieved but excessive force could not retrieve the barrel, the core barrel was sometimes "drilled over," meaning after the inner core barrel was successfully shot into the formation, the drill bit was advanced to total depth to free the APC barrel.

Nonmagnetic core barrels were used during all APC deployments. Most APC cores recovered during Expedition 342 were oriented using the FlexIT tool (see **"Paleomagnetism"**). Formation temperature measurements were made to obtain temperature gradients and heat flow estimates (see **"Downhole logging"**).

The XCB system was used to advance the hole when APC refusal occurred before the target depth was reached. The XCB is a rotary system with a small cutting shoe that extends below the large rotary APC/XCB bit. The smaller bit can cut a semi-indurated core with less torque and fluid circulation than the main bit, optimizing recovery. The XCB cutting shoe (bit) extends ~30.5 cm ahead of the main bit in soft sediments but retracts into the main bit when hard formations are encountered.

The bottom-hole assembly (BHA) is the lowermost part of the drill string. The exact configuration of the BHA is reported in the operations section in each site chapter. A typical APC/XCB BHA consists of a drill bit (outer diameter = 11 7/16 inches), a bit sub, a seal bore drill collar, a landing saver sub, a modified top sub, a modified head sub, a nonmagnetic drill collar (for APC/XCB), a number of 8 inch (~20.32 cm) drill collars, a tapered drill collar, six joints (two stands) of 5½ inch (~13.97 cm) drill pipe, and one crossover sub. A lockable flapper valve was used to collect downhole logs without dropping the bit when APC/XCB coring.

Drilling disturbance

Cores may be significantly disturbed as a result of the drilling process and contain extraneous material as a result of the coring and core handling process. In formations with loose sand layers, sand from intervals higher in the hole may be washed down by drilling circulation, accumulate at the bottom of the hole, and be sampled with the next core. The uppermost 10–50 cm of each core must therefore be examined critically during description for potential "cave-in." Common coring-induced deformation includes the concave-downward appearance of originally horizontal bedding. Piston action may result in fluidization (flow-in) at the bottom of APC cores. Retrieval from depth to the surface may result in elastic rebound. Gas that is in solution at depth may become free and drive core segments within the liner apart. When gas content is high, pressure must be relieved for safety reasons before the cores are cut into segments. This is accomplished by drilling holes into the liner, which forces some sediment as well as gas out of the liner. Drilling disturbances are described in "Lithostratigraphy" in each site chapter and are graphically indicated on the graphic core summary reports, also referred to as visual core descriptions (VCDs), in **"Core descriptions."**

Core handling and analysis

Cores recovered during Expedition 342 were extracted from the core barrel in plastic liners. These liners were carried from the rig floor to the core processing area on the catwalk outside the Core Laboratory and cut into ~1.5 m sections. The exact section length was noted and later entered into the database as "created length" using the Sample Master application. This number was used to calculate recovery. The curated length was set equal to the created length and very rarely had to be modified. Depth in hole calculations are based on the curated length. Headspace samples were taken from selected section ends (typically one per core) using a syringe for immediate hydrocarbon analysis as part of the shipboard safety and pollution prevention program. Similarly, microbiology samples were taken immediately after the core was sectioned. Core catcher samples were taken for biostratigraphic analysis. When catwalk sampling was complete, liner caps (blue = top; colorless = bottom) were glued with acetone onto liner sections and the sections were placed in core racks in the laboratory for analysis.

The numbering of sites, holes, cores, and samples followed standard IODP procedure. A full curatorial sample identifier consists of the following information: expedition, site, hole, core number, core type, section number, and offset in centimeters measured from the top of the core section. For example, a sample identification of "342-U1403A-1H-2, 10–12 cm" represents a sample taken from the interval between 10 and 12 cm below the top of Section 2 of Core 1 ("H" designates that this core was taken with the APC system) of Hole A of Site U1403 during Expedition 342. The "U" preceding the hole number indicates that the hole was drilled by the United States Implementing Organization (USIO) platform, the *JOIDES Resolution*.

Sample depth calculations

Sample depth calculations are based on the methods described in IODP Depth Scales Terminology v.2 at **www.iodp.org/program-policies/procedures/guidelines**). Depths of samples and measurements were calculated at the applicable depth scale either by fixed protocol or by combinations of protocols with user-defined correlations as summarized below. The definition of these depth scale types, and the distinction in nomenclature, should keep the user aware that a nominal depth value at two different depth scale types usually does not refer to exactly the same stratigraphic interval in a hole.

Depths of cored intervals were measured from the drill floor based on the length of drill pipe deployed beneath the rig floor and referred to as drilling depth below rig floor (DRF). The depth of the cored interval was referenced to the seafloor by subtracting the seafloor depth from the DRF depth of the interval. The seafloor referenced depth of the cored interval is referred to as the drilling depth below seafloor (DSF). In most cases, the seafloor depth was the length of pipe deployed minus the length of the mudline core recovered. In some cases the seafloor depth was adopted from a previous hole drilled at the site.

Depths of samples and measurements in each core are computed based on the assumption that (1) the top depth of a recovered core corresponds to the top depth of its cored interval (at DSF scale) and (2) the recovered material is a contiguous section even if core segments are separated by voids when recovered. These depths are referred to as core depth below seafloor, method A (CSF-A). Voids in the core were closed by pushing core segments together, if possible, during core handling. This convention was also applied when a core had incomplete recovery, in which case the true position of the core within the cored interval is unknown and should be considered a sample depth uncertainty when analyzing data associated with the core material. Depths of subsamples and associated measurements at the CSF-A scale were calculated by adding the offset of the subsample or measurement from the top of its section, and the lengths of all higher sections in the core, to the top depth of the cored interval.

A soft to semisoft sediment core from less than a few hundred meters below seafloor expands upon recovery (typically a few percent to as much as 15%), so the length of the recovered core exceeds that of the cored interval. Therefore, a stratigraphic interval may not have the same nominal depth at the DSF and CSF scales in the same hole. When core recovery (the ratio of recovered core to cored interval times 100%) is >100%, the CSF-A depth of a sample taken from the bottom of a core will be deeper than that of a sample from the top of the subsequent core (i.e., the data associated with the two core intervals overlap at the CSF-A scale). The core depth below sea floor, method B (CSF-B), depth scale is a solution to the overlap problem. This method scaled the recovered core length back into the interval cored, from >100% to exactly 100% recovery. If cores had <100% recovery to begin with, they were not scaled. When downloading data using the IODP-USIO Laboratory Information Management System (LIMS) Reports pages at **web.iodp.tamu.edu/UWQ,** depths for samples and measurements are by default presented at both CSF-A and CSF-B scales. The CSF-B depth scale is primarily useful for data analysis and presentations in single-hole situations.

Core composite depth scales (CCSF) were constructed for each site, whenever feasible, to mitigate the CSF-A core overlap problem as well as the coring gap problem, and to create as continuous a stratigraphic record as possible. Using shipboard core logging data, and for some intervals postcruise XRF scanning data, core depths in adjacent holes at a site were vertically shifted to maximize the correlation of the data from cores recovered in adjacent holes. The correlation process resulted in affine tables, indicating the vertical shift of cores at the CCSF scale relative to the CSF-A scale. Once the CCSF scale was constructed, a splice was defined that best represented the stratigraphy of a site by utilizing and splicing the best core intervals from each hole at a site. Because of core expansion, the CCSF depths of stratigraphic intervals are typically 10%–15% deeper than their CSF-A depths (see **"Stratigraphic correlation"**). CCSF construction also revealed that coring gaps on the order of 1 m typically occur between cores in each hole, despite the apparent >100% recovery.

More on sample depth terminology

IODP Depth Scales Terminology v.1, adopted in June 2007, established the above summarized framework to distinguish between and refer to the different depth scale types used in scientific ocean drilling. Unfortunately, that document lacked clear directives for the use of the terminology in the editorial context, which resulted in rather inconsistent use since its implementation. IODP Depth Scales Terminology v.2 (April 2011), following a number of workshops and panel meetings, attempted to clarify this issue with the following directive:

1. A detailed description of the depth scales used during operations and data collection must be presented in the "Methods" chapter of reports and publications. The description in the "Methods" chapter should include designation of default depth terminology for use in the publication or report, to be used in all cases where depth was determined using the specified method.
2. The terms "meters below seafloor" or "meters below rig floor" and abbreviations "mbsf" and "mbrf" should be used throughout the report or publication in both text and figures where the depth being referenced was determined using the depth scale specified as the default depth scale for that report or publication in the "Methods" chapter.
3. If depth being referenced was not determined using the depth scale specified as the default depth scale for that report or publication, the abbreviation of the actual method should be used in both text (e.g., 12.34 m CCSF) and figure labels (e.g., Depth CCSF [m]).
4. The relationship between the default depth scale and the depth scale used in more specific investigations should, where possible, be clearly documented in the "Methods" chapter (e.g., the relationship between mbsf and CCSF as used in 3. above). If it is not possible to establish such a relationship, this should be stated in the "Methods" chapter.

These guidelines, aimed at continuing some of the old terminology that the new framework meant to differentiate and replace, resulted in a hybrid nomenclature recommendation including pieces of the old and the new concepts and names. For example, we now have statements such as "mbsf to CCSF growth rates" rather than "CSF-A to CCSF growth rates." Furthermore, the directive required that each science party designate one particular depth scale type as the "default," with the assumption that in most cases the CSF-A scale type would be designated the default scale.

During Expedition 342, we used the IODP depth scales DRF, DSF, CSF-A, and CCSF, and all depths were consistently expressed in terms of these four scale types throughout text, tables, and figures of the expedition *Preliminary Report*. After the expedition, in an attempt to make the reports more compatible with the above cited nomenclature directive, Publications Staff replaced all occurrences of "m CSF-A" in all text, figure and table documents with "mbsf."

Shipboard core analysis

When the cores reached equilibrium with laboratory temperature (typically after ~4 h), whole-round core sections were run through the Whole-Round Multisensor Logger (WRMSL), which measures *P*-wave velocity, density, and magnetic susceptibility, and the Natural Gamma Radiation Logger (NGRL). Thermal conductivity measurements were also taken before the cores were split lengthwise from bottom to top into working and archive halves. Investigators should note that older material might have been transported upward on the split face of each section during splitting. The working half of each core was sampled for shipboard analysis (biostratigraphy, physical properties, carbonate, paleomagnetism, and bulk X-ray diffraction [XRD] mineralogy). The archive half of each core was scanned on the Section Half Image Logger (SHIL) and measured for color reflectance and magnetic susceptibility on the Section Half Multisensor Logger (SHMSL). At the same time, the archive halves were described macroscopically as

well as microscopically by means of smear slides. Finally, the archive halves were run through the cryogenic magnetometer. Both halves of the core were then put into labeled plastic tubes that were sealed and transferred to cold storage space aboard the ship.

At the end of the expedition, all working section halves were transported from the ship to permanent cold storage at the Bremen Core Repository (BCR) at the University of Bremen, Germany. Archive section halves were divided into three batches and shipped directly to the Scripps Institution of Oceanography (SIO), the Gulf Coast Repository at Texas A&M University (TAMU), and the BCR for X-ray fluorescence (XRF) scanning. Most of the archive section halves measured at the SIO and TAMU were shipped to the BCR in February 2013 to be available for U-channel sampling at the 18 February–3 March postexpedition sampling party at the BCR, during which >30,000 samples were taken for studies in the investigators' laboratories.

Lithostratigraphy

The lithostratigraphy of sediments recovered during Expedition 342 was determined by a combination of core description, smear slide and thin section analyses, digital color imaging, spectrophotometry, and visual color determination. The methods employed are adapted from those used during Ocean Drilling Program (ODP) Leg 199 (Lyle, Wilson, Janecek, et al., 2002) and IODP Expedition 320/321 (Pälike, Lyle, Nishi, Raffi, Gamage, Klaus, and the Expedition 320/321 Scientists, 2010).

Visual core descriptions

VCDs of the archive half of the split cores provide a visual summary of lithostratigraphic, biostratigraphic, magnetostratigraphic, and physical property data obtained during shipboard analyses. IODP VCDs are equivalent to the "barrel sheets" used during the Deep Sea Drilling Program (DSDP) and ODP. Lithostratigraphic data for VCDs were recorded digitally in real time using the DESClogik software (version 3.32.5.1). Prior to drilling operations, a spreadsheet template with seven tabs was constructed in Tabular Data Capture and customized for Expedition 342 (Fig. F1). The tabs were used to record the following information:

1. Drilling disturbance,
2. General (lithologic core description),
3. Detail (higher level detail than general core description),
4. Smear slides (quantified texture and relative abundance of biogenic and lithologic components),
5. Core summary (written description of major lithologic findings by core),
6. Stratigraphic unit, and
7. Age.

DESClogik also includes a graphic display mode of core data (e.g., aligned digital images of section halves and various measurement data) that can be used to aid core description.

During Expedition 342, the Strater software package was used to compile the VCDs for each core. Site, hole, and core number are given at the top of the VCD together with a summary core description (Fig. F2). The written description for each core contains a succinct overview of major and minor lithologies, their Munsell colors, and notable features such as sedimentary structures and major disturbances resulting from the coring process (Fig. F3). Core depth below seafloor (recorded in meters), core length (recorded in centimeters), section breaks, and lithostratigraphic unit are indicated along the left side of the digital color image of the core and Graphic lithology column. Columns to the right of the Graphic lithology column include age and data collected by the WRMSL and SHMSL (see **"Physical properties"**). These include natural gamma radiation (NGR), lightness (L*) and color (a* and b*) as determined by color reflectance, and corrected magnetic susceptibility. Columns to the right of these data show drilling disturbance, biostratigraphy (nannofossils, planktonic foraminifers, and radiolarian biozones), drilling disturbance and intensity, sedimentary structures, lithologic accessories, and shipboard sampling.

Digital color image

The SHIL imaged the flat face of the archive half of the split cores using a line-scan camera. Sediment cores were split and the archive half scraped with the edge of a glass slide to provide a "clean" surface for imaging. The cleaned, flat face of the archive section halves were imaged as soon as possible after splitting to minimize color changes that occur through oxidation and drying. Images are taken at an interval of 10 lines/mm. Camera height is adjusted so that image pixels are square. Light is provided by three pairs of Advanced Illumination high-current focused LED line lights with fully adjustable angles to the lens axis. Note that compression of line-scanned images into compiled stacks (like the core image shown in the VCDs) may result in visual artifacts (e.g., the false appearance of lamination).

Sediment classification

Lithologic names consist of a principal name based on composition, degree of lithification, and/or tex-

ture as determined from visual examination and smear slide or thin section observations. For a mixture of components, the principal name is preceded by major modifiers (in order of increasing abundance) that refer to components making up ≥25% of the sediment (Fig. F4). Minor components that represent between 10% and 25% of the sediment follow the principal name (after "with") in order of increasing abundance. For example, an unconsolidated sediment containing 30% nannofossils, 25% clay minerals, 20% foraminifers, 15% quartz silt, and 10% manganese nodules would be described as a clayey nannofossil ooze with manganese nodules, quartz silt, and foraminifers. Our naming conventions mostly follow the ODP sediment classification scheme of Mazzullo et al. (1988). However, the mixed sediment class is replaced by a more descriptive set of terms (Fig. F4).

Sediments were divided into lithostratigraphic units on the basis of composition and abundance of different grain types estimated from visual examination of the core, smear slides, thin sections, shipboard measurements of carbonate content, and shipboard XRD analyses. When encountered, pebble-sized fragments and larger particles (e.g., dropstones, pumice, etc.) are noted in each VCD. Size divisions for grains are those of Wentworth (1922).

Terms that describe lithification vary depending upon the dominant composition, as described below:

1. Sediments derived predominantly from calcareous pelagic organisms (e.g., calcareous nannofossils and foraminifers): the lithification terms "ooze," "chalk," and "limestone" reflect whether the sediment can be deformed with a finger (ooze), can be scratched easily by a fingernail (chalk), or is unable to be scratched with a fingernail (limestone).
2. Sediments derived predominantly from siliceous microfossils (e.g., diatoms and radiolarians): the lithification terms "ooze," "diatomite/radiolarite," "porcellanite," and "chert" reflect whether the sediment can be deformed with a finger (ooze), cannot be easily deformed manually (diatomite/radiolarite), or displays a glassy luster (chert). We use the term "porcellanite" as defined by Keene (1975) to describe a siliceous limestone/claystone that has a dull luster and is less hard and compact than chert. Porcellanite may contain a mix of opal, quartz, clay minerals, and carbonate. Note that the terms "porcellanite" and "chert" do not imply crystallinity of the silica.
3. Sediments derived predominantly from siliciclastic material: if the sediment can be deformed easily with a finger, no lithification term is added and the sediment is named for the dominant grain size. For more consolidated material, the lithification suffix "-stone" is appended to the dominant size classification (e.g., "clay" versus "claystone").

Each recovered lithology is shown in the Graphic lithology column on the VCD (Fig. F2). For intervals composed of more than one lithology, symbols are arranged within the column from left to right in order of their relative abundance. Graphic lithologies are used for all components that comprise 25% or more of the total sediment. The width of each pattern in the column approximates the relative abundance of that component. For instance, for nannofossil clay, the left half of the column would show the "clay" graphic lithology and the right half of the column would show the "nannofossil" graphic lithology. For nannofossil ooze with clay, the leftmost 75% of the column would show "nannofossil ooze" and the rightmost 25% of the column would show "clay." For nannofossil clay with radiolarians, the Graphic lithology column would show (from left to right) 50% clay, 25% nannofossils, and 25% radiolarians.

Smear slide descriptions

Smear slide samples were taken by toothpick sampling of the section halves to define the lithologies. Visual percentage estimates of biogenic, nonbiogenic, and textural features were made from each slide. Biogenic components were divided into major microfossil groups (e.g., nannofossils, radiolarians, and foraminifers). Basic mineralogies were identified. In order to quantify the components observed in the smear slides, we used the following categories:

0 = absent (0%).
P = present (<1%).
F = few (1%–10%).
C = common (>10%–25%).
A = abundant (>25%–50%).
VA = very abundant (>50%).

Spectrophotometry and visual color determination

Spectrophotometry and magnetic susceptibility of the archive section halves were measured with the SHMSL. The SHMSL also takes measurements on empty intervals and in places where the core surface is well below the level of the core liner, resulting in spurious measurements. Spurious measurements can also result from small cracks, sediment disturbance caused by the drilling process, or plastic section dividers. These data points are to be edited out of the

data set by the user. Additional detailed information about measurement and interpretation of spectral data can be found in Balsam et al. (1997, 1998) and Balsam and Damuth (2000).

Reflectance of visible light from the archive halves of sediment cores was measured using an Ocean Optics USB4000 spectrophotometer mounted on the automated SHMSL. Freshly split cores were covered with clear plastic wrap and placed on the SHMSL. Measurements were taken at 1–5 cm spacing to provide a high-resolution stratigraphic record of color variation for visible wavelengths. Each measurement was recorded in 2 nm wide spectral bands from 400 to 900 nm.

In addition to the digital color image captured by the SHIL, VCDs include a description of sediment color and the corresponding hue, value, and chroma data as determined qualitatively using Munsell Soil Color Charts for each major and minor lithology (Munsell Color Company, 1994). These data were recorded immediately after cores were split to avoid color changes associated with drying and redox reactions.

Sedimentary structures

Sedimentary structures formed by natural processes (i.e., not a result of drilling disturbance) are represented on the VCD with symbols in the Structures column (see Fig. F3 for the definition of structures and symbols). Structures formed by both biogenic and physical processes are included. An estimate of bioturbation intensity is indicated on the left side of the Biostratigraphy column. Bioturbation intensity is classified as

- Absent, for laminated sediments;
- Slight, for sediments with still-visible horizontal bedding;
- Moderate, for sediments with obvious burrows;
- Heavy, for sediments with a nearly uniform appearance and rare burrows; and
- Complete, for completely uniform (homogeneous) sediments with no obvious burrows or sedimentary layers.

When identifiable, ichnofossils such as *Zoophycos, Chondrites,* and *Planolites* burrows were reported in the lithologic description. Sedimentary structure types are indicated on the right side of the Structures column (e.g., traction structures, soft-sediment deformation structures, etc.). All contacts between lithologies are gradational unless otherwise specified.

Drilling disturbance

Sediment disturbance resulting from the coring process is illustrated in the Drilling disturbance column on the VCD (e.g., fall-in, flow-in, biscuits, and drilling breccia) (Fig. F2). If the feature extends over an interval, the symbol appears centered on a vertical line to denote the extent of occurrence. Blank regions indicate an absence of drilling disturbance. Disturbance intensity follows the following subjective scheme:

- Slight
- Slight to moderate
- Moderate
- Moderate to high
- High
- Destroyed

Shipboard sampling

VCDs display the interval where sample material was taken for shipboard analysis (all whole rounds and all samples taken to aid core description). Whole rounds consist of samples taken for interstitial water and micropaleontology samples. Samples taken to aid core description include toothpick samples that were analyzed for smear slides, thin section billets, and discrete samples for mineralogical XRD analysis (Fig. F2). Typically, three or four smear slides were made per core, but more samples were selected in cores showing a high degree of lithologic variability. Interstitial water samples were taken at designated intervals, and a micropaleontology sample was obtained from the core catcher of most cores. XRD samples were taken only where needed to assess the lithologic components.

X-ray diffraction analyses

Bulk sample XRD analyses were performed using a Bruker D-4 Endeavor X-ray diffractometer with a Vantec detector using Ni-filtered CuKα radiation. Instrument settings were

Voltage = 40 kV.
Current = 40 mA.
Goniometer scan = 2°–70°2θ (air-dried samples).
Step size = 0.01°2θ.
Scan speed = 1.2°2θ/min.
Count time = 0.5 s.

Biostratigraphy

Preliminary age assignments were based on biostratigraphic analyses of calcareous nannofossils, planktonic foraminifers, and radiolarians. Paleodepth interpretations were based on benthic foraminifers. The biostratigraphy is tied to the geomagnetic polarity timescale (GPTS) used for Expedition 342, which is based upon the timescale of Gradstein et al. (2012) (Fig. F5). The age of events based on the previous

timescales of Gradstein et al. (2004), IODP Expedition 320 (Pälike, Lyle, Nishi, Raffi, Gamage, Klaus, and the Expedition 320/321 Scientists, 2010), and Cande and Kent (1995) are also shown in Tables T1, T2, and T3.

Calcareous nannofossil, planktonic and benthic foraminifer, and radiolarian data were collected from core catcher samples. Where possible, an additional sample was analyzed from each working section half in Hole A. At critical levels, extra samples from section halves were also analyzed. Sample depths are cited in the text as midpoint depths within the sample interval, where appropriate. Datum and zone boundary levels are cited as the midpoint between the datum level and the nearest sample without the datum taxon. Microfossil preservation, abundance, preliminary assemblage composition, datum level, and zonal assignment data were entered through DESClogik into the LIMS database (www.iodp.tamu.edu/UWQ). Biostratigraphic analyses focused on Hole A. In this Expedition Report, we present the biostratigraphic data for each site in datum tables, stratigraphic distribution charts, integrated biozonation figures, age-depth plots, and microfossil group abundance and preservation figures. It should be noted that the distribution charts are based on shipboard study only and are, therefore, biased toward age-diagnostic species.

Calcareous nannofossils

Calcareous nannofossil zonal scheme and taxonomy

The zonal scheme of Martini (1971), zonal code numbers NP and NN, was used for Cenozoic calcareous nannofossil biostratigraphy. The zonal scheme of Burnett (1998), zonal code numbers UC, was used for Cretaceous calcareous nannofossil biostratigraphy. These zonations represent a general framework for the biostratigraphic classification of middle- to low-latitude nannofossil assemblages and are presented in Figure F5. The age estimates presented are based on the Gradstein et al. (2012) timescale (Table T1). We have added several additional secondary nannofossil marker species not included in Gradstein et al. (2012) to our datum table and also provide revised calibration ages for several existing datum levels; references for these calibrations are provided in Table T1. Nannofossil taxonomy follows Bown (1998, 2005) and Perch-Nielsen (1985a, 1985b), in which full taxonomic lists can be found. A taxonomic list of nannofossil datums is given in Table T4.

Critical boundaries tend not to coincide precisely with nannofossil datum levels but may be approximated by the closest events, as follows:

1. Oligocene/Miocene boundary (23.03 Ma): the top of *Sphenolithus delphix* (23.11 Ma) occurs just below and the top of *Sphenolithus capricornutus* (22.97 Ma) occurs just above the boundary.
2. Eocene/Oligocene boundary (33.89 Ma): the boundary falls within Zone NP21, 0.55 m.y. above the top of *Discoaster saipanensis* (34.44 Ma) and 0.46 m.y. below the top acme of *Clausicoccus subdistichus* (33.43 Ma).
3. Middle Eocene Climatic Optimum (MECO): the onset of the MECO is approximated by the top of *Sphenolithus furcatolithoides* and the base of *Dictyococcites bisectus* (>10 µm), and the termination can be approximated by the base of *Sphenolithus predistentus* and top common occurrence of *Sphenolithus spiniger*.
4. Paleocene/Eocene Thermal Maximum (PETM): the carbon isotope excursion (CIE) interval is approximated by the base of *Rhomboaster* spp. and *Discoaster araneus* (Subzone NP9b of some authors), and the latter "excursion taxon" is restricted to this interval. The base of *Tribrachiatus* (or *Rhomboaster*) *bramlettei* and therefore the base of Zone NP10 is estimated to occur ~0.5 m.y. above the CIE onset (Raffi et al., 2005).

Methods of study for calcareous nannofossils

Calcareous nannofossils were examined in smear slides using standard light microscope techniques under crossed polarizers, transmitted light, and phase contrast at 1000× magnification.

Total calcareous nannofossil abundance within the sediment is recorded as

A = abundant (>50% of sediment particles).
C = common (>10%–50% of sediment particles).,
F = few (1%–10% of sediment particles).
R = rare (<1% of sediment particles).
VR = very rare (<5 specimens seen while logging slide).
B = barren (no specimens).

Abundance of individual calcareous nannofossil taxa is recorded as

A = abundant (>10 specimens per field of view [FOV]).
C = common (>1–10 specimens per FOV).
F = few (1 specimen per 1–10 FOV).
R = rare (<1 specimen per 10 FOV).
VR = very rare (<5 specimens seen while logging slide).

For selected age-diagnostic species, abundance is presented as specimens counted.

Preservation of the calcareous nannofossils is recorded as

G = good (little or no evidence of dissolution and/or recrystallization, primary morphological characteristics only slightly altered, and specimens were identifiable to the species level).
M = moderate (specimens exhibit some etching and/or recrystallization, primary morphological characteristics somewhat altered; however, most specimens were identifiable to the species level).
P = poor (specimens were severely etched or overgrown, primary morphological characteristics largely destroyed, fragmentation has occurred, and specimens often could not be identified at the species and/or generic level).

Foraminifers

Planktonic foraminifer zonal scheme and taxonomy

The zonal scheme of Berggren and Pearson (2005) as modified by Wade et al. (2011) was used for the Paleogene (zonal codes P, E, and O), and Berggren et al. (1995) as modified by Wade et al. (2011) was used for the Neogene (zonal codes M, PL, and PT). The planktonic foraminifer zonal scheme used during Expedition 342 is illustrated in Figure F5. The Cretaceous planktonic foraminifer zones are based on the tropical zonal schemes of Caron (1985) and Sliter (1989), with modifications by Hardenbol et al. (1998). Age estimates for planktonic foraminiferal datums follow Gradstein et al. (2012) (Table T2). Planktonic foraminifer taxonomic concepts in the Cenozoic selectively follow those of Jenkins (1971), Blow (1979), Kennett and Srinivasan (1983), Bolli and Saunders (1985), Toumarkine and Luterbacher (1985), Scott et al. (1990), Spezzaferri (1994), Pearson (1995), Chaisson and Pearson (1997), Olsson et al. (1999), and Pearson et al. (2006). The Cretaceous taxonomic concepts are based on Robaszynski et al. (1979, 1984), Leckie (1984), Caron (1985), Nederbragt (1990), and data at services.chronos.org:9090/resources/interactiveforams.html. A taxonomic list of planktonic foraminifer datum species is given in Table T5.

Benthic foraminifer taxonomy and paleodepth determination

Taxonomic assignments mainly follow Pflum and Frerichs (1976), Tjalsma and Lohmann (1983), van Morkhoven et al. (1986), Miller and Katz (1987), Thomas (1990), Katz and Miller (1991), Kaminski et al. (1993), Jones (1994), Nomura (1995), and Holbourn and Henderson (2002). The generic classification of Loeblich and Tappan (1988) was used and updated in some instances, in particular for uniserial taxa (Hayward, 2002). Species identification was made routinely on core catcher samples and on selected working section halves. Additional samples taken from working section halves are utilized for the description of relative abundance of individual morphogroups and preservation.

Paleodepth estimates are based on van Morkhoven et al. (1986) using the following categories:

Neritic = <200 meters below sea level (mbsl).
Bathyal = 200–2000 mbsl.
Abyssal = >2000 mbsl.

Methods of study for foraminifers

Sediments were washed with tap water over a 63 µm wire mesh sieve. For clay-rich sediments, samples were boiled in water with added Borax first. Subsequently, samples were washed and dried repeatedly until a clear residue formed. Lithified samples were treated with a 3% hydrogen peroxide solution for several minutes before washing.

Planktonic foraminiferal age determination was initially established using the wet samples in sieves. Subsequently, all samples were dried in sieves or on filter papers in a low-temperature oven (~50°C) and then examined under a binocular light microscope for benthic and planktonic foraminiferal assemblages. To minimize contamination of foraminifers between samples, the empty sieves were placed in a sonicator for several minutes and thoroughly checked between samples to enable identification of contaminants from previous samples. Species identification for planktonic foraminifers was generally made on the >250 and >150 µm size fractions. The 63–150 µm size fraction was scanned for distinctive taxa. Planktonic foraminifer species distribution and range charts are presented in each site chapter. Benthic foraminifer assemblage composition, paleodepth estimates, and relative abundance of morphogroups were based on counts of ~150 specimens from the >150 µm size fraction, where possible.

The preservation status of planktonic and benthic foraminifers was estimated as

VG = very good (no evidence of overgrowth, dissolution, or abrasion).
G = good (little evidence of overgrowth, dissolution, or abrasion).
M = moderate (calcite overgrowth, dissolution, or abrasion are common but minor).
P = poor (substantial overgrowth, dissolution, or fragmentation).

Planktonic foraminifer abundance estimates

The following planktonic foraminifer abundance categories relative to total sediment particles were es-

timated from visual examination of the dried sample in the >63 µm fraction as

D = dominant (>30% of sediment particles).
A = abundant (>10%–30% of sediment particles).
F = few (>5% to <10% of sediment particles).
R = rare (>1% to <5% of sediment particles).
P = present (<1% of sediment particles).
B = barren.

The number of individuals of each planktonic foraminifer species was categorized as

A = abundant (>50 specimens on the tray).
C = common (20–49 specimens on the tray).
F = few (10–19 specimens on the tray).
R = rare (2–9 specimens on the tray).
P = present (<2 specimens on the tray).
B = barren.

Benthic foraminifer abundance estimates

The following benthic foraminifer abundance categories relative to total sediment particles >150 µm were estimated from visual examination of the dried sample as

D = dominant (>30% of total sediment particles).
A = abundant (>10%–30% of total sediment particles).
F = few (>5% to <10% of total sediment particles).
R = rare (>1% to <5% of total sediment particles).
P = present (<1% of total sediment particles).
B = barren.

The number of individuals of each benthic foraminifer species was categorized as

D = dominant (>30% of benthic assemblage).
A = abundant (>10%–30% of benthic assemblage).
F = few (>1% to <10% of benthic assemblage).
P = present (<1% of benthic assemblage).

The number of individuals of each benthic morphotype was counted for selected working half section samples and categorized as

D = dominant (>30% of benthic assemblage).
A = abundant (>10%–30% of benthic assemblage).
F = few (>5% to <10% of benthic assemblage).
R = rare (>1% to <5% of benthic assemblage).
P = present (<1% of benthic assemblage).
B = barren.

Radiolarians

Radiolarian zonal scheme and taxonomy

The radiolarian zonal scheme used during Expedition 342 is described in Sanfilippo and Nigrini (1998), Nigrini et al. (2006), and Kamikuri et al. (2012). Age estimates for radiolarian datums from the Quaternary to the lower Eocene are based on the magnetobiochronology established for equatorial Pacific Leg 199 and Expedition 320 (Nigrini et al., 2006; Kamikuri et al., 2012), complemented by earlier compilations (Sanfilippo and Nigrini, 1998; Nigrini and Sanfilippo, 2001). For the lowermost Eocene through Upper Cretaceous, age estimates are based on correlation with calcareous microfossil datums (Sanfilippo and Riedel, 1985; Sanfilippo and Nigrini, 1998). For Expedition 342, these age estimates were calibrated to four timescales, where possible (Cande and Kent, 1995 [CK95]; Berggren et al. 1995; Gradstein et al., 2004 [GTS2004]; Ogg et al., 2008; Pälike, Lyle, Nishi, Raffi, Gamage, Klaus, and the Expedition 320/321 Scientists, 2010; Gradstein et al. 2012 [GTS2012]) (Table T3). All ages cited in the text and shown in figures are based on GTS2012. The primary references for the taxonomy of radiolarians studied during Expedition 342 were Nigrini and Lombari (1984), Sanfilippo et al. (1985), Nishimura (1992), Nigrini and Sanfilippo (2001), Sanfilippo and Blome (2001), Nigrini et al. (2006), Funakawa et al. (2006), and Kamikuri et al. (2012). Additional sources are noted in the taxonomic list (Table T6).

Methods of study for radiolarians

Samples were disaggregated by warming in a solution of 10% H_2O_2 and a generous squirt of dilute Borax (laundry detergent, acting as a clay dispersant). After effervescence subsided, calcareous components were dissolved by adding a 10% solution of hydrochloric acid. The solution was then washed through a 63 µm sieve. Strewn slides were prepared by pipetting the residue onto a microscope coverslip that was then dried on a hot plate. Norland mounting medium was applied to the coverslip (8–10 drops) while the coverslip was still warm. The coverslip was then inverted and gently placed on the slide. The mounting medium was fixed by placing the slide under an ultraviolet lamp for 15 min.

Abundance estimates of the radiolarian assemblage are qualitative estimates of the concentration of radiolarians in individual sediment samples, with the following categories:

A = abundant (>10,000 specimens in a 5 cm^3 sample).
C = common (2000–10,000 specimens in a 5 cm^3 sample).
R = rare (500–1999 specimens in a 5 cm^3 sample).
F = few (<500 specimens in a 5 cm^3 sample).
B = barren (absent).

Abundance of individual radiolarian species was based on a census of 300 specimens and recorded as

A = abundant (>16% of census).
C = common (>4%–16% of census).
F = few (>1%–4% of census).
R = rare (<1% of census).

P = present but not observed in census.
? = identification uncertain.

Preservation of the radiolarian assemblage was recorded as

G = good (most specimens complete, fine structures preserved).
M = moderate (minor dissolution and/or breakage).
P = poor (common dissolution, recrystallization, and/or breakage).

Paleomagnetism

Samples, instruments, and measurements

Paleomagnetic investigations during Expedition 342 focused mainly on measuring the natural remanent magnetization (NRM) of archive section halves before and after alternating field (AF) demagnetization. We also collected one discrete sample per section from most Hole A working section halves for use in bulk magnetic susceptibility, anisotropy of magnetic susceptibility (AMS), and AF demagnetization experiments. Discrete samples were taken in plastic Natsuhara-Giken sampling cubes (7 cm^3 sample volume) (Fig. **F6A, F6B**). Cubes were pushed into the working half of the core by hand with the "up" arrow on the cube pointing upsection. For indurated intervals, cubes were cut with a table saw and trimmed to fit in the plastic containers. The coordinate system of the discrete samples follows the right-hand rule and is oriented so that the cube is pushed toward the double lines on the core liner and the +*z*-axis points downsection.

Remanence measurements of archive section halves were made using a 2G Enterprises Model-760R superconducting rock magnetometer (SRM) equipped with direct-current superconducting quantum interference devices (SQUIDs) and an in-line, automated AF demagnetizer capable of reaching a peak field of 80 mT. The coordinate system for the SRM is shown in Figure **F6C.** Prior to every working shift (i.e., every ~12 h), we washed the length of the sample track with antistatic solution and the top and bottom of the sample tray with isopropyl alcohol. The magnetization of the sample tray was measured at the beginning of every shift to monitor any changes to the sample tray during the course of the expedition and to maintain accurate tray correction values. Every section half was wrapped in plastic wrap prior to measurement. Finally, we regularly checked the tuning of the SQUIDs and made adjustments when necessary. This procedure ensured that the magnetometer was kept as clean and noise free as laboratory conditions permitted.

We measured NRM every 2.5 cm along the archive section halves after 0 and 20 mT AF demagnetization. Additional intermediate steps were deemed unnecessary for the goals of shipboard analysis. We did not measure sections that were entirely visibly disturbed. Similarly, when analyzing SRM data we removed measurements from within 7.5 cm of section ends and within intervals with drilling-related core disturbance as described by the lithostratigraphers.

Remanence of the discrete samples was measured on an AGICO JR-6A spinner magnetometer. Discrete samples were placed into the "automatic holder" of the JR-6A as shown in Figure **F7.** Following measurement, the JR-6A data were transformed from the instrument coordinate system to the core coordinate system. AF demagnetization of discrete samples was made with an ASC D-2000 AF demagnetizer. AF demagnetization of these samples was usually conducted at a peak field of 20 mT. Some selected discrete samples were step-wise demagnetized up to 60 or 80 mT if core flow permitted and if full demagnetization was necessary for directional interpretations.

AMS measurements were made on an AGICO KLY 4S Kappabridge instrument using the AMSSpin LabVIEW program designed by Gee et al. (2008) and adapted for use with the shipboard KLY 4S. The KLY 4S Kappabridge measures anisotropy of magnetic susceptibility by rotating the sample along three axes, stacking the data, and calculating the best-fit second-order tensor. It also measures the volume-normalized, calibrated bulk susceptibility (χ). Tensor elements were converted to eigenparameters (eigenvectors V_1, V_2, and V_3 with associated eigenvalues τ_1, τ_2, and τ_3, in which τ_1 is the maximum and τ_3 is the minimum [terminology of Tauxe, 2010]). These parameters can be interpreted in terms of particle alignment within the sample (Fig. **F8**). Normal sedimentary fabrics are oblate with vertical axes of minimum susceptibility (e.g., Fig. **F8B**). Disturbance by slumping or other deformation generally yields triaxial fabrics (e.g., Fig. **F8D**). AMS data were analyzed using the Pmag.Py Python software package (Tauxe, 2010; freely available at **magician.ucsd.edu/Software/PmagPy**).

Low-field magnetic susceptibility was measured on all whole-core sections using the WRMSL and the Special Task Multisensor Logger (STMSL) (see **"Physical properties"**). Magnetic susceptibility was measured with a Bartington loop meter (Model MS2 with an MS2C sensor. The MS2C meter in the STMSL had a coil with an internal diameter of 90 mm and an operating frequency of 565 Hz. The modified MS2C in the WRMSL had a coil with an internal diameter of 80 mm and an operating frequency of 513 Hz. The "units" option for the meters was set to SI units, and

the values were stored in the database and are reported in raw instrument units. To convert to approximate SI volume susceptibilities for the 80 mm loop, instrument units are multiplied by ~0.578 × 10^{-5} ($1/K_{REL}$; K_{REL} = 3.45 × $(d/D)^3$; d = core diameter [~70 mm] and D = loop sensor diameter + 8 mm [88 mm]). For the 90 mm loop, the factor changes accordingly. This conversion factor may vary downhole with changes in core diameter and core volume.

Paleomagnetic data collected on the pass-through SRM were uploaded to the LIMS database. Data from discrete samples are tabulated in each site chapter.

Coring and core orientation

Cores were collected using nonmagnetic core barrels and cutting shoes. The FlexIT core orientation tool was used with all APC deployments except when partial strokes were experienced because of hard stratigraphic layers (i.e., cherts) or when core liners repeatedly failed during recovery. The orientation tool uses three orthogonally mounted fluxgate magnetometers to record the orientation of the double lines scribed on the core liner with respect to magnetic north. The tool also has three orthogonally mounted accelerometers to monitor the movement of the drill assembly, which helps determine when the most stable and thus most robust core orientation data were gathered. The tool declination, inclination, total magnetic field, and temperature are recorded at regular intervals until the internal memory of the tool is filled to capacity. These data are downloaded, processed, and uploaded to the LIMS database on the ship by shipboard support staff. Core orientation tool deployment and core orientation data are also indicated in our site reports.

In general, the quality of magnetic data from APC-recovered intervals is much higher than data from XCB-recovered cores. For example, magnetic directions and intensity are substantially less noisy within and between cores in a single hole and more coherent between holes at a given site for APC-recovered intervals than they are from XCB intervals. XCB-recovered intervals often, but not always, have higher magnetic intensities attributable to more pervasive magnetic overprinting during the coring process. These intervals are frequently disturbed by "biscuiting," which is characterized by intervals of coherent or relatively undisturbed stratigraphy that are a few to tens of centimeters long and are separated by hydrated clay and pulverized rock intervals as thick as several centimeters. The clay layers between biscuits are especially prone to remagnetization. Moreover, rotation (primarily on the vertical axis but random for biscuits smaller than the diameter of the core liner) between biscuits effectively randomizes downhole magnetic declination through these intervals. Therefore, our general shipboard strategy is to interpret only the magnetostratigraphy from APC-recovered intervals; we occasionally interpret the magnetostratigraphy from XCB-recovered intervals when the magnetic data are unusually good and unambiguous.

Magnetostratigraphy

Expedition 342 drill sites are located at ~40°N; therefore, typical magnetic polarity zones can be easily identified by distinct changes in inclination. The present-day normal field in this region, as calculated from the geocentric axial dipole (GAD), has a positive inclination of ~59°. Negative inclination values, therefore, indicate reversed field polarity. Magnetozones identified from the shipboard data were correlated to the GPTS with the aid of biostratigraphic datums.

We used the GTS2012 timescale, which is summarized in Table **T7** and Figure **F5** (see **"Biostratigraphy"**). In GTS2012, boundary ages for Chrons C1n–C13n and C24n.1n–C34n are orbitally tuned, whereas those for Chrons C13r–C23r are spline fitted. Cryptochrons not described in Gradstein et al. (2012) are referred from Cande and Kent (1995) and are described in the Remarks column in Table **T7.** Cryptochron C18n.1n-1, found in sediments from Site U1333 (Expedition 320/321 Scientists, 2010), is also noted in this table.

Age models and mass accumulation rates

Age models

The age models developed for each site are based on shipboard micropaleontology and paleomagnetic measurements. For most sites, the age model is based on Hole A, which was the hole that was examined in the most detail by the micropaleontology team. The age-depth model was constructed from tabulations of biostratigraphic and paleomagnetic datums. Datums were placed at midpoints between bounding samples for biostratigraphy and between inflection points in the declination or inclination curves for magnetochron boundaries. The bounding samples and inflection points represent datum uncertainty in age-depth plots. Age determinations are based on GTS2012. See Figure **F5** and Tables **T1, T2,** and **T3** for a more detailed description of this timescale and biostratigraphic datums, including notes on additional biostratigraphic datums utilized during Expedition 342; see **"Paleomagnetism"** for a detailed description of the GPTS utilized during Expedition 342.

Linear sedimentation rates

Shipboard micropaleontology and magnetostratigraphy were used to construct a linear sedimentation rate (LSR) curve for each site. For Sites U1403–U1410, depths are based on Hole A. For Site U1411, depths are based on Hole B, which was the principal first hole. Construction of the LSR curve was an iterative process involving refinements of magnetochron identification coupled with review of the reliability of specific biostratigraphic datums. The final LSR curve is drawn through the finalized paleomagnetic datums and the most robust biostratigraphic datums, taking care to avoid age inversions. Because of known calibration uncertainties (Gradstein et al., 2012) and the potential for significant diachroneity (e.g., Sanfilippo and Blome, 2001), we chose to construct LSR curves based on a selection of tie points rather than incorporate all biostratigraphic datums in the age model. This strategy minimizes the potential for spurious variations in LSR and mass accumulation rate (MAR) over short timescales that can result from poorly calibrated or diachronous biostratigraphic events.

Datum reliability was evaluated on the basis of

1. Uncertainty relating to the shipboard sampling interval and intervals of poor microfossil recovery,
2. Reliability of the calibration of the datum to GTS2012, and
3. Relative reliability of datums when datums were in contradiction.

Selected datum ties were chosen as the tie points for LSR line segments.

Datum tie points are denoted by a tie point number that increases with depth (e.g., D01 to D12 in Table **T18** in the "Site U1403" chapter [Norris et al., 2014]). The slope of line segments between datum ties is the LSR used in the MAR calculations. Using this approach, the LSR creates a square wave pattern that is imparted to the MAR record; this artifact must be considered when interpreting MAR calculations.

Clusters of biostratigraphic events of varying ages at or close to specific depth horizons were used to infer hiatuses. Hiatuses were also inferred where shipboard magnetostratigraphy could not be continuously correlated to the GPTS or became inconsistent with well-calibrated biostratigraphic datums. Where possible, these hiatuses were verified with reference to physical property and lithostratigraphic data.

Mass accumulation rates

MARs were calculated for the Expedition 342 drill sites using (1) LSR derived from shipboard age-depth models and (2) dry bulk density calculated from shipboard moisture and density (MAD) analyses. MARs of carbonate (CAR) and noncarbonate (nCAR) fractions were then calculated by multiplying the MAR by carbonate weight percent, which was calculated from shipboard coulometry measurements of inorganic carbon (IC) weight percent, where

$$CaCO_3 \text{ wt\%} = \text{IC wt\%} \times 8.33.$$

This calculation assumes that all of the inorganic carbon is present as calcite and aragonite.

Dry bulk density

Shipboard MAD measurements provided wet mass, dry mass, and dry volume values for discrete samples at a resolution of one sample per section (see **"Physical properties"**); dry bulk density values were calculated from these data. All of these data are tabulated in the "Age-depth models and mass accumulation rates" section of each site chapter. The shipboard age models were applied to the dry bulk density records.

Time step for mass accumulation rate calculations

The time step for the MAR calculations was selected on the basis of the sampling resolution of the shipboard MAD samples. Considerations taken into account for the time step of MAR calculations are (1) consistency in the time step between sites and (2) the geological period of interest that is best represented in each site. A 200 k.y. time step was chosen and the dry bulk density (DBD) and carbonate data were resampled at this new sampling interval using the Analyseries software. Average values between age midpoints were calculated using linear interpolation. MAR, CAR, and nCAR values (g/cm^2/k.y.) for each 200 k.y. time step are therefore

$$\text{MAR} = \text{LSR (cm/k.y.)} \times \text{DBD (g/cm}^3),$$

$$\text{CAR} = \text{LSR} \times \text{DBD} \times CaCO_3 \text{ (wt\%), and}$$

$$\text{nCAR} = \text{MAR} - \text{CAR}.$$

Geochemistry

Shipboard geochemistry for Expedition 342 included routine sets of analyses for

- Hydrocarbon gases;
- Interstitial water composition;
- Sedimentary geochemistry including inorganic carbon, sedimentary organic carbon, total carbon and nitrogen, and C/N ratios; and

- Pyrolysis characterization of sedimentary organic matter.

These analyses were conducted to satisfy routine shipboard safety and pollution prevention requirements, to characterize interstitial water and sediment geochemistry for shipboard interpretation, to guide shore-based sampling, and to provide samples for shore-based research. The procedures and instruments used during Expedition 342 are generally similar to those used during recent IODP expeditions; many of these are described by Pimmel and Claypool (2001). Comments on routine sampling and deviations from standard practice are noted below and in the individual site chapters.

Hydrocarbon gases

Sediment gas composition was typically determined at each interstitial water sampling point once every core. The routine headspace procedure involved the placement of a 5 cm^3 sediment sample in a 21 cm^3 glass serum vial that was sealed with a septum and metal crimp cap and heated at 70°C for 30 min for standard IODP hydrocarbon safety monitoring. After heating, a 5 cm^3 volume of headspace gas was removed with a glass syringe for analysis by gas chromatography. A second gas sampling procedure using a vacuum container was used when gas pockets or expansion voids appeared in the core while still in the core liner. A device with a heavy-duty needle was used to penetrate the core liner, and an attached syringe was employed to collect the gas.

Headspace gas samples were analyzed with an Agilent/HP 6890 Series II gas chromatograph equipped with a 2.4 m × 2.0 mm stainless steel column packed with 80/100 mesh HayeSep R and a flame ionization detector (FID). The instrument quickly measures concentrations of methane (C_1), ethane (C_2), ethene ($C_{2=}$), propane (C_3), and propene ($C_{3=}$). Gases were introduced by injection from a 5 mL syringe directly connected to the gas chromatograph system through a 1 cm^3 sample loop. Helium was used as the carrier gas, and the gas chromatograph oven temperature was programmed to start at 80°C and hold that temperature for 8.25 min before ramping at 40°C/min to 150°C, with a final holding time of 5 min. The FID temperature was 250°C.

In instances where samples were collected in vacuum containers, gases were analyzed with an Agilent/HP 6890A Series II gas chromatograph equipped with a FID and a thermal conductivity detector (TCD) to measure concentrations of C_1–C_6 hydrocarbons, N_2, O_2, and CO_2. Gases were introduced by injection from a 5 mL syringe directly connected to the gas chromatograph system through a 1 cm^3 sample loop.

TCD separation used three columns:

1. A 6 ft × 2.0 mm inner diameter (ID) stainless steel column (Poropak T; 50/80 mesh),
2. A 3 ft × 2.00 mm ID stainless steel molecular sieve column (13X; 60/80 mesh), and
3. A 2.4 m × 3.2 mm ID stainless steel column packed with 80/100 mesh HayeSep R (Restek).

FID separation was performed on a DB1 capillary column (60 m × 0.32 mm) with 1.5 µm phase thickness. FID separation used helium as the carrier gas, and the gas chromatograph oven temperature was programmed to hold for 2 min at 50°C, ramp at 8°C/min to 70°C, and then ramp at 25°C/min to 200°C, with a final holding time of 5 min. The FID temperature was 250°C.

Data were collected and evaluated with an Agilent ChemStation data-handling program. Chromatographic response was calibrated to different gas standards with variable quantities of low–molecular weight hydrocarbons. Gas components are reported as parts per million by volume (ppmv) of the injected sample. Methane in the uppermost headspace samples is also expressed as millimoles per liter per volume (mM), assuming a porosity of 0.45 µm, a sample volume of 5 cm^3, and a vial volume of 21.5 cm^3:

$$C_1 \text{ (mM)} = \text{ppmv } C_1 \times [(21.5 - 5)/(22{,}400 \times 5 \times 0.45)] = \text{ppmv } C_1 \times 0.0003.$$

Interstitial water analyses

Interstitial water analyses were carried out on cores from Sites U1402–U1407. Interstitial water was extracted from 5 to 10 cm long whole-round sections that were cut and capped immediately after core retrieval on deck. Whole-round sections for interstitial water analyses were taken from the bottom of Section 6 in Hole A or, alternatively, from the bottom of Section 1 in Hole A. This strategy was used to avoid removing whole rounds from the middle of cores, thereby preserving material integral to the splicing process (see **"Stratigraphic correlation"**). Occasionally, samples from more than one hole were analyzed and integrated in a single depth profile (splice) using the appropriate composite depth scale as the depth reference, if possible. Before squeezing, samples were removed from the core liner and the outer surfaces were carefully scraped with spatulas to minimize potential contamination by the coring process.

Whole rounds were placed into a titanium and steel squeezing device modified after the stainless steel

squeezer of Manheim and Sayles (1974) and squeezed at ambient temperature with a hydraulic press at pressures of up to 170 MPa (~25,000 psi). The interstitial water squeezed out of the sediment was extruded into a prewashed (in 10% HCl) 60 mL plastic syringe attached to the bottom of the squeezer assembly. The solution was subsequently split into five parts:

1. One part (10 mL) was filtered through a 0.45 µm polysulfone disposable filter (Whatman) into a vial for shipboard routine analyses of salinity, pH and alkalinity, chlorinity, dissolved inorganic carbon (DIC), anions and cations (Cl^-, SO_4^{2-}, Na^+, K^+, Ca^{2+}, and Mg^{2+}), nutrients (PO_4^{3-}, NH_4^+, and $NO_2^- + NO_3^-$), and minor elements (Li, B, Mn, Fe, Sr, Ba, Si, and P).
2. One part (5 mL) was added to 225 µL mercuric chloride and 10 µL of concentrated sulfuric acid and refrigerated in headspace-free vials for shore-based ammonium $\delta^{15}N$ measurements.
3. One part (2 mL) was added to 100 µL of mercuric chloride for shore-based liquid DIC measurement.
4. A water split was placed into a 5 mL cryovial and spiked with 10 µL HNO_3 for inductively coupled plasma–atomic emission spectroscopy (ICP-AES) analysis.
5. The remaining interstitial fluids were sealed in glass ampules and archived.

Following interstitial water removal, squeeze cakes were removed from the squeezing device, placed in sterile bags, and stored at –20°C for postcruise molecular biomarker analyses.

Interstitial water was also sampled at higher resolution (every 50 cm) from Hole U1404C to test for the presence of gas hydrates with Rhizon samplers. Originally developed as soil moisture samplers for root zones, rhizon samplers consist of thin tubes of hydrophilic porous polymer that extract water from sediment under vacuum. Rhizon samplers have recently been applied to sampling of sediment interstitial water, including during IODP Expeditions 302 (Dickens et al., 2007) and 320/321. Rhizon CSS-F 5 cm core solution samplers (Rhizosphere Research Products) were soaked in distilled water for ~1 h before use. Rhizon samplers were wiped clean of excess water and carefully inserted through holes drilled through the core liner at a 55° angle so that the 5 cm porous tube was in contact with presumably undisturbed sediment away from the core liner on either side. Samples were taken after the core was run through the STMSL. Acid-washed 10 mL syringes were attached to each Rhizon sampler, pulled to generate vacuum, and held open by hand. The first ~1 mL of water was discarded, with the rest collected and split for shore-based and shipboard analyses. Collection of 10–12 mL typically took 30 min.

Salinity, pH, and alkalinity analyses

Interstitial water analyses followed the procedures outlined by Gieskes et al. (1991), Murray et al. (2000), and user manuals for new shipboard instrumentation with modifications, as indicated. Interstitial water was analyzed for salinity with a Fischer Model S66366 salinity refractometer previously calibrated using the International Association of Physical Sciences of the Ocean (IAPSO) seawater standard. Alkalinity and pH were measured by Gran titration with a Brinkman pH electrode Metrohm autotitrator. The IAPSO seawater standard was used for standardization of alkalinity.

Ion chromatography

Sulfate, chloride, magnesium, calcium, sodium, and potassium concentrations in interstitial water were determined with a Dionex ICS-3000 ion chromatograph on 1:200 diluted aliquots in 18 MΩ water. The IAPSO seawater standard was used for standardization of measurements made on the ion chromatograph.

Spectrophotometric analyses

Phosphate, ammonium, and total nitrate and nitrite concentrations in interstitial water were determined by an Agilent Cary 100 UV-Vis spectrophotometer unit, an automated system that controls sample analysis and reagent aspiration, dispensing, heating, and mixing. In the phosphate method, orthophosphate reacts with Mo(VI) and Sb(III) in an acidic solution to form an antimony phosphomolybdate complex. Ascorbic acid reduces this complex to form a blue color, measured at 885 nm. Potassium phosphate monobasic (KH_2PO_4) was used to produce a calibration curve and as an internal standard. In the ammonium method, phenol undergoes diazotization and the subsequent diazo compound is oxidized by sodium hypochlorite to yield a blue color, measured spectrophotometrically at 640 nm. Ammonium chloride (NH_4Cl) was used to produce a calibration curve and as an internal standard. In the nitrate/nitrite method, the sample passes through an open, tubular, copperized cadmium coil that reduces nitrate to nitrite. Both the reduced nitrate and any preexisting nitrite are diazotized with sulfanilamide and coupled with N-(1-naphthyl)ethylenediamine dihydrochloride to form a colored azo dye, measured spectrophotometrically at 540 nm.

Major and trace element analyses by ICP-AES

Concentrations of selected elements (Li, B, Mn, Fe, Sr, Ba, and Si) in interstitial water were determined by ICP-AES with a Teledyne Prodigy high-dispersion ICP-AES. The method for shipboard ICP-AES analysis of samples is described in detail in Murray et al. (2000).

Each batch of ~20 samples run on the ICP-AES contained six artificial standards of known increasing concentrations for all elements of interest, as well as two additional standards to monitor instrumental drift. Samples were analyzed in batches to take advantage of achieved calibration, and each sample was analyzed three times from the same dilute solution (i.e., in triplicate) within a given sample run. Samples and standards were diluted 1:10 using 2% HNO_3 prior to analyses.

Following each run of the instrument, the measured raw-intensity values are transferred to a data file. Instrument drift was negligible during analyses of interstitial water, and therefore no correction was applied. A calibration line for each element was calculated using the results for the known standard solutions. Element concentrations in the samples were subsequently calculated from the relevant calibration line. Replicate analyses of one of the artificial standards were used to estimate precision and accuracy for minor elements, which typically was between 2% and 5%.

Depletion of shipboard supplies of the laboratory strontium standard at Site U1407 prompted a mission to collect seawater for preparation as a replacement standard. Four batches of 150 mL of seawater were filtered with 0.2 µm filters to remove colloidal particles, transferred to precleaned 200 mL beakers and heated to concentrate solutions by evaporation until ~2% of the original volumes remained. When complete and cooled, batches were combined to make one uniform solution, which was then acidified to 2% nitric acid, the same as the original standard used aboard Expedition 342. We were ultimately unable to confirm the calibration range; therefore, strontium values for Sites U1407–U1411 are not reported.

Bulk sediment geochemistry

We routinely took one 5 cm^3 sample of sediment for bulk geochemistry from the working section half of each core. Sample intervals were occasionally adjusted depending on the prevailing lithology, and not all samples were analyzed for every element in order to best approach the scientific questions in the available time and with the available resources. Whenever possible, samples were taken adjacent to moisture and density samples to maximize integration of analytical data (e.g., calcium carbonate content), to calibrate higher resolution core logging data, and to calculate mass accumulation rates. Samples were freeze-dried for 24 h and ground in a mortar for subsequent analyses. Geochemical analyses included percent carbonate and elemental analyses of carbon and nitrogen.

For intervals sampled for microbiology, squeeze cakes from the interstitial water samples were freeze-dried for onshore elemental analyses (C/N) and intact polar lipids.

Inorganic carbon and carbonate

Inorganic carbon content of sediment samples was determined using a Coulometrics 5011 CO_2 coulometer. One carbonate determination was performed typically every 1.5 m section of core and at higher resolution (up to every 10 cm) across selected lithologic transitions or in zones of pronounced changes.

Freeze-dried and ground sediment (~10–15 mg) was reacted with 2N HCl. The liberated CO_2 was backtitrated to a colorimetric end point. Sediment carbonate content (in weight percent) was calculated from inorganic carbon (IC) content by assuming all carbonate occurs as calcium carbonate:

$$\text{wt\% } CaCO_3 = \text{wt\% IC} \times 8.33.$$

Reproducibility was determined by replicate measurements of selected samples and standards (100 wt% $CaCO_3$) treated as samples (every 10 samples). Typical standard deviations are 0.3–0.4 wt% on sample and standard replicates.

Elemental analyses

Total carbon (TC) and total nitrogen (TN) contents of sediment samples were determined with a ThermoElectron FlashEA elemental analyzer 1112 equipped with a ThermoElectron packed column (CHNS/NCS) and a TCD. An aliquot of ~8–20 mg of freeze-dried, ground sediment was weighed into tin cups, and the sample was combusted in a stream of oxygen at 950°C. The reaction gases were passed through a reduction column to reduce CO_3 to CO_2, nitrogen oxides to nitrogen, SO_3 to SO_2, and H_2O to H_2. The gases were then separated by the CHNS/NCS multiseparation column (Thermo 26008215) before detection by the TCD. H_2 values are not useful because they represent hydrogen from both organic matter and (clay) minerals. Sulfur values were not reported after Site U1403 because the vanadium pentoxide catalyst was contaminated.

All measurements were calibrated to two reference materials: the National Institute of Standards and Technology (NIST) 1646a Estuarine Sediment reference material (TN = 16.27 wt%; TC = 41.84 wt%) or La Luna Shale (TC = 11.32 wt%). Reference material was run after every 10 samples. Analyses were only continued if standard data varied by <1% from these values for N and C. During Expedition 342, the mean total organic carbon (TOC) value measured for NIST1646a Estuarine Sediment reference material was 0.87 ± 0.01 wt% (1σ; N = 10).

Typical precision was assessed using 10 replicate analyses of a rock standard from Weatherford Laboratories (99986; PWDR5) with a minimal TOC content of 3.11 wt% and an IC content of 0.43 ± 0.02 wt% based on coulometry (total carbon = 3.54 wt%). These replicate analyses show standard deviations of 0.032 and 0.046 for N and C, respectively. The coefficients of variation are 0.055 and 0.013 wt% for N and C, respectively.

TOC_{DIFF} content was calculated as the difference between TC (measured on the elemental analyzer) and IC (measured by the coulometry):

$$TOC_{DIFF} = TC - IC.$$

These values are probably overestimates because they are determined as a small difference between two numbers comparable in magnitude.

Total organic carbon measurement

During Expedition 342, TOC values determined against the two reference materials gave different values by a factor of ~3 (2.913 derived from cross-calibration and duplicate sample runs under each standard calibration), even for cases where their calibration ranges overlap. For example, low-carbonate samples determined under the La Luna Shale calibration yielded a TC value of 0.5 wt% but ~1.5 wt% under the Estuarine Sediment calibration. This discrepancy seriously compromises confidence in the shipboard total carbon results. The sources of this discrepancy should be resolved for future shipboard measurements. In order to recover an estimate of TC from the data we had in hand, Scientist Zhonghui Liu developed a mixed-model correction scheme using data from the two calibrations. This method is based on the supposition that the Estuarine Sediment standard applies best for samples with low TC, whereas La Luna Shale applies best for samples with high TC. Using the calibration maximum points we applied onboard (2.2 wt% for Estuarine Sediment and 15.36 wt% for La Luna Shale, normalized to a typical 15 mg sediment sample to be analyzed), mathematically, correction factors can be derived for both calibrations. Under the Estuarine Sediment calibration, if TC < 2.2 wt%, no correction is applied, and if TC > 2.2 wt%,

$$\text{wt\% corrected TC} = 2.2 + (x - 2.2) \times (15.36 - 2.2)/(15.36 \times 2.913 - 2.2),$$

where x is the measured value and 2.913 is the difference factor between the two standards. Under the La Luna Shale calibration, if TC < 2.2 wt%,

$$\text{wt\% corrected TC} = x \times 2.913.$$

If TC > 2.2 wt%,

$$\text{wt\% corrected TC} = 2.2 + (x - 2.2/2.913) \times (15.36 - 2.2)/(15.36 - 2.2/2.913).$$

We therefore report TC measurements with the understanding that they should be considered provisional and are likely subject to substantial nonrandom errors that we cannot, at present, estimate. Postexpedition research on these cores should not rely on the TC values reported here, and should seek to make more reliable TC determinations.

The "acidification method" of TOC analysis was also applied to determine if the analytical precision of TOC in high-$CaCO_3$–low-TOC sediment could be improved. A pilot study from Hole U1404A of 10 freeze-dried samples (~30 mg) in precombusted silver capsules were treated with small aliquots (10 µL) of 2 N HCl at room temperature to remove $CaCO_3$; samples were treated with repeated aliquots until no further reaction was visible and then dried. The 10 selected samples have variable carbonate contents (1.9–56.9 wt%) and thus variable original IC contents (2.9–10.35 wt%) (Fig. F9).

TOC concentration was determined using a Thermo Electron Flash EA 1112 element analyzer for TC. Decarbonated TOC varied from showing increases relative to TOC by difference (two cases with increases of 29% and 75%) to the remainder showing moderate to strong decreases, with reductions of up to 85% compared to original TOC. Removing carbonate should lead to an increase in TOC in the residue weight, not a decrease, so bulk removal of carbonate using the technique described above alters and removes a portion of organic matter. This means that the technique commonly used to measure TOC (bulk offline removal of carbonates by acid digestion followed by TC measurement) results in under-reporting of organic carbon and nitrogen content in the samples in the process.

Organic matter characterization

The type and quantity of organic matter in some sediments was evaluated by pyrolysis assay using the source rock analyzer (SRA) (Weatherford Laboratories). Between 60 and 180 mg of freeze-dried, ground sediment was weighed into SRA crucibles. Volatile hydrocarbon content (HC) was released when the sample was heated at 340°C for 3 min as the S1 peak (mg HC/g rock). Hydrocarbons were released during the pyrolysis of kerogen as the temperature was increased from 340°C to 640°C at 25°C/min as the S2 peak (mg HC/g rock). The nominal temperature of the maximum rate of hydrocarbon yield during the S2 analysis is T_{max}. CO_2 (as mg C/g rock) released during pyrolysis between 340°C and 390°C is the S3 peak. CO_2 (as mg C/g rock) produced by oxidizing the pyrolysis residue at 580°C is the S4 peak, but this is not directly reported. TOC_{SRA} was calculated from S1, S2, and S4, assuming that S1 and S2 are 83% carbon:

$$\text{wt\% TOC}_{SRA} = (0.83 \times [S1 + S2] + S4)/10.$$

The carbon-normalized hydrogen index (HI) (mg HC/g C) and the oxygen index (OI) (mg CO_2/g C) were calculated from pyrolysis values:

$$HI = (100 \times S2)/TOC \text{ and}$$

$$OI = (100 \times S3)/TOC.$$

All measurements were preceded by a blank and then calibrated to a rock standard from Weatherford Laboratories (99986; PWDR5). The same standard was used for quality control every 10 samples. Analysis was only continued if quality control data fell within the permitted range for this standard, as defined by Weatherford Laboratories. Typical precision was assessed using eight replicate analyses of the rock standard. Coefficients of variation for this data set fell between 0.005 (T_{max}) and 0.1 (OI).

Physical properties

High-resolution physical property measurements were made during Expedition 342 mainly to aid lithostratigraphic correlations and interpretations and to help document the Cenozoic behavior of the carbonate compensation depth (CCD) in the North Atlantic. More specifically, physical property data are used for

- Hole-to-hole stratigraphic correlations for the construction of composite depth scales and sampling splices at each site (see **"Stratigraphic correlation"**),
- Site-to-site stratigraphic correlations,
- Detection of discontinuities and lateral inhomogeneities caused either naturally or by the drilling process,
- Collection of information about differences in the composition and texture of sediment,
- Correlation with orbital cycles and tuning to reference cores for stratigraphic purposes, and
- Identification of major seismic reflectors and construction of synthetic seismic profiles.

Measured physical properties include gamma ray attenuation (GRA) bulk density, magnetic susceptibility with loop (MSL) and point (MSP) sensors, NGR with the NGRL, thermal conductivity, color reflectance, MAD, and compressional *P*-wave velocity.

The measurement sequence included several core logging and discrete sample measurement systems designed and built at IODP-TAMU for specific shipboard workflow requirements. First, physical properties were measured using three whole-round core logging systems:

1. The STMSL was run on selected sections immediately after cores were sectioned on the catwalk to obtain data that could guide coring operations (see **"Stratigraphic correlation"**).
2. All core sections were run on the WRMSL after they had warmed to ambient laboratory temperature (20°–21°C).
3. All core sections were also run on the NGRL.

Both the STMSL and WRMSL include a GRA bulk densitometer and an MSL system. In addition, the WRMSL employs a compressional *P*-wave velocity logger (PWL).

After the whole-round sections were logged, thermal conductivity was measured on selected whole-round sections (typically Section 3 of each core in one hole per site, usually Hole A). The sections were subsequently split into working and archive halves. The archive half was processed through the SHIL to acquire high-resolution core images, followed by the SHMSL for color reflectance and magnetic susceptibility measurements. The working half was placed on the Section Half Measurement Gantry (SHMG), on which instruments are set up to measure compressional *P*-wave velocity using a caliper-type system (PWC). *P*-wave measurements on section halves are often of better quality than those on whole-round sections because of better coupling between those sensors and the sediment. PWL measurements have the advantage of being of much higher spatial resolution than those produced by the PWC. Dis-

crete samples were collected from the working halves of every section for MAD analysis.

The following sections describe the measurement methods and systems in more detail. A full discussion of all methodologies and calculations used aboard the *JOIDES Resolution* in the Physical Properties Laboratory is available in Blum (1997).

Gamma ray attenuation bulk density

The measurement of GRA can be directly related to the bulk density of sediment (Evans, 1965). The GRA densitometers on the STMSL and WRMSL operate by passing gamma radiation from a Cesium-137 (^{137}Cs) source through a whole-round core into a 75 mm × 75 mm sodium iodide detector situated directly below the core. The gamma ray peak has a principal energy of 662 KeV and is attenuated as it passes through the core. The attenuation of gamma radiation, mainly by Compton scattering, through a known sample thickness is proportional to the bulk density. The GRA densitometer has a spatial resolution of <1 cm. Because of this high spatial resolution, the quality of GRA data is highly dependent on the structural integrity of the sediment (i.e., the measurements are significantly affected by cracks, voids, biscuiting, etc.). The absolute values will be lower if the sediment does not completely fill the core liner (i.e., if a gap between the sediment and the core liner or cracks in the core exist). Bulk density can also be affected by vertical compaction during the collection of APC cores.

GRA precision is proportional to the square root of the counts measured, as gamma ray emission is subject to Poisson statistics. Measurements with the present system typically have count rates of 10,000 (dense rock) to 20,000 cps (soft mud). If measured for 4 s, the statistical error is therefore <40,000 ± 200, or 0.5% (i.e., the high flux of the ^{137}Cs source does not require excessive counting times. Calibration of the densitometer was performed using core liners filled with distilled water and aluminum blocks. GRA density measurement intervals on both the STMSL and WRMSL were 2.5 cm.

Magnetic susceptibility

Magnetic susceptibility is the degree to which a material can be magnetized in an external magnetic field.

Both the STMSL and WRMSL incorporate a Bartington (United Kingdom) MS2C meter. The MS2C meter in the STMSL had a coil with an internal diameter of 90 mm and an operating frequency of 565 Hz. The modified MS2C in the WRMSL had a coil with an internal diameter of 80 mm and ran at an operating frequency of 513 Hz. On both instruments, measurements were taken at intervals of 2.5 cm.

The SHMSL included a Bartington Instruments MS2E MSP, which is a high-resolution surface scanning sensor with an operating frequency of 2 kHz. This sensor integrates a volume of 10.5 mm × 3.8 mm × 4 mm, where 10.5 mm is the length perpendicular to the core axis, 3.8 mm is the width in the core axis, and 4 mm is the depth. Because the MS2E demands flush contact between the probe and the section-half surface, the archive halves were covered with clear plastic wrap to avoid contamination. Measurements were taken at 2.5 cm when time permitted; the interval was increased to 5 cm when required because of high core recovery rates.

Magnetic susceptibility from all three instruments is reported in instrument units. To obtain results in dimensionless SI units, the instrument units need to be multiplied by a geometric correction factor that is a function of the probe type, core diameter, and loop size (see **"Paleomagnetism"** for parameter examples). Because we are not measuring the core diameter, application of a correction factor has no benefit over reporting instrument units. If normalized magnetic susceptibility values are needed, the best method is to measure discrete samples with good accuracy and precision using a Kappabridge to calibrate the logs (see **"Paleomagnetism"** for shipboard Kappabridge measurements).

Compressional *P*-wave velocity

Compressional *P*-wave velocity is the distance an ultrasonic *P*-wave travels through a sample per unit time. *P*-wave velocity varies with material composition, porosity, and bulk density, as well as state of stress, temperature, and fabric or degree of fracturing. In soft sediment, velocity is also controlled by the degree of consolidation and lithification and the occurrence and abundance of free gas and gas hydrate. Together with bulk density, velocity data are used to calculate acoustic impedance and reflection coefficients in order to construct synthetic seismic profiles and to estimate the depth of specific seismic horizons.

The PWL system on the WRMSL transmits a 500 kHz *P*-wave pulse across the whole-round core section at a specified repetition rate. Pulser and receiver are mounted on a caliper-type device and are aligned so that wave propagation is perpendicular to the section's long axis. Core diameter is measured using a linear variable differential transducer. Torque applied by the actuator to clamp the pulser and receiver against the core liner ensures good acoustic contact.

The first arrival of the wave at the receiver is picked by signal processing software with 50 ns precision and assessed against coefficients derived during calibration. The precision of the velocity on standard materials (e.g., water and acrylic calibration standards) is ±20 m/s.

The PWC system on the SHMG also uses a caliper-type configuration for the pulser and receiver. Typically, two measurements were performed per section (at ~50 and 100 cm). The system uses Panametrics-NDT Microscan delay line transducers that transmit at 0.5 MHz. The user has the option to override the automated pulse arrival and, particularly in the case of a weak signal, pick the first arrival manually. The distance between transducers was measured with a built-in linear voltage displacement transformer (LDVT).

Calibration of both the PWL and the PWC systems was performed with a series of acrylic cylinders of varying thicknesses and a known *P*-wave velocity of 2750 ± 20 m/s. The determined system time delay from calibration was subtracted from the picked arrival time to give a traveltime of the *P*-wave through the sample. The thickness of the sample, corrected for liner thickness, was divided by the traveltime to calculate *P*-wave velocity in meters per second.

Natural gamma radiation

Gamma radiation in geological formations arise primarily from the decay of mineral-hosted uranium (U), thorium (Th), and potassium (K) isotopes. In general, high counts identify fine-grained deposits containing K-rich clay minerals and their absorbed U and Th atoms. The NGR data reveal stratigraphic details that aid in stratigraphic correlations and formation characterization and can be compared directly against downhole logs of NGR for core-log integration.

The NGRL designed and built at the TAMU IODP-USIO facility from 2006 to 2008 (Vasiliev et al., 2011) measures gamma rays emitted from whole-round core sections. The main NGR detector unit consists of 8 sodium iodide (NaI) scintillation detectors, spaced at ~20 cm intervals along the core axis, surrounding the lower half of the core section to be measured; 7 active shield plastic scintillation detectors; 22 photomultipliers; and passive lead shielding.

A measurement run generally consists of counting one position in each core section for 5 min for a total of 8 measurements per 150 cm section and a second position for another 5 min for another 8 measurements, yielding a depth resolution of one data point per ~10 cm.

Thermal conductivity

Thermal conductivity is the rate at which heat flows through a material and is dependent on chemical composition, porosity, density, and fabric of material (e.g., Jumikis, 1966). It is used in conjunction with downhole temperature measurements to calculate heat flow.

A TeKa (Germany) TK04 system measures and records the changes in temperature with time after an initial heating of a needle probe inserted into the whole-round section through a small hole drilled through the plastic core liner. The temperature of the superconductive probe has a linear relationship with the natural logarithm of the time after the initiation of heat. Core sections and needle probes were equilibrated together and subsequently measured in a Styrofoam sleeve to minimize the effect of rapid but small temperature changes introduced by air currents in the laboratory. The instrument internally measures drift and does not begin a heating run until sufficient thermal equilibrium is attained.

We attempted to conduct thermal conductivity measurements but were ultimately unsuccessful for all J-Anomaly Ridge sites and for SENR Site U1407. The instrument was placed in a shielded box to minimize external environmental effects. Although we obtained good results on an equilibrated standard and a core from Site U1402, we were unable to obtain stable temperature readings on cores from the sites listed above even after (in one case) the core was measured continually for 48 h. However, we successfully measured thermal conductivity in several core sections from Sites U1408–U1411.

Moisture and density

Procedure

Working section halves were sampled for MAD analysis using plastic syringes with a diameter of only slightly less than the diameter of the preweighed 16 mL Wheaton glass vials used to process and store the samples of ~10 cm^3 volume. In some cases, where sediment was too indurated to be sampled with a syringe, a spatula was used to take several pieces. Typically one sample per section (at ~35 cm from the top of the section) was collected.

First, the mass of wet samples was determined to a precision of 0.005 g using two Mettler Toledo electronic balances and a computer averaging system to compensate for the ship's motion. The samples were then heated in an oven at 105° ± 5°C for 24 h and allowed to cool in a desiccator. The mass of the dry sample was then determined with the same balance system.

Dry sample volume was determined using a six-celled, custom-configured Micromeritics AccuPyc 1330TC helium-displacement pycnometer system. The precision of each cell volume is 1% of the full-scale volume. Volume measurement was preceded by three purges of the sample chamber with helium warmed to ~28°C. Three measurement cycles were run for each sample. A reference volume (calibration sphere) was placed sequentially in one of the chambers to check for instrument drift and systematic error. The volumes of the numbered Wheaton vials were calculated before the cruise by multiplying each vial's mass against the average density of the vial glass.

The procedures for the determination of physical properties comply with the American Society for Testing and Materials (ASTM) designation (D) 2216 (ASTM International, 1990). The phase relationships and assumptions for the calculations of all MAD parameters are discussed by Blum (1997) and summarized below in **"Mass and volume calculation"** and **"Calculation of bulk properties."** The method applicable to saturated, fine-grained sediments is called "method C." Method C is based on the measurement of wet mass, dry mass, and volume. It is not reliable or adapted for coarse-grained sediments in which water can be easily lost during the sampling (e.g., in foraminifer sands often found at the top of the hole).

Mass and volume calculation

Wet mass (M_{wet}), dry mass (M_{dry}), and dry volume (V_{dry}) were measured in the laboratory. The mass ratio (rm) is a computational constant of 0.965 (i.e., 0.965 g of freshwater per 1 g of seawater). Salt precipitated in sediment pores during the drying process is included in the M_{dry} and V_{dry} values. The mass of the evaporated water (M_{water}) and salt (M_{salt}) in the sample are given by

$$M_{water} = M_{wet} - M_{dry} \text{ and}$$

$$M_{salt} = M_{water}\,[s/(1 - s)],$$

where s is the assumed saltwater salinity (0.035) corresponding to a pore water density (ρ_{pw}) of 1.024 g/cm^3 and a salt density (ρ_{salt}) of 2.22 g/cm^3. The corrected mass of pore water (M_{pw}), volume of pore water (V_{pw}), mass of solids excluding salt (M_{solid}), volume of salt (V_{salt}), volume of solids excluding salt (V_{solid}), and wet volume (V_{wet}) are

$$M_{pw} = (M_{wet} - M_{dry})/rm,$$

$$V_{pw} = M_{pw}/\rho_{pw},$$

$$M_{solid} = M_{wet} - M_{pw},$$

$$M_{salt} = M_{pw} - (M_{wet} - M_{dry}),$$

$$V_{salt} = M_{salt}/\rho_{salt},$$

$$V_{solid} = V_{dry} - V_{salt}, \text{ and}$$

$$V_{wet} = V_{solid} + V_{pw}.$$

Calculation of bulk properties

For all sediment samples, water content (w) is expressed as the ratio of mass of pore water to wet sediment (total) mass,

$$w = M_{pw}/M_{wet}.$$

Wet bulk density (ρ_{wet}), dry bulk density (ρ_{dry}), sediment grain density (ρ_{solid}), porosity (ϕ), and void ratio (VR) are calculated as

$$\rho_{wet} = M_{wet}/V_{wet},$$

$$\rho_{dry} = M_{solid}/V_{wet},$$

$$\rho_{solid} = M_{solid}/V_{solid},$$

$$\phi = V_{pw}/V_{wet}, \text{ and}$$

$$VR = V_{pw}/V_{solid}.$$

Color reflectance

Reflectance of visible light from the archive halves of sediment cores was measured using an Ocean Optics USB4000 spectrophotometer mounted on the automated SHMSL. Freshly split cores were covered with clear plastic wrap and placed on the SHMSL. Measurements were taken at 2.5 cm intervals when time permitted and at 5 cm intervals when the rate of core recovery required faster processing to provide a high-resolution stratigraphic record of color variation for visible wavelengths. Each measurement was recorded in 2 nm wide spectral bands from 400 to 900 nm.

Spurious measurements can result from small cracks, sediment disturbance caused by the drilling process, or plastic section dividers.

Additional detailed information about measurement and interpretation of spectral data can be found in Balsam et al. (1997, 1998) and Balsam and Damuth (2000).

Stratigraphic correlation

The scientific objectives of Expedition 342 required the recovery of complete stratigraphic sections; however, recovery of a continuous section from a single borehole is technically impossible. Despite 100% or more nominal recovery, core recovery gaps occur between successive APC and XCB cores (e.g., Ruddiman et al., 1987; Hagelberg et al., 1995; Lisiecki and Herbert, 2007). Tides, ship heave, core expansion, and coring deformation also prohibit complete recovery in a single hole. Luckily, tidal variations (calculated using OTPS software from **volkov.oce.orst.edu/tides/otps.html**) during the expedition were <0.8 m for all sites (Egbert and Erofeeve, 2002). However, several storms transpired during operations and occasional damaged core liners impeded depth corrections. Depth corrections were also affected by differences in mudline depths between adjacent holes (likely because of seafloor bedforms) and local variations in stratigraphic thicknesses. Construction of a complete stratigraphic section requires the construction of a composite depth scale for multiple holes and assembly of stratigraphic intervals from two or more holes cored at the same site into a spliced record. By offsetting the recovery depth of cores below seafloor between each hole, it is possible to maximize the probability that adjacent holes recover most core gaps within previous holes. Expedition 342 cored at least two holes at all sites in order to construct the splice where stratigraphic control and recovery allowed.

The Expedition 342 composite depth and splice construction methodology followed a number of previous ODP legs and IODP expeditions (e.g., Hagelberg et al., 1992; Curry, Shackleton, Richter, et al., 1995; Jansen, Raymo, Blum, et al., 1996; Lyle, Koizumi, Richter, et al., 1997; Wefer, Berger, Richter, et al., 1998; Gersonde, Hodell, Blum, 1999; Wang, Prell, Blum, et al., 2000; Lyle, Wilson, Janecek, et al., 2002; Mix, Tiedemann, Blum, et al., 2003; Zachos, Kroon, Blum, et al., 2004; Channell, Kanamatsu, Sato, Stein, Alvarez Zarikian, Malone, and the Expedition 303/306 Scientists, 2006; Pälike et al., 2009, 2012). After generating a composite depth scale, it is possible to produce a stratigraphically continuous and complete splice using representative intervals from multiple holes. Ideally, this spliced record does not include core recovery gaps or intervals with coring deformation.

Core composite depth scale

The goal of constructing a composite depth scale is to place coeval, laterally continuous stratigraphic features into a common frame of reference, which is achieved by shifting the depths of individual cores from the original CSF-A scale to the CCSF scale in order to maximize correlation between holes. In the composite depth scale, the rule is to shift the depths of individual cores by a constant amount (affine transformation). Core-by-core depth shifting does not permit corrections for expansion or contraction within cores. This method provides good first-order correlation between cores from different holes without adding more subjective, and potentially erroneous, interpretations and also preserves the "true" relationship between curated core sections and the depth scale.

The CCSF depth scale overcomes many of the inadequacies of the CSF-A depth scale. The CSF-A scale is unique to each hole and derives from the length that the drill string advanced. Between-hole variations in mbsf can occur because of ship heave (not compensated for in APC coring), tidal variations in sea level, and other sources of error. In contrast, the CCSF scale is built by using the uppermost sediment (mudline) in the first core from a given hole as the "anchor" in the composite depth scale. The mudline anchor core is the only one with equivalent depths on the CSF-A and CCSF scales. From this anchor, physical property data generated on cores (e.g., bulk density and magnetic susceptibility) allow correlation among holes. For each core, we added a constant depth offset to the mbsf depth that best aligned the physical property variations to equivalent cores in adjacent holes.

For Expedition 342, we primarily based the CCSF scale and the splice on stratigraphic correlation of data from the STMSL, WRMSL, SHMSL, and NGRL (see **"Physical properties"**). The measurement interval is 2.5 cm for the multisensor logger data and 10 cm for the NGRL data. We used STMSL magnetic susceptibility and GRA density only for preliminary stratigraphic correlation in Microsoft Excel with the goal of directing drilling operations to avoid between-core gaps in one hole becoming aligned with those in the hole being cored. Unfortunately, real-time correlation was not always possible because many of the drilled strata had very low magnetic susceptibility (<20 IU). In these cases, we made few "live" depth adjustments and interpreted the overlap between holes primarily based on the top depths of cores reported on the drill floor.

These preliminary susceptibility and GRA density data sets were subsequently replaced with data series collected on the WRMSL, which was used to measure all cores after they equilibrated to room temperature. We used WRMSL magnetic susceptibility and GRA bulk density as well as NGR, color reflectance, and the intensity of magnetization following 20 mT AF demagnetization to assign tie points between cores from adjacent holes. All of these measurements are described in **"Physical properties"** and **"Paleomagnetism."** We used additional data as appropriate, such as biozones and core images (see **"Biostratigraphy"** and **"Lithostratigraphy"**). Of all the shipboard data sets considered, we typically considered magnetic susceptibility our prime variable for sediments with >40 wt% calcium carbonate. In clay-dominated sediments, our choice of the prime variable depended on the signal-to-noise ratio of all data sets.

To generate the CCSF depth scale, we imported the raw stratigraphic data into Microsoft Excel and culled as necessary to remove anomalous data influenced by edge effects at section boundaries or by coring disturbance. We identified additional one-off outliers by eye and removed these from the record; however, all raw data (including outliers) are available through the LIMS database. We used plots of physical property data for all available holes to assess the stratigraphic continuity of the recovered sedimentary sequences and to add appropriate depth offsets between holes to build the CCSF depth scale and splice.

It is impossible to align all correlative features within cores without squeezing or stretching depth intervals. The appearance of apparently compressed or expanded intervals when comparing cores from different holes may reflect small-scale differences in sedimentation and/or distortion caused by the coring and archiving processes. The tops of APC cores are generally stretched and the bottoms are compressed, although this effect is lithology dependent. When there was only a small overlap between cores, we chose tentative ties rather than appending cores (which inserts arbitrarily large coring gaps).

The CCSF depth scale denotes the new, depth-shifted data. Each site chapter contains an affine table that summarizes the depth offsets of all cores. These tables are necessary for converting depth in mbsf to depths in mcd. The mcd depth for any point within a core equals the mbsf depth plus the cumulative offset.

Splicing

After depth shifting to align stratigraphic features, we built a splice from segments selected from multiple holes to form a complete record at each site. The splice includes core sections from adjacent holes such that coring gaps in one hole are filled with core intervals from an adjacent hole. The shipboard splice is a guide for core sampling for detailed depth-continuous paleoceanographic studies. A table and figure presented in each site chapter summarize the intervals from each hole used to construct the splice.

The choice of tie points (and hence of a splice) is partly a subjective exercise. Our method in the construction of each splice followed two key rules. First, where possible we avoided using the top and bottom ~50 cm of each core, where disturbance resulting from drilling artifacts (even if not apparent in physical property data) is most likely. Second, we attempted to incorporate those portions of the recovered core that are most representative of the overall stratigraphic section. Splice ties connect two points in two splice intervals at the same CCSF depth.

The length of the spliced section (on the CCSF scale) at a given site is typically 5%–15% greater than the length of the cored section in any one hole as indicated by the CSF-A scale. Reasons for this difference include sediment expansion resulting from elastic rebound, stretching during the coring process, gas expansion during the core recovery process, and curation practices, in which slurry commonly occurring at the tops of cores is curated as part of the core (e.g., Moran, 1997; Acton et al., 2001; Lisiecki and Herbert, 2007).

Ideally, the splice is continuous to the bottom of the deepest core recovered from the deepest hole. In practice, however, the splice is continuous until gaps align across all holes, the data quality no longer allows reliable correlations between holes, or not all holes were drilled to equivalent depths. It is not possible to directly tie cores below an interval with aligned core gaps between multiple holes into the overlying and continuous CCSF scale. However, it is sometimes possible to correlate cores from two or more holes below the base of the continuous CCSF scale in order to create a floating splice. In this case, we add the average differential offset of the last several cores to the floating cores.

Changes in CSF-A depth scales

The mbsf depths assigned to WRMSL measurements in the LIMS database are not always the same as the mbsf depths used in the construction of the splice table. Below-seafloor depths associated with measurement on the WRMSL derive from liner length, measured when the cores are cut into sections on the catwalk. At some later time, typically 10–36 h after measurement on the WRMSL, core sections are split and analyzed further (see **"Core handling and anal-**

ysis"). At this time, section lengths are sometimes remeasured because the sections may have expanded during the period between the whole-round core logging measurements and the section-half analyses, or shifted during splitting and handling. If section length has changed by >1 cm, the database record is updated, which means the CSF-A depth scale is slightly changed. General database queries return depths based on the last updated section length, and the depths associated with the WRMSL data at the time of measurement are therefore not identical to the final depths assigned to a given interval in the database. For each site, we updated our final composite section and splice using the final section lengths. This means that, for a particular stratigraphic feature, mbsf depths used in the splice may not align precisely with mbsf depths reported for WRMSL measurements.

Drift deposits

The drilling of drift deposits complicated the construction of shipboard composite sections for some of the sites on Expedition 342. Side-scan sonar images of the seafloor near the *Titanic* wreckage location (proximal to the Expedition 342 sites) show clear erosional scours. This indicates persistent deep western-boundary currents, coming from the Gulf of Mexico, the Labrador Sea, and/or the East Greenland Sea, have influenced deposition and erosion on a local scale. These currents generally follow the bathymetric contours of continental margins but can interact with topographies (e.g., ridges, seamounts, etc.) that focus and redirect flow, resulting in spatially variable current energies. The Deep Western Boundary Current redistributes deep-sea sediments to form drift deposits (mainly biogenic mud, clay, silt, and rarely sand) or to erode preexisting sediments. The thickness of surficial Pleistocene deposits varied, in some cases, by a few meters—easily enough to distort hole-to-hole correlations based upon mudline depths. As a result of local erosion/deposition of sediment on the seafloor, the mudline is typically not the strongest anchor for our composite depth scales. In contrast, prominent color and/or sediment compositional changes as deep as 10 m below the sediment surface provide the strongest anchors between holes at a given site.

Evidence from studies of the seafloor and shallow subsurface using seismic reflection profiles indicates that some drifts are characterized by lateral discontinuity because of the effects of changes in local sedimentation and erosion through time. For example, fields of migrating mudwaves (as high as 50 m with wavelengths of hundreds of meters to kilometers) can develop in drift systems (Wynn and Masson, 2008). The seismic character of the drifts targeted in this expedition is generally uniform, sometimes transparent, but subtle reflector geometries suggestive of mudwaves are also visible. The lateral discontinuity of sedimentation rates (including hiatuses) might add further complexity.

Shore-based splice construction

In addition to the possibility of lateral discontinuities between holes at a single site, the homogeneity of drift sediments typically corresponds to low variability in shipboard physical properties. The absence of clear, prominent, meter-scale features in physical properties and the low magnetic susceptibility in clay-rich lithologies impeded shipboard stratigraphic correlation and splice construction for some sites, particularly Sites U1404 and U1405. As a result, we devised a strategy to revise tentative splice tie points using data collected from XRF analyses at TAMU in College Station, Texas, and at the Scripps Institution of Oceanography in La Jolla, California.

XRF elemental measurements are generally assumed to show a larger signal-to-noise ratio compared to shipboard physical property measurements and have been used to improve shipboard composite depth scale and splice construction (Röhl and Abrams, 2000; Evans et al., 2004; Westerhold et al., 2007, 2008; Westerhold and Röhl, 2009). XRF scanning allows the construction of high-resolution, nondestructive estimates of elemental composition from the surfaces of split core sections (Jansen et al., 1998; Richter et al., 2006). Constraints imposed by time and cost caused us to prioritize collection of XRF measurements across intervals where shipboard correlation was ambiguous and across intervals with heavy sampling requests. Individual site chapters include descriptions of the XRF scanning strategy for each site as well as the extent to which the collected data were used to revise the composite depth scale and splice as of January 2013.

Downhole logging

Downhole logs are used to determine physical, chemical, and structural properties of the formation penetrated by a borehole. The data are rapidly collected, continuous with depth, and measured in situ. The sampling (vertical sampling intervals ranging from 2.5 mm to 15 cm) is intermediate between laboratory measurements on core samples and geophysical surveys. Downhole logs are useful in calibrating the interpretation of geophysical survey data (e.g., through the use of synthetic seismograms) and provide a necessary link for the integrated understanding of physical properties on all scales.

Downhole logs can be interpreted in terms of the stratigraphy, lithology, mineralogy, and geochemical composition of the penetrated formation. Where core recovery is incomplete or disturbed, log data may help to characterize the borehole section. Where core recovery is good, log and core data complement one another and may be interpreted jointly.

Downhole logs also provide information on the condition, shape, and size of the borehole and on possible deformations induced by drilling or formation stress.

Unfortunately, logging attempts were aborted at the first site because of technical problems with the logging tool, and time did not become available for logging during the remainder of the cruise. For detailed descriptions of the logging methodologies, see other IODP *Proceedings* volumes.

In situ temperature measurements

In situ temperature measurements were made with the advanced piston corer temperature tool (APCT-3) in Holes U1405A and U1408A. The APCT-3 fits directly into the coring shoe of the APC and consists of a battery pack, data logger, and platinum resistance-temperature device calibrated over a temperature range from 0° to 30°C. Before entering the borehole, the tool is first stopped at the mudline for 5 min to thermally equilibrate with bottom water and give a bottom water temperature. After the APC penetrated the sediment, it was held in place for 10 min as the APCT-3 recorded the temperature of the cutting shoe every second. When the APC is plunged into the formation, frictional heating creates an instantaneous rise in the temperature profile. This heat gradually dissipates into the surrounding sediments as the temperature at the APCT-3 equilibrates toward the temperature of the sediments.

The equilibrium temperature of the sediments was estimated by applying a mathematical heat-conduction model to the temperature decay record (Horai and Von Herzen, 1985). The synthetic thermal decay curve for the APCT-3 is a function of the geometry and thermal properties of the probe and the sediment (Bullard, 1954; Horai and Von Herzen, 1985). The equilibrium temperature must be estimated by applying a fitting procedure (TPFIT by Martin Heesemann, 2006). However, when ship heave pulls the APC up from full penetration, the temperature equilibration curve will be disturbed and temperature determination is more difficult. The nominal accuracy of the APCT-3 temperature measurements is ±0.05°C with a total error of 0.1°–0.5°C.

The APCT-3 temperature data were combined with measurements of thermal conductivity (see **"Physical properties"**) obtained from whole-core samples to obtain heat flow values. Heat flow was calculated according to the Bullard method, to be consistent with the synthesis of ODP heat flow data by Pribnow et al. (2000).

Acknowledgment

We thank Heiko Pälike for site-specific tide calculations.

References

Acton, G.D., Borton, C.J., and the Leg 178 Shipboard Scientific Party, 2001. Palmer Deep composite depth scales for Leg 178 Sites 1098 and 1099. *In* Barker, P.F., Camerlenghi, A., Acton, G.D., and Ramsay, A.T.S. (Eds.), *Proc. ODP, Sci. Results,* 178: College Station, TX (Ocean Drilling Program), 1–35. **doi:10.2973/odp.proc.sr.178.202.2001**

Agnini, C., Fornaciari, E., Raffi, I., Rio, D., Röhl, U., and Westerhold, T., 2007. High-resolution nannofossil biochronology of middle Paleocene to early Eocene at ODP Site 1262: implications for calcareous nannoplankton evolution. *Mar. Micropaleontol.,* 64(3–4):215–248. **doi:10.1016/j.marmicro.2007.05.003**

Agnini, C., Muttoni, G., Kent, D.V., and Rio, D., 2006. Eocene biostratigraphy and magnetic stratigraphy from Possagno, Italy: the calcareous nannofossil response to climate variability. *Earth Planet Sci. Lett.,* 241(3–4):815–830. **doi:10.1016/j.epsl.2005.11.005**

Aguirre, E., and Pasini, G., 1985. The Pliocene–Pleistocene boundary. *Episodes,* 8:11–120.

ASTM International, 1990. Standard method for laboratory determination of water (moisture) content of soil and rock (Standard D2216–90). In *Annual Book of ASTM Standards for Soil and Rock* (Vol. 04.08): Philadelphia (Am. Soc. Testing Mater.). [revision of D2216-63, D2216-80]

Backman, J., 1986. Late Paleocene to middle Eocene calcareous nannofossil biochronology from the Shatsky Rise, Walvis Ridge and Italy. *Palaeogeogr., Palaeoclimatol., Palaeoecol.,* 57(1):43–59. **doi:10.1016/0031-0182(86)90005-2**

Backman, J., 1987. Quantitative calcareous nannofossil biochronology of middle Eocene through early Oligocene sediment from DSDP Sites 522 and 523. *Abh. Geol. Bundesanst. (Austria),* 39:21–31.

Balsam, W.L., and Damuth, J.E., 2000. Further investigations of shipboard vs. shore-based spectral data: implications for interpreting Leg 164 sediment composition. *In* Paull, C.K., Matsumoto, R., Wallace, P., and Dillon, W.P. (Eds.), *Proc. ODP, Sci. Results,* 164: College Station, TX (Ocean Drilling Program), 313–324. **doi:10.2973/odp.proc.sr.164.222.2000**

Balsam, W.L., Damuth, J.E., and Schneider, R.R., 1997. Comparison of shipboard vs. shore-based spectral data from Amazon Fan cores: implications for interpreting

sediment composition. *In* Flood, R.D., Piper, D.J.W., Klaus, A., and Peterson, L.C. (Eds.), *Proc. ODP, Sci. Results,* 155: College Station, TX (Ocean Drilling Program), 193–215. **doi:10.2973/odp.proc.sr.155.210.1997**

Balsam, W.L., Deaton, B.C., and Damuth, J.E., 1998. The effects of water content on diffuse reflectance spectrophotometry studies of deep-sea sediment cores. *Mar. Geol.,* 149(1–4):177–189. **doi:10.1016/S0025-3227(98)00033-4**

Berggren, W.A., Hilgen, F.J., Langereis, C.G., Kent, D.V., Obradovich, J.D., Raffi, I., Raymo, M.E., and Shackelton, N.J., 1995. Late Neogene chronology: new perspectives in high-resolution stratigraphy. *Geol. Soc. Am. Bull.,* 107(11):1272–1287. **doi:10.1130/0016-7606(1995)107<1272:LNCNPI>2.3.CO;2**

Berggren, W.A., Kent, D.V., Swisher, C.C., III, and Aubry, M.-P., 1995. A revised Cenozoic geochronology and chronostratigraphy. *In* Berggren, W.A., Kent, D.V., Aubry, M.-P., and Hardenbol, J. (Eds.), *Geochronology, Time Scales and Global Stratigraphic Correlation*. Spec. Publ.—SEPM (Soc. Sediment. Geol.), 54:129–212. **doi:10.2110/pec.95.04.0129**

Berggren, W.A., and Pearson, P.N., 2005. A revised tropical to subtropical Paleogene planktonic foraminiferal zonation. *J. Foraminiferal Res.,* 35(4):279–298. **doi:10.2113/35.4.279**

Blaj, T., Backman, J., and Raffi, I., 2009. Late Eocene to Oligocene preservation history and biochronology of calcareous nannofossils from paleo-equatorial Pacific Ocean sediments. *Riv. Ital. Paleontol. Stratigr.,* 115(1):67–84.

Blow, W.H., 1979. *The Cainozoic* Globigerinida: *A Study of the Morphology, Taxonomy, Evolutionary Relationships and the Stratigraphical Distribution of Some* Globigerinida *(mainly* Globigerinacea): Leiden (E.J. Brill).

Blum, P., 1997. Physical properties handbook: a guide to the shipboard measurement of physical properties of deep-sea cores. *ODP Tech. Note,* 26. **doi:10.2973/odp.tn.26.1997**

Bolli, H.M., and Saunders, J.B., 1985. Oligocene to Holocene low latitude planktic foraminifera. *In* Bolli, H.M., Saunders, J.B., and Perch-Nielsen, K. (Eds.), *Plankton Stratigraphy* (Vol. 1): *Planktic Foraminifera, Calcareous Nannofossils and Calpionellids:* Cambridge (Cambridge Univ. Press), 155–262.

Bown, P.R. (Ed.), 1998. *Calcareous Nannofossil Biostratigraphy:* London (Chapman and Hall).

Bown, P.R., 2005. Palaeogene calcareous microfossils from the Kilwa and Lindi areas of coastal Tanzania (Tanzania Drilling Project 2003–4). *J. Nannoplankton Res.,* 27(1):21–95.

Bullard, E.C., 1954. The flow of heat through the floor of the Atlantic Ocean. *Proc. R. Soc. London, Ser. A,* 222(1150):408–429. **doi:10.1098/rspa.1954.0085**

Burnett, J.A., 1998. Upper Cretaceous. *In* Bown, P.R. (Ed.), *Calcareous Nannofossil Biostratigraphy:* Dordrecht, The Netherlands (Kluwer Academic Publ.), 132–199.

Cande, S.C., and Kent, D.V., 1995. Revised calibration of the geomagnetic polarity timescale for the Late Cretaceous and Cenozoic. *J. Geophys. Res., [Solid Earth],* 100(B4):6093–6095. **doi:10.1029/94JB03098**

Caron, M., 1985. Cretaceous planktic foraminifera. *In* Bolli, H.M., Saunders, J.B., and Perch-Nielsen, K. (Eds.), *Plankton Stratigraphy:* Cambridge (Cambridge Univ. Press), 17–86.

Chaisson, W.P., and Pearson, P.N., 1997. Planktonic foraminifer biostratigraphy at Site 925: middle Miocene–Pleistocene. *In* Shackleton, N.J., Curry, W.B., Richter, C., and Bralower, T.J. (Eds.), *Proc. ODP, Sci. Results,* 154: College Station, TX (Ocean Drilling Program), 3–31. **doi:10.2973/odp.proc.sr.154.104.1997**

Channell, J.E.T., Kanamatsu, T., Sato, T., Stein, R., Alvarez Zarikian, C.A., Malone, M.J., and the Expedition 303/306 Scientists, 2006. *Proc. IODP,* 303/306: College Station, TX (Integrated Ocean Drilling Program Management International, Inc.). **doi:10.2204/iodp.proc.303306.2006**

Coccioni, R., Marsili, A., Montanari, A., Bellanca, A., Neri, R., Bice, D.M., Brinkhuis, H., Church, N., Macalady, A., McDaniel, A., Deino, A., Lirer, F., Sprovieri, M., Maiorano, P., Monechi, S., Nini, C., Nocchi, M., Pross, J., Rochette, P., Sagnotti, L., Tateo, F., Touchard, Y., Van Simaeys, S., and Williams, G.L., 2008. Integrated stratigraphy of the Oligocene pelagic sequence in the Umbria-Marche Basin (northeastern Apennines, Italy): a potential Global Stratotype Section and Point (GSSP) for the Rupelian/Chattian boundary. *Geol. Soc. Am. Bull.,* 120(3–4):487–511. **doi:10.1130/B25988.1**

Curry, W.B., Shackleton, N.J., Richter, C., et al., 1995. *Proc. ODP, Init. Repts.,* 154: College Station, TX (Ocean Drilling Program). **doi:10.2973/odp.proc.ir.154.1995**

Dallanave, E., Agnini, C., Muttoni, G., and Rio, D., 2012. Paleocene magneto-biostratigraphy and climate-controlled rock magnetism from the Belluno Basin, Tethys Ocean, Italy. *Palaeogeogr., Palaeoclimatol., Palaeoecol.,* 337–338:130–142. **doi:10.1016/j.palaeo.2012.04.007**

Dickens, G.R., Koelling, M., Smith, D.C., Schneiders, L., and the IODP Expedition 302 Scientists, 2007. Rhizon sampling of pore waters on scientific drilling expeditions: an example from the IODP Expedition 302, Arctic Coring Expedition (ACEX). *Sci. Drill.,* 4: 22–25. **doi:10.2204/iodp.sd.4.08.2007**

Egbert, G.D., and Erofeeva, S.Y., 2002. Efficient inverse modeling of barotropic ocean tides. *J. Atmos. Oceanic Technol.,* 19(2):183–204. **doi:10.1175/1520-0426(2002)019<0183:EIMOBO>2.0.CO;2**

Ellis, D.V., and Singer, J.M., 2007. *Well Logging for Earth Scientists* (2nd ed.): New York (Elsevier).

Evans, H.B., 1965. GRAPE—a device for continuous determination of material density and porosity. *Trans. SPWLA Annu. Logging Symp.:* 6(2):B1–B25.

Expedition 320/321 Scientists, 2010. Site U1333. *In* Pälike, H., Lyle, M., Nishi, H., Raffi, I., Gamage, K., Klaus, A., and the Expedition 320/321 Scientists, *Proc. IODP,* 320/321: Tokyo (Integrated Ocean Drilling Program Management International, Inc.). **doi:10.2204/iodp.proc.320321.105.2010**

Fornaciari, E., Agnini, C., Catanzariti, R., Rio, D., Bolla, E.M., and Valvasoni, E., 2010. Mid-latitude calcareous

nannofossil biostratigraphy and biochronology across the middle to late Eocene transition. *Stratigraphy,* 7(4):229–264. **http://www.micropress.org/micropen2/articles/1/7/94581_articles_article_file_1717.pdf**

Funakawa, S., Nishi, H., Moore, T.C., and Nigrini, C.A., 2006. Radiolarian faunal turnover and paleoceanographic change around Eocene/Oligocene boundary in the central equatorial Pacific, ODP Leg 199, Holes 1218A, 1219A, and 1220A. *Palaeogeogr., Palaeoclimatol., Palaeoecol.,* 230(3–4):183–203. **doi:10.1016/j.palaeo.2005.07.014**

Gee, J.S., Tauxe, L., and Constable, C., 2008. AMSSpin: a LabVIEW program for measuring the anisotropy of magnetic susceptibility with the Kappabridge KLY-4S. *Geochem., Geophys., Geosyst.,* 9(8):Q08Y02. **doi:10.1029/2008GC001976**

Gersonde, R., Hodell, D.A., Blum, P., et al., 1999. *Proc. ODP, Init. Repts.,* 177: College Station, TX (Ocean Drilling Program). **doi:10.2973/odp.proc.ir.177.1999**

Gieskes, J.M., Gamo, T., and Brumsack, H., 1991. Chemical methods for interstitial water analysis aboard *JOIDES Resolution*. *ODP Tech. Note,* 15. **doi:10.2973/odp.tn.15.1991**

Goldberg, D., 1997. The role of downhole measurements in marine geology and geophysics. *Rev. Geophys.,* 35(3):315–342. **doi:10.1029/97RG00221**

Gradstein, F.M., Ogg, J.G., Schmitz, M.D., and Ogg, G.M. (Eds)., 2012. *The Geological Time Scale 2012:* Amsterdam (Elsevier).

Gradstein, F.M., Ogg, J.G., and Smith, A. (Eds.), 2004. *A Geologic Time Scale 2004:* Cambridge (Cambridge Univ. Press). **doi:10.2277/0521786738**

Hagelberg, T., Shackleton, N., Pisias, N., and Shipboard Scientific Party, 1992. Development of composite depth sections for Sites 844 through 854. *In* Mayer, L., Pisias, N., Janecek, T., et al., *Proc. ODP, Init. Repts.,* 138: College Station, TX (Ocean Drilling Program), 67–77. **doi:10.2973/odp.proc.ir.138.105.1992**

Hagelberg, T.K., Pisias, N.G., Shackleton, N.J., Mix, A.C., and Harris, S., 1995. Refinement of a high-resolution, continuous sedimentary section for studying equatorial Pacific Ocean paleoceanography, Leg 138. *In* Pisias, N.G., Mayer, L.A., Janecek, T.R., Palmer-Julson, A., and van Andel, T.H. (Eds.), *Proc. ODP, Sci Results,* 138: College Station, TX (Ocean Drilling Program), 31–46. **doi:10.2973/odp.proc.sr.138.103.1995**

Hardenbol, J., Thierry, J., Farley, M.B., Jacquin, T., de Graciansky, P.-C., and Vail, P.R., 1998. Mesozoic and Cenozoic sequence chronostratigraphic framework of European basins. *In* de Graciansky, P.-C., Hardenbol, J., Jacquin, T., and Vail, P.R. (Eds.), *Mesozoic and Cenozoic Sequence Stratigraphy of European Basins*. Spec. Publ.—SEPM (Soc. Sediment. Geol.), 60:3–13. **doi:10.2110/pec.98.02.0003**

Hayward, B.W., 2002. Late Pliocene to middle Pleistocene extinctions of deep-sea benthic foraminifera ("*Stilostomella* extinction") in the southwest Pacific. *J. Foraminiferal Res.,* 32(3):274–307. **doi:10.2113/32.3.274**

Heesemann, M., Villinger, H., Fisher, A.T., Tréhu, A.M., and White, S., 2006. Data report: testing and deployment of the new APCT-3 tool to determine in situ temperatures while piston coring. *In* Riedel, M., Collett, T.S., Malone, M.J., and the Expedition 311 Scientists. *Proc. IODP,* 311: Washington, DC (Integrated Ocean Drilling Program Management International, Inc.). **doi:10.2204/iodp.proc.311.108.2006**

Hicks, J.F., Obradovich, J.D., and Tauxe, L., 1995. A new calibration point for the Late Cretaceous time scale: the $^{40}Ar/^{39}Ar$ isotopic age of the C33r/C33n geomagnetic reversal from the Judith River Formation (Upper Cretaceous), Elk Basin, Wyoming, USA. *J. Geol.,* 103(3):243–256. **doi:10.1086/629744**

Holbourn, A.E., and Henderson, A.S., 2002. Re-illustration and revised taxonomy for selected deep-sea benthic foraminifers. *Paleontol. Electron.,* 4(2):1–34. **http://palaeo-electronica.org/2001_2/foram/issue2_01.htm**

Hollis, C.J., 1997. *Cretaceous-Paleocene Radiolaria of Eastern Marlborough, New Zealand*. Inst. Geol. Nucl. Sci. Monogr., 17.

Hollis, C.J., 2002. Biostratigraphy and paleoceanographic significance of Paleocene radiolarians from offshore eastern New Zealand. *Mar. Micropaleontol.,* 46:265–316. **doi:10.1016/S0377-8398(02)00066-X**

Horai, K., and Von Herzen, R.P., 1985. Measurement of heat flow on Leg 86 of the Deep Sea Drilling Project. *In* Heath, G.R., Burckle, L.H., et al., *Init. Repts. DSDP,* 86: Washington, DC (U.S. Govt. Printing Office), 759–777. **doi:10.2973/dsdp.proc.86.135.1985**

Husson, D., Galbrun, B., Laskar, J., Hinnov, L.A., Thibault, N., Gardin, S., and Lockair, R.E., 2011. Astronomical calibration of the Maastrichtian (Late Cretaceous). *Earth Planet. Sci. Lett.,* 305(3–4):328–340. **doi:10.1016/j.epsl.2011.03.008**

Jansen, E., Raymo, M.E., Blum, P., et al., 1996. *Proc. ODP, Init. Repts.,* 162: College Station, TX (Ocean Drilling Program). **doi:10.2973/odp.proc.ir.162.1996**

Jansen, J.H.F., Van der Gaast, S.J., Koster, B., and Vaars, A.J., 1998. CORTEX, a shipboard XRF-scanner for element analyses in split sediment cores. *Mar. Geol.,* 151(1–4):143–153. **doi:10.1016/S0025-3227(98)00074-7**

Jenkins, D.G., 1971. New Zealand Cenozoic planktonic foraminifera. *N. Z. Geol. Surv. Paleontol. Bull.,* 42.

Jones, R.W., 1994. *The Challenger Foraminifera:* New York (Oxford).

Jovane, L., Florindo, F., Coccioni, R., Dinarès-Turell, J., Marsili, A., Monechi, S., Roberts, A.P., and Sprovieri, M., 2007. The middle Eocene climatic optimum event in the Contessa Highway section, Umbrian Appennines, Italy. *Geol. Soc. Am. Bull.,* 119(3–4):413–427. **doi:10.1130/B25917.1**

Jumikis, A.R., 1966. *Thermal Soil Mechanics:* New Brunswick, N.J. (Rutgers Univ. Press).

Kamikuri, S., Moore, T.C., Ogane, K., Suzuki, N., Pälike, H., and Nishi, H., 2012. Early Eocene to early Miocene radiolarian biostratigraphy for the low-latitude Pacific Ocean. *Stratigraphy,* 9(1):77–108. **http://www.micropress.org/micropen2/articles/1/7/27546_articles_article_file_1785.pdf**

Kaminski, M.A., Geroch, S., and Kaminski, D.G. (Eds.), 1993. *The Origins of Applied Micropalaeontology: The School of Jozef Grzybowski*. Spec. Publ.– Grzybowski Found., 1.

Katz, M.E., and Miller, K.G., 1991. Early Paleogene benthic foraminiferal assemblages and stable isotopes in the Southern Ocean. *In* Ciesielski, P.F., Kristoffersen, Y., et al., *Proc. ODP, Sci. Results,* 114: College Station, TX (Ocean Drilling Program), 481–512. **doi:10.2973/odp.proc.sr.114.147.1991**

Keene, J.B., 1975. Cherts and porcellanites from the North Pacific DSDP, Leg 32. *In* Larson, R.L., Moberly, R., et al. *Init. Repts. DSDP,* 32: Washington, DC (U.S. Govt. Printing Office), 429–507. **doi:10.2973/dsdp.proc.32.114.1975**

Kennett, J.P., and Srinivasan, M.S., 1983. *Neogene Planktonic Foraminifera: A Phylogenetic Atlas:* Stroudsburg, PA (Hutchinson Ross).

Lazarus, D., Spencer-Cervato, C., Pianka-Biolzi, M., Beckmann, J.P., von Salis, K., Hilbrecht, H., and Thierstein, H., 1995. Revised chronology of Neogene DSDP holes from the world ocean. *ODP Tech. Note,* 24. **doi:10.2973/odp.tn.24.1995**

Leckie, R.M., 1984. Mid-Cretaceous planktonic foraminiferal biostratigraphy off central Morocco, Deep Sea Drilling Project Leg 79, Sites 545 and 547. *In* Hinz, K., Winterer, E.L., et al., *Init. Repts. DSDP,* 79: Washington, DC (U.S. Govt. Printing Office), 579–620. **doi:10.2973/dsdp.proc.79.122.1984**

Lisiecki, L.E., and Herbert, T.D., 2007. Automated composite depth scale construction and estimates of sediment core extension. *Paleoceanography,* 22(4):PA4213. **doi:10.1029/2006PA001401**

Loeblich, A.R., and Tappan, H., 1988. *Foraminiferal Genera and Their Classification* (Vol. 2): New York (Van Nostrand Reinhold Co.).

Lourens, L., Hilgen, F., Shackleton, N.J., Laskar, J., and Wilson, D., 2004. The Neogene period. *In* Gradstein, F.M., Ogg, J.G., and Smith, A. (Eds.), *A Geologic Time Scale 2004:* Cambridge (Cambridge Univ. Press), 409–440.

Lovell, M.A., Harvey, P.K., Brewer, T.S., Williams, C., Jackson, P.D., and Williamson, G., 1998. Application of FMS images in the Ocean Drilling Program: an overview. *In* Cramp, A., MacLeod, C.J., Lee, S.V., and Jones, E.J.W. (Eds.), *Geological Evolution of Ocean Basins: Results from the Ocean Drilling Program.* Geol. Soc. Spec. Publ., 131(1):287–303. **doi:10.1144/GSL.SP.1998.131.01.18**

Lyle, M., Koizumi, I., Richter, C., et al., 1997. *Proc. ODP, Init. Repts.,* 167: College Station, TX (Ocean Drilling Program). **doi:10.2973/odp.proc.ir.167.1997**

Lyle, M., Wilson, P.A., Janecek, T.R., et al., 2002. *Proc. ODP, Init. Repts.,* 199: College Station, TX (Ocean Drilling Program). **doi:10.2973/odp.proc.ir.199.2002**

Manheim, F.T., and Sayles, F.L., 1974. Composition and origin of interstitial waters of marine sediments, based on deep sea drill cores. *In* Goldberg, E.D. (Ed.), *The Sea* (Vol. 5): *Marine Chemistry: The Sedimentary Cycle:* New York (Wiley), 527–568.

Martini, E., 1971. Standard Tertiary and Quaternary calcareous nannoplankton zonation. *In* Farinacci, A. (Ed.), *Proc. Second Planktonic Conf. Roma 1970:* Rome (Ed. Tecnosci.), 2:739–785.

Mazzullo, J.M., Meyer, A., and Kidd, R.B., 1988. New sediment classification scheme for the Ocean Drilling Program. *In* Mazzullo, J.M., and Graham, A.G. (Eds.), *Handbook for shipboard sedimentologists*. ODP Tech. Note, 8:45–67. **doi:10.2973/odp.tn.8.1988**

Miller, K.G., and Katz, M.E., 1987. Oligocene to Miocene benthic foraminiferal and abyssal circulation changes in the North Atlantic. *Micropaleontology,* 33(2):97–149. **doi:10.2307/1485489**

Mix, A.C., Tiedemann, R., Blum, P., et al., 2003. *Proc. ODP, Init. Repts.,* 202: College Station, TX (Ocean Drilling Program). **doi:10.2973/odp.proc.ir.202.2003**

Moran, K., 1997. Elastic property corrections applied to Leg 154 sediment, Ceara Rise. *In* Shackleton, N.J., Curry, W.B., Richter, C., and Bralower, T.J. (Eds.), *Proc. ODP, Sci. Results,* 154: College Station, TX (Ocean Drilling Program), 151–155. **doi:10.2973/odp.proc.sr.154.132.1997**

Munsell Color Company, Inc., 1994. *Munsell Soil Color Chart* (Revised ed.): Newburgh, MD (Munsell Color).

Murray, R.W., Miller, D.J., and Kryc, K.A., 2000. Analysis of major and trace elements in rocks, sediments, and interstitial waters by inductively coupled plasma–atomic emission spectrometry (ICP-AES). *ODP Tech. Note,* 29. **doi:10.2973/odp.tn.29.2000**

Nederbragt, A.J., 1990. Biostratigraphy and paleoceanographic potential of the Cretaceous planktic foraminifera Heterohelicidae [Ph.D. thesis]. Centrale Huisdrukkerij Vrije Univ., Amsterdam.

Nigrini, C., and Lombari, G., 1984. *A Guide to Miocene Radiolaria*. Spec. Publ.—Cushman Found. Foraminiferal Res., 22.

Nigrini, C., and Sanfilippo, A., 2001. Cenozoic radiolarian stratigraphy for low and middle latitudes with descriptions of biomarkers and stratigraphically useful species. *ODP Tech. Note,* 27. **doi:10.2973/odp.tn.27.2001**

Nigrini, C., Sanfilippo, A., and Moore, T.C., Jr., 2006. Cenozoic radiolarian biostratigraphy: a magnetobiostratigraphic chronology of Cenozoic sequences from ODP Sites 1218, 1219, and 1220, equatorial Pacific. *In* Wilson, P.A., Lyle, M., and Firth, J.V. (Eds.), *Proc. ODP, Sci. Results,* 199: College Station, TX (Ocean Drilling Program), 1–76. **doi:10.2973/odp.proc.sr.199.225.2006**

Nishimura, A., 1992. Paleocene radiolarian biostratigraphy in the northwest Atlantic at Site 384, Leg 43, of the Deep Sea Drilling Project. *Micropaleontology,* 38(4):317–362. **doi:10.2307/1485764**

Nomura, R., 1995. Paleogene to Neogene deep-sea paleoceanography in the eastern Indian Ocean: benthic foraminifera from ODP Sites 747, 757 and 758. *Micropaleontology,* 41(3):251–290. **doi:10.2307/1485862**

Norris, R.D., Wilson, P.A., Blum, P., Fehr, A., Agnini, C., Bornemann, A., Boulila, S., Bown, P.R., Cournede, C., Friedrich, O., Ghosh, A.K., Hollis, C.J., Hull, P.M., Jo, K., Junium, C.K., Kaneko, M., Liebrand, D., Lippert, P.C., Liu, Z., Matsui, H., Moriya, K., Nishi, H., Opdyke, B.N., Penman, D., Romans, B., Scher, H.D., Sexton, P., Takagi, H., Turner, S.K., Whiteside, J.H., Yamaguchi, T., and

Yamamoto, Y., 2014. Site U1403. *In* Norris, R.D., Wilson, P.A., Blum, P., and the Expedition 342 Scientists, *Proc. IODP,* 342: College Station, TX (Integrated Ocean Drilling Program). **doi:10.2204/iodp.proc.342.104.2014**

Ogg, J.G., Ogg, G., and Gradstein, F.M., 2008. *The Concise Geologic Time Scale*: Cambridge (Cambridge Univ. Press). **http://www.cambridge.org/catalogue/catalogue.asp?isbn=9780521898492**

Olsson, R.K., Hemleben, C., Berggren, W.A., and Huber, B.T. (Eds.), 1999. Atlas of Paleocene planktonic foraminifera. *Smithson. Contrib. Paleobiol.,* 85. **http://hdl.handle.net/10088/2001**

Pälike, H., Lyle, M., Nishi, H., Raffi, I., Gamage, K., Klaus, A., and the Expedition 320/321 Scientists, 2010. *Proc. IODP,* 320/321: Tokyo (Integrated Ocean Drilling Program Management International, Inc.). **doi:10.2204/iodp.proc.320321.2010**

Pälike, H., Norris, R.D., Herrle, J.O., Wilson, P.A., Coxall, H.K., Lear, C.H., Shackleton, N.J., Tripati, A.K., and Wade, B.S., 2006. The heartbeat of the Oligocene climate system. *Science,* 314(5807):1894–1898. **doi:10.1126/science.1133822**

Pearson, P.N., 1995. Planktonic foraminifer biostratigraphy and the development of pelagic caps on guyots in the Marshall Islands group. *In* Haggerty, J.A., Premoli Silva, I., Rack, F., and McNutt, M.K. (Eds.), *Proc. ODP, Sci. Results,* 144: College Station, TX (Ocean Drilling Program), 21–59. **doi:10.2973/odp.proc.sr.144.013.1995**

Pearson, P.N., Olsson, R.K., Huber, B.T., Hemleben, C., and Berggren, W.A. (Eds.), 2006. *Atlas of Eocene Planktonic Foraminifera.* Spec. Publ.—Cushman Found. Foraminiferal Res., 41.

Perch-Nielsen, K., 1985a. Cenozoic calcareous nannofossils. *In* Bolli, H.M., Saunders, J.B., and Perch-Nielsen, K. (Eds.), *Plankton Stratigraphy:* Cambridge (Cambridge Univ. Press), 427–554.

Perch-Nielsen, K., 1985b. Mesozoic calcareous nannofossils. *In* Bolli, H.M., Saunders, J.B., and Perch-Nielsen, K. (Eds.), *Plankton Stratigraphy:* Cambridge (Cambridge Univ. Press), 329–426.

Pessagno, E.A., Jr., 1976. Radiolarian zonation and stratigraphy of the Upper Cretaceous portion of the Great Valley Sequence, California Coast Ranges. *Micropaleontology, Spec. Publ.,* 2:1–95.

Pflum, C.E., and Frerichs, W.E., 1976. Gulf of Mexico Deep-Water Foraminifers. *Spec. Publ.—Cushman Found. Foraminiferal Res.,* 14:1–122.

Pimmel, A., and Claypool, G., 2001. Introduction to shipboard organic geochemistry on the *JOIDES Resolution. ODP Tech. Note,* 30. **doi:10.2973/odp.tn.30.2001**

Pribnow, D., Kinoshita, M., and Stein, C., 2000. *Thermal Data Collection and Heat Flow Recalculations for Ocean Drilling Program Legs 101–180:* Hanover, Germany (Inst. Joint Geosci. Res., Inst. Geowiss. Gemeinschaftsauf. [GGA]). **http://www-odp.tamu.edu/publications/heatflow/ODPReprt.pdf**

Raffi, I., Backman, J., Fornaciari, E., Pälike, H., Rio, D., Lourens, L., and Hilgen, F., 2006. A review of calcareous nannofossil astrobiochronology encompassing the past 25 million years. *Quat. Sci. Rev.,* 25(23–24):3113–3137. **doi:10.1016/j.quascirev.2006.07.007**

Raffi, I., Backman, J., and Pälike, H., 2005. Changes in calcareous nannofossil assemblages across the Paleocene/Eocene transition from the paleo-equatorial Pacific Ocean. *Palaeogeogr., Palaecoclimatol., Palaeoecol.,* 226(1–2):93–126. **doi:10.1016/j.palaeo.2005.05.006**

Rider, M.H., 1996. *The Geological Interpretation of Well Logs* (2nd ed.): Caithness (Whittles Publ.).

Robaszynski, F., and Caron, M., 1979. Atlas de foraminifères planctoniques du Cretace moyen (Mer Boreale et Tethys) (Vols. 1 and 2). *Cah. Micropaleontol.*

Robaszynski, F., Caron, M., Gonzales-Donoso, J.-M., Wonders, A.A.H., and the European Working Group on Planktonic Foraminifera, 1984. Atlas of Late Cretaceous globotruncanids. *Rev. Micropaleontol.,* 26:145–305.

Ruddiman, W.F., Cameron, D., and Clement, B.M., 1987. Sediment disturbance and correlation of offset holes drilled with the hydraulic piston corer: Leg 94. *In* Ruddiman, W.F., Kidd, R.B., Thomas, E., et al., *Init. Repts. DSDP,* 94: Washington, DC (U.S. Govt. Printing Office), 615–634. **doi:10.2973/dsdp.proc.94.111.1987**

Sanfilippo, A., and Blome, C.D., 2001. Biostratigraphic implications of mid-latitude Paleocene–Eocene radiolarian faunas from Hole 1051A, ODP Leg 171B, Blake Nose, western North Atlantic. *In* Kroon, D., Norris, R.D., and Klaus, A. (Eds.), *Western North Atlantic Palaeogene and Cretaceous Palaeoceanography.* Geol. Soc. Spec. Publ., 183(1):l85–224. **doi:10.1144/GSL.SP.2001.183.01.10**

Sanfilippo, A., and Nigrini, C., 1998. Code numbers for Cenozoic low latitude radiolarian biostratigraphic zones and GPTS conversion tables. *Mar. Micropaleontol.,* 33(1–2):109–117, 121–156. **doi:10.1016/S0377-8398(97)00030-3**

Sanfilippo, A., and Riedel, W.R., 1985. Cretaceous radiolaria. *In* Bolli, H.M., Saunders, J.B., and Perch-Nielsen, K. (Eds.), *Plankton Stratigraphy:* Cambridge (Cambridge Univ. Press), 573–630.

Sanfilippo, A., Westberg-Smith, M.J., and Riedel, W.R., 1985. Cenozoic Radiolaria. *In* Bolli, H.M., Saunders, J.B., and Perch-Nielsen, K. (Eds.), *Plankton Stratigraphy* (Vol. 2): *Radiolaria, Diatoms, Silicoflagellates, Dinoflagellates, and Ichthyoliths:* Cambridge (Cambridge Univ. Press), 631–712.

Schlumberger, 1989. *Log Interpretation Principles/Applications:* Houston (Schlumberger Educ. Serv.), SMP–7017.

Schlumberger, 1994. *IPL Integrated Porosity Lithology:* Houston (Schlumberger Wireline Testing), SMP-9270.

Scott, G.H., Bishop, S., and Burt, B.J., 1990. Guide to some Neogene Globotalids (Foraminiferida) from New Zealand. *N. Z. Geol. Surv. Paleontol. Bull.,* 61:1–135.

Serra, O., 1984. *Fundamentals of Well-Log Interpretation* (Vol. 1): *The Acquisition of Logging Data:* Amsterdam (Elsevier).

Serra, O., 1986. *Fundamentals of Well-Log Interpretation* (Vol. 2): *The Interpretation of Logging Data.* Amsterdam (Elsevier).

Serra, O., 1989. *Formation MicroScanner Image Interpretation:* Houston (Schlumberger Educ. Serv.), SMP-7028.

Sliter, W.V., 1989. Biostratigraphic zonation for Cretaceous planktonic foraminifers examined in thin section. *J. Foraminiferal Res.,* 19(1):1–19. **doi:10.2113/gsjfr.19.1.1**

Spezzaferri, S., 1994. Planktonic foraminiferal biostratigraphy and taxonomy of the Oligocene and lower Miocene in the oceanic record: an overview. *Palaeontographica Ital.,* 81:1–187.

Tauxe, L., 2010. *Essentials of Paleomagnetism:* La Jolla, California (Univ. California Press). **http://www.ucpress.edu/book.php?isbn=9780520260313**

Thibault, N., Husson, D., Harlou, R., Gardin, S., Galbrun, B., Huret, E., Minoletti, F., 2012. Astronomical calibration of upper Campanian–Maastrichtian carbon isotope events and calcareous plankton biostratigraphy in the Indian Ocean (ODP Hole 762C): implication for the age of the Campanian–Maastrichtian boundary. *Palaeogeogr., Palaeoclimatol., Paleoecol.,* 337–338:52–71. **doi:10.1016/j.palaeo.2012.03.027**

Thomas, E., 1990. Late Cretaceous through Neogene deep-sea benthic foraminifers (Maud Rise, Weddell Sea, Antarctica). *In* Barker, P.F., Kennett, J.P., et al., *Proc. ODP, Sci. Results,* 113: College Station, TX (Ocean Drilling Program), 571–594. **doi:10.2973/odp.proc.sr.113.123.1990**

Tjalsma, R.C., and Lohmann, G.P., 1983. Paleocene–Eocene bathyal and abyssal benthic foraminifera from the Atlantic Ocean. *Micropaleontology, Spec. Publ.,* 4.

Toumarkine, M., and Luterbacher, H., 1985. Paleocene and Eocene planktic foraminifera. *In* Bolli, H.M., Saunders, J.B., and Perch-Nielsen, K. (Eds.), *Plankton Stratigraphy:* Cambridge (Cambridge Univ. Press), 87–154.

van Morkhoven, F.P.C.M., Berggren, W.A., and Edwards, A.S., 1986. *Cenozoic Cosmopolitan Deep-Water Benthic Foraminifera*. Bull. Cent. Rech. Explor.—Prod. Elf-Aquitaine, 11.

Vasiliev, M.A., Blum, P., Chubarian, G., Olsen, R., Bennight, C., Cobine, T., Fackler, D., Hastedt, M., Houpt, D., Mateo, Z., and Vasilieva, Y.B., 2011. A new natural gamma radiation measurement system for marine sediment and rock analysis. *J. Appl. Geophys.,* 75:455–463. **doi:10.1016/j.jappgeo.2011.08.008**

Villa, G., Fioroni, C., Pea, L., Bohaty, S., and Persico, D., 2008. Middle Eocene–late Oligocene climate variability: calcareous nannofossil response at Kerguelen Plateau, Site 748. *Mar. Micropaleontol.,* 69(2):173–192. **doi:10.1016/j.marmicro.2008.07.006**

Wade, B.S., Pearson, P.N., Berggren, W.A., and Pälike, H., 2011. Review and revision of Cenozoic tropical planktonic foraminiferal biostratigraphy and calibration to the geomagnetic polarity and astronomical time scale. *Earth-Sci. Rev.,* 104(1–3):111–142. **doi:10.1016/j.earscirev.2010.09.003**

Wang, P., Prell, W.L., Blum, P., et al., 2000. *Proc. ODP, Init. Repts.,* 184: College Station, TX (Ocean Drilling Program). **doi:10.2973/odp.proc.ir.184.2000**

Wefer, G., Berger, W.H., and Richter, C., et al., 1998. *Proc. ODP, Init. Repts.,* 175: College Station, TX (Ocean Drilling Program). **doi:10.2973/odp.proc.ir.175.1998**

Wentworth, C.K., 1922. A scale of grade and class terms for clastic sediments. *J. Geol.,* 30(5):377–392. **doi:10.1086/622910**

Wynn, R.B., and Masson, D.G., 2008. Sediment waves and bedforms. *Dev. Sedimentol.,* 60:289–300. **doi:10.1016/S0070-4571(08)10015-2**

Zachos, J.C., Kroon, D., Blum, P., et al., 2004. *Proc. ODP, Init. Repts.,* 208: College Station, TX (Ocean Drilling Program. **doi:10.2973/odp.proc.ir.208.2004**

Publication: 3 March 2014
MS 342-102

Figure F1. Example of the DESClogik interface for recording visual core description data, Expedition 342. A similar interface is also used for the recording of smear slide data.

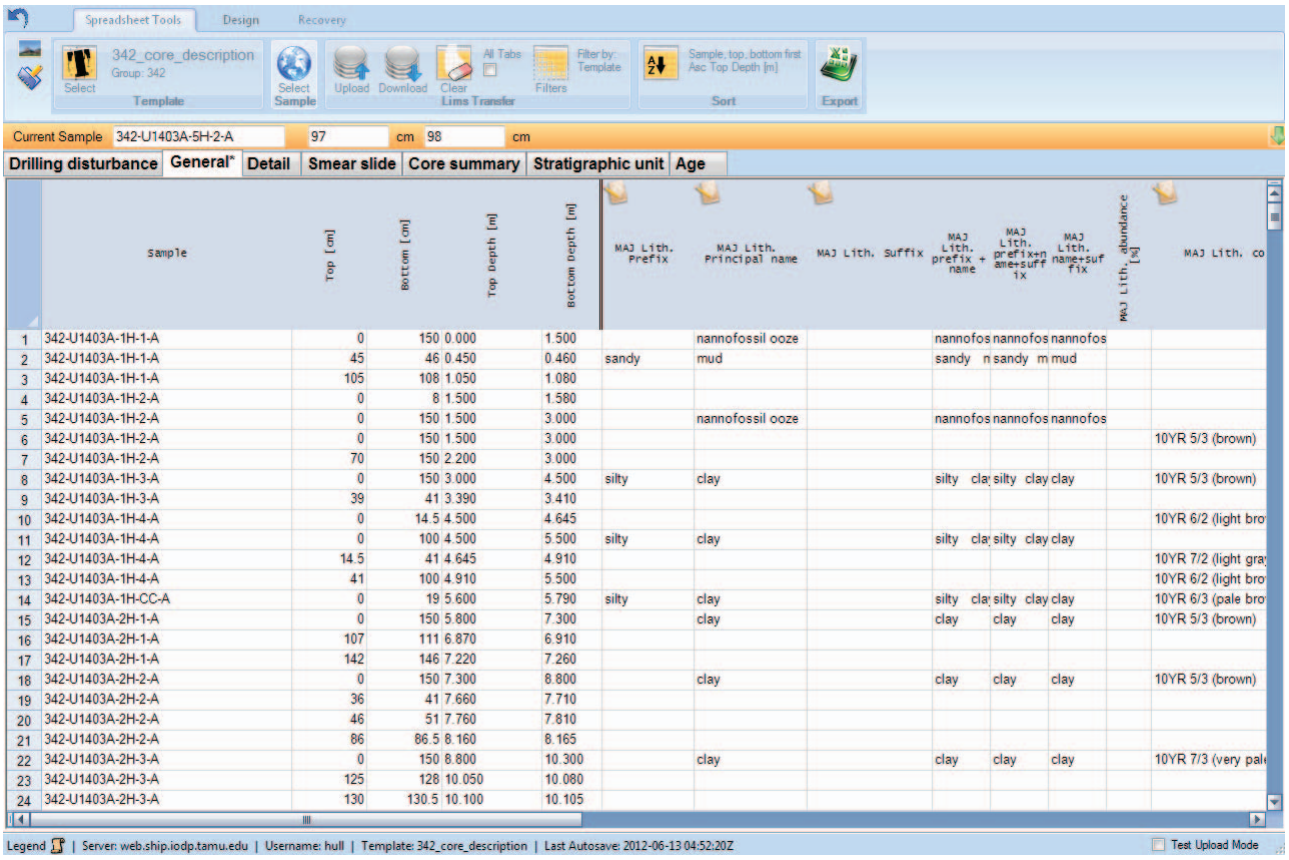

	Sample	Top [cm]	Bottom [cm]	Top Depth [m]	Bottom Depth [m]	MAJ Lith. Prefix	MAJ Lith. Principal name	MAJ Lith. Suffix	MAJ Lith. prefix + name	MAJ Lith. prefix+name+suffix	MAJ Lith. name+suffix	MAJ Lith. abundance [%]	MAJ Lith. co
1	342-U1403A-1H-1-A	0	150	0.000	1.500		nannofossil ooze		nannofos	nannofos	nannofos		
2	342-U1403A-1H-1-A	45	46	0.450	0.460	sandy	mud		sandy n	sandy m	mud		
3	342-U1403A-1H-1-A	105	108	1.050	1.080								
4	342-U1403A-1H-2-A	0	8	1.500	1.580								
5	342-U1403A-1H-2-A	0	150	1.500	3.000		nannofossil ooze		nannofos	nannofos	nannofos		
6	342-U1403A-1H-2-A	0	150	1.500	3.000								10YR 5/3 (brown)
7	342-U1403A-1H-2-A	70	150	2.200	3.000								
8	342-U1403A-1H-3-A	0	150	3.000	4.500	silty	clay		silty cla	silty clay	clay		10YR 5/3 (brown)
9	342-U1403A-1H-3-A	39	41	3.390	3.410								
10	342-U1403A-1H-4-A	0	14.5	4.500	4.645								10YR 6/2 (light bro
11	342-U1403A-1H-4-A	0	100	4.500	5.500	silty	clay		silty cla	silty clay	clay		
12	342-U1403A-1H-4-A	14.5	41	4.645	4.910								10YR 7/2 (light gra
13	342-U1403A-1H-4-A	41	100	4.910	5.500								10YR 6/2 (light bro
14	342-U1403A-1H-CC-A	0	19	5.600	5.790	silty	clay		silty cla	silty clay	clay		10YR 6/3 (pale bro
15	342-U1403A-2H-1-A	0	150	5.800	7.300		clay		clay	clay	clay		10YR 5/3 (brown)
16	342-U1403A-2H-1-A	107	111	6.870	6.910								
17	342-U1403A-2H-1-A	142	146	7.220	7.260								
18	342-U1403A-2H-2-A	0	150	7.300	8.800		clay		clay	clay	clay		10YR 5/3 (brown)
19	342-U1403A-2H-2-A	36	41	7.660	7.710								
20	342-U1403A-2H-2-A	46	51	7.760	7.810								
21	342-U1403A-2H-2-A	86	86.5	8.160	8.165								
22	342-U1403A-2H-3-A	0	150	8.800	10.300		clay		clay	clay	clay		10YR 7/3 (very pal
23	342-U1403A-2H-3-A	125	128	10.050	10.080								
24	342-U1403A-2H-3-A	130	130.5	10.100	10.105								

Figure F2. Example of the visual core description "barrel sheet" that compiles initial lithologic data taken from core description and smear slide analyses and preliminary physical property data, Expedition 342.

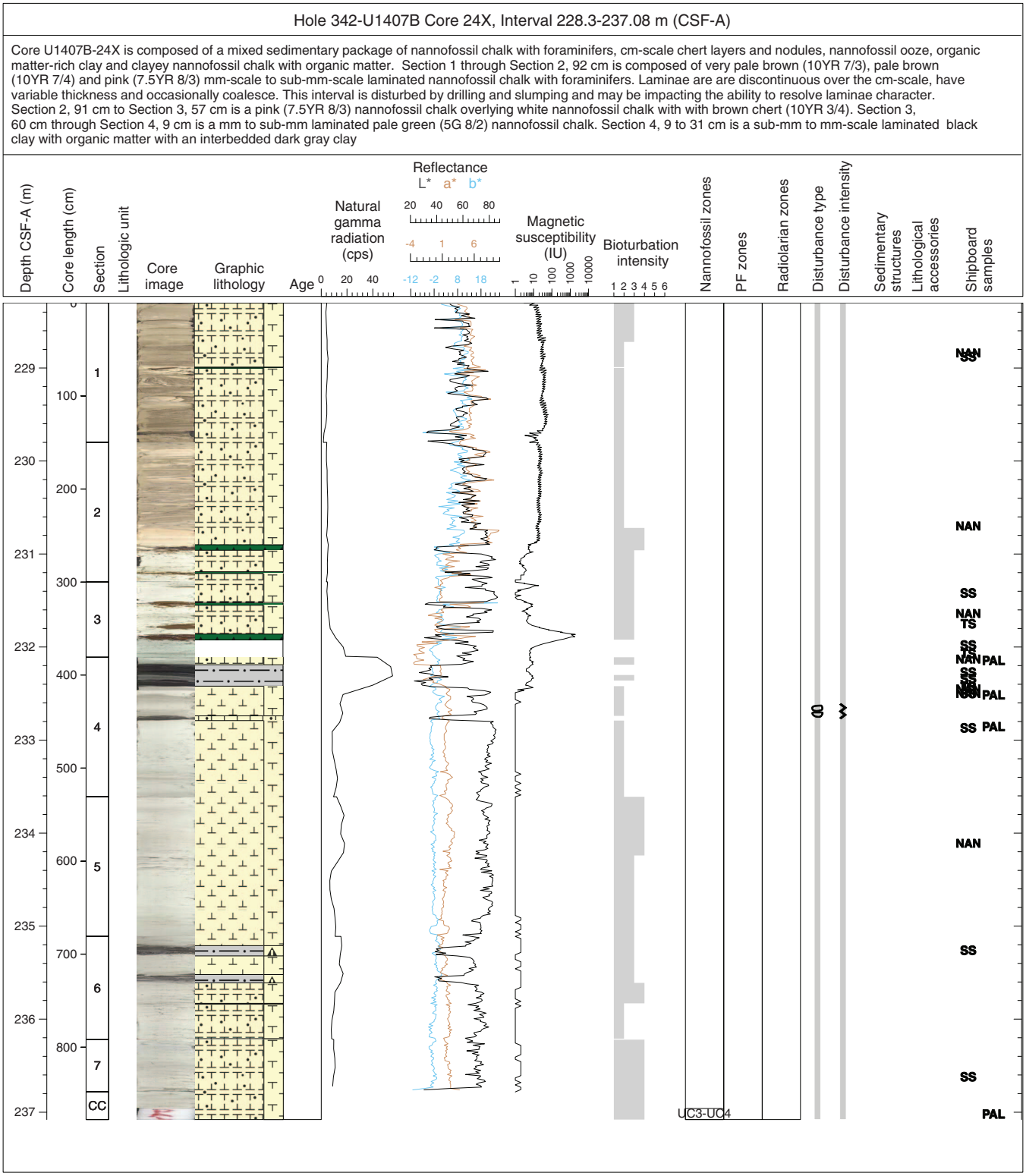

Figure F3. Key of symbols used on visual core description sheets and graphic logs, Expedition 342. **A.** Lithology symbols. (Continued on next page.)

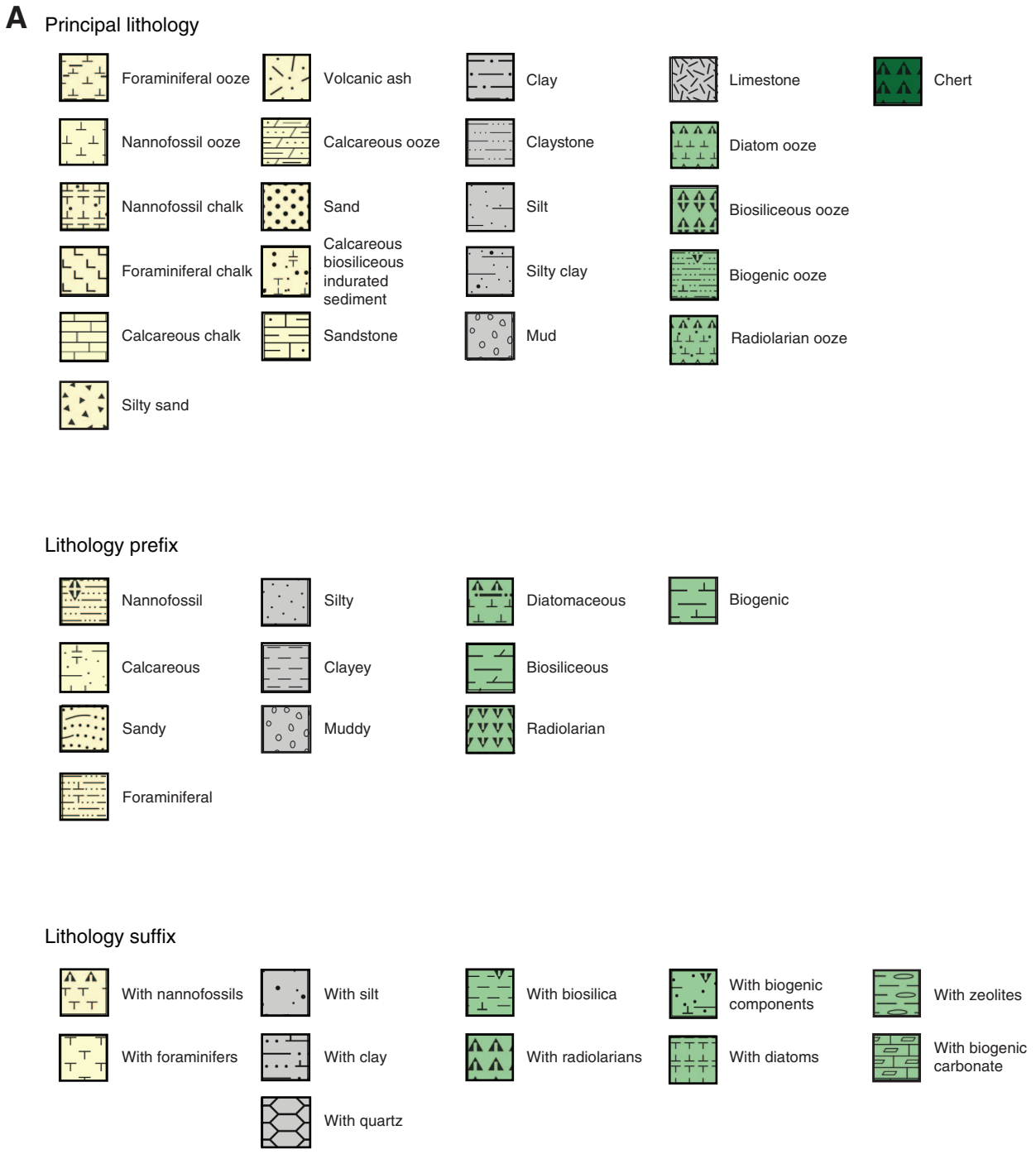

Figure F3 (continued). B. Other symbols.

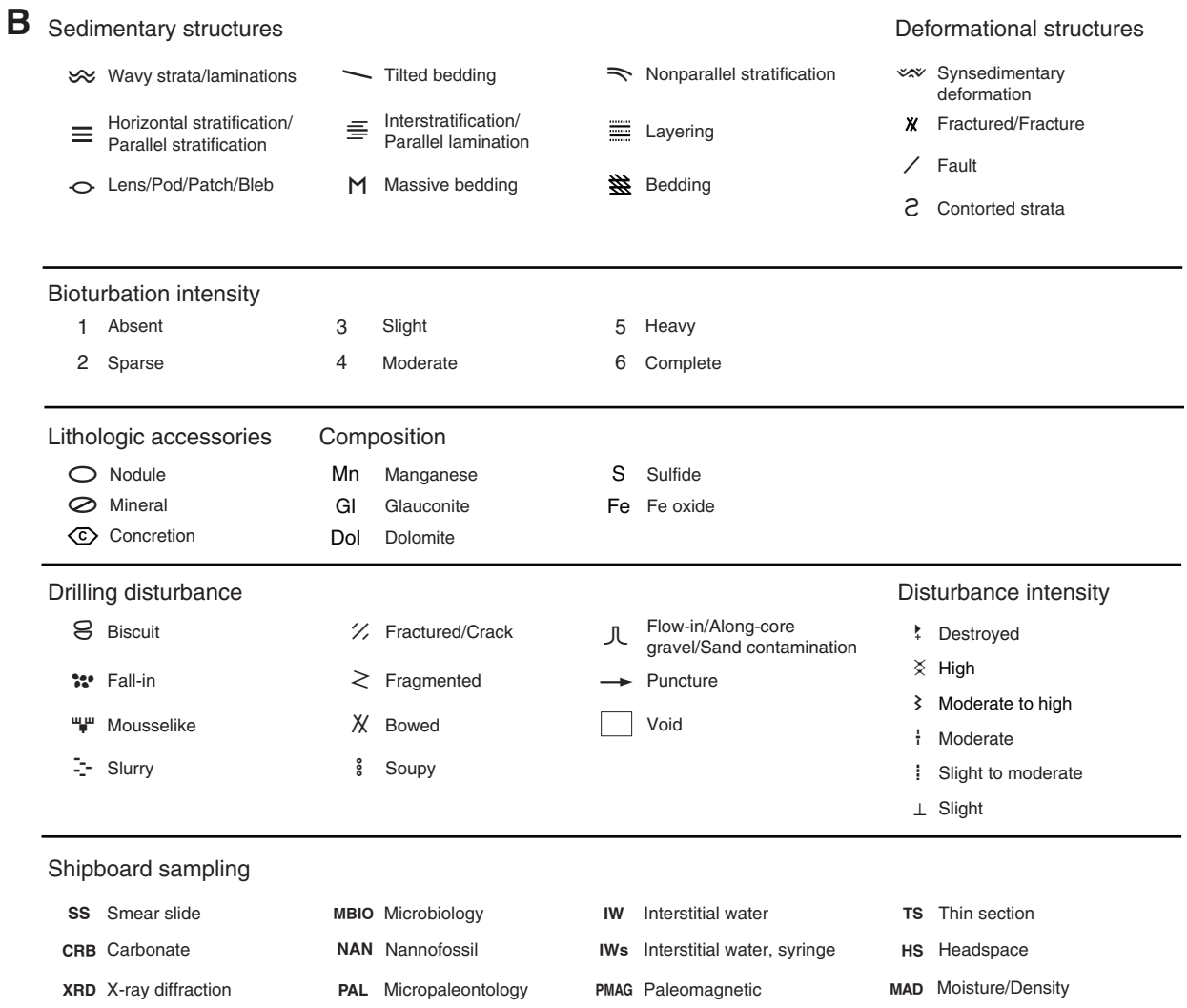

Figure F4. Lithology ternary diagram utilized for the assignment of lithology names, Expedition 342.

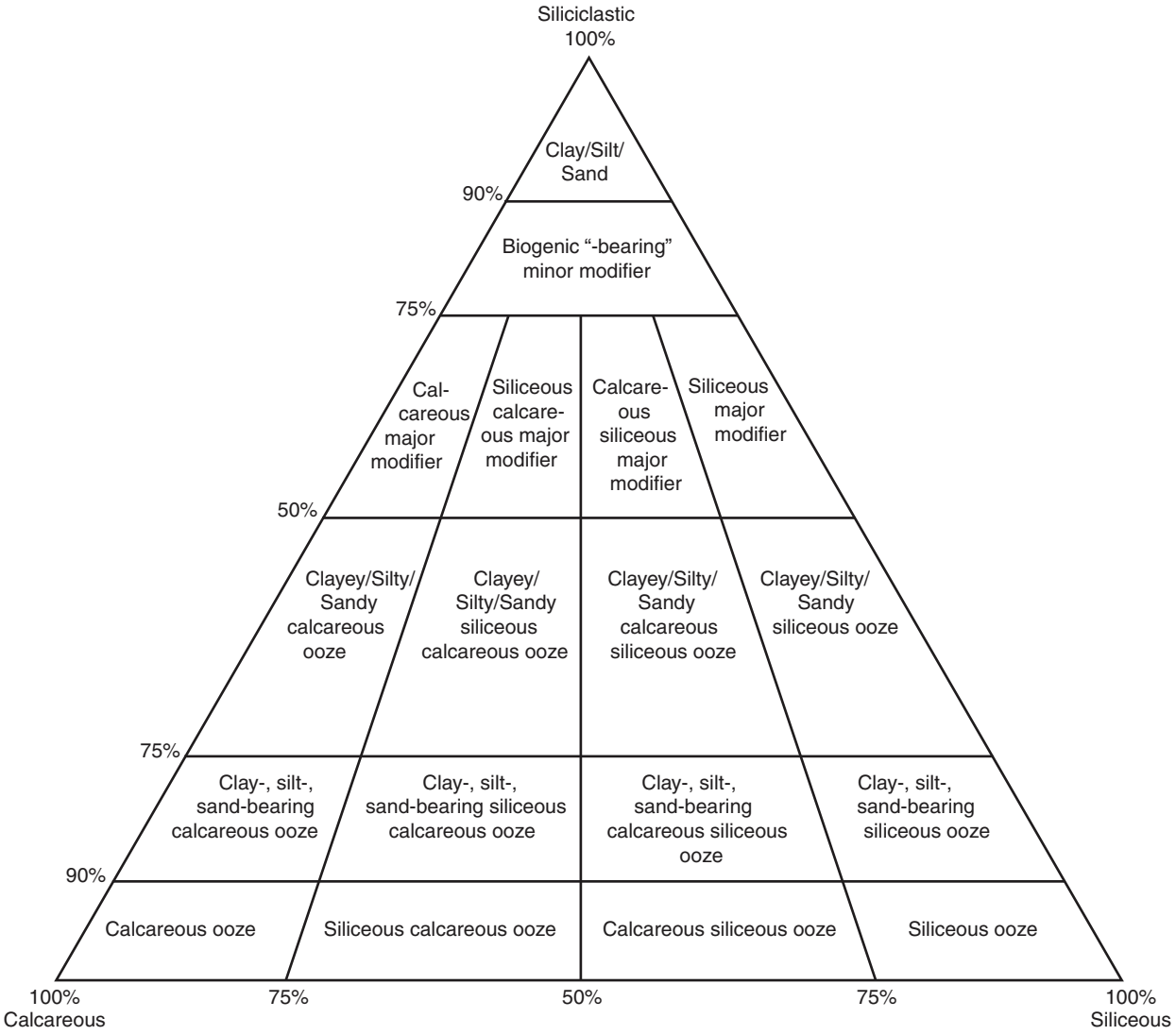

Figure F5. Timescales used during Expedition 342 with calcareous nannofossil, planktonic foraminifer, and radiolarian zones and datums through the 0–85 Ma interval. B = base, T = top, Tc = top common, Ta = top of acme, Bc = base common, Br = base reentrance, X = abundance cross-over in nannofossils or coiling change in planktonic foraminifers. **A.** 0–12 Ma. (Continued on next five pages.)

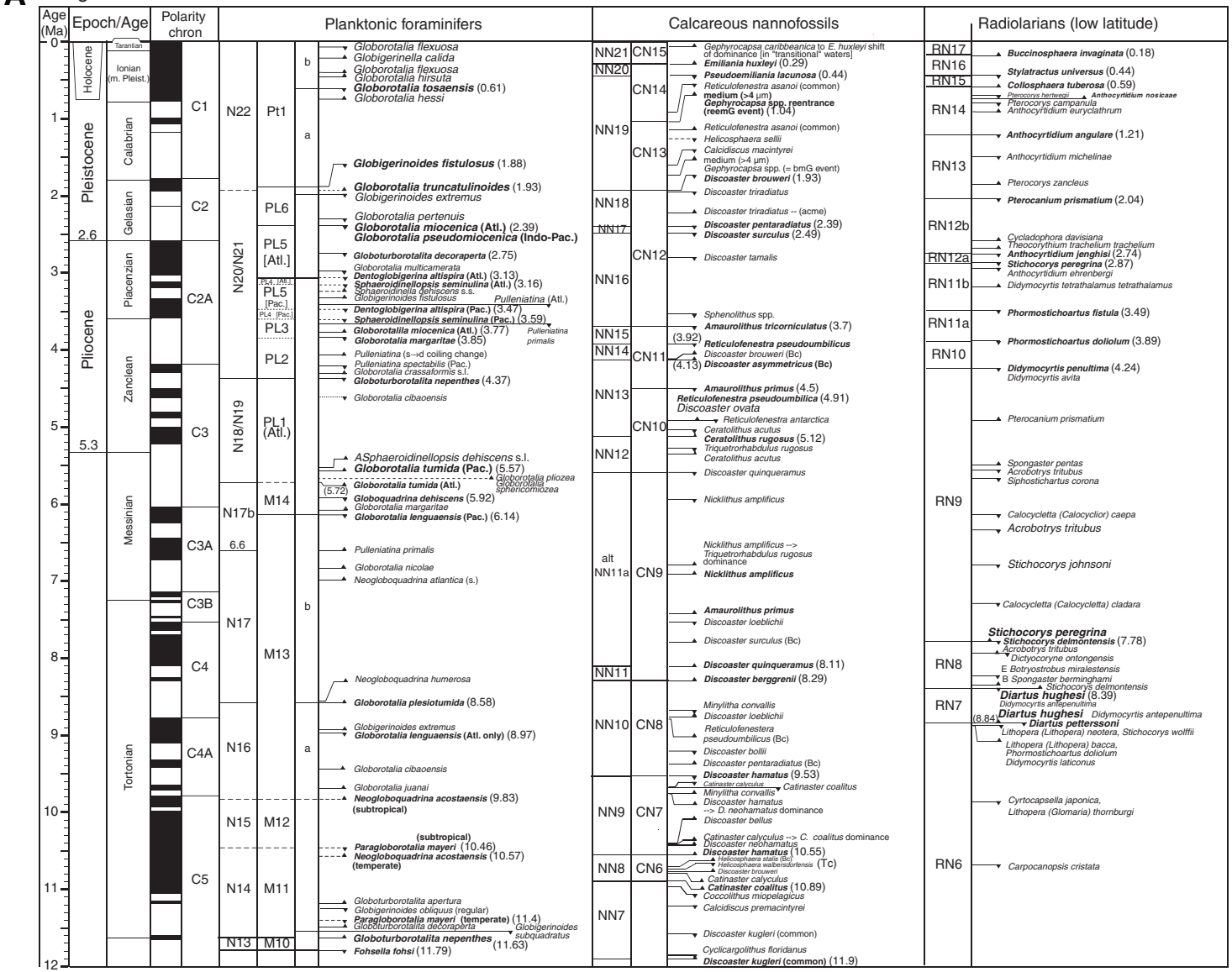

Figure F5 (continued). B. 12–24 Ma. (Continued on next page.)

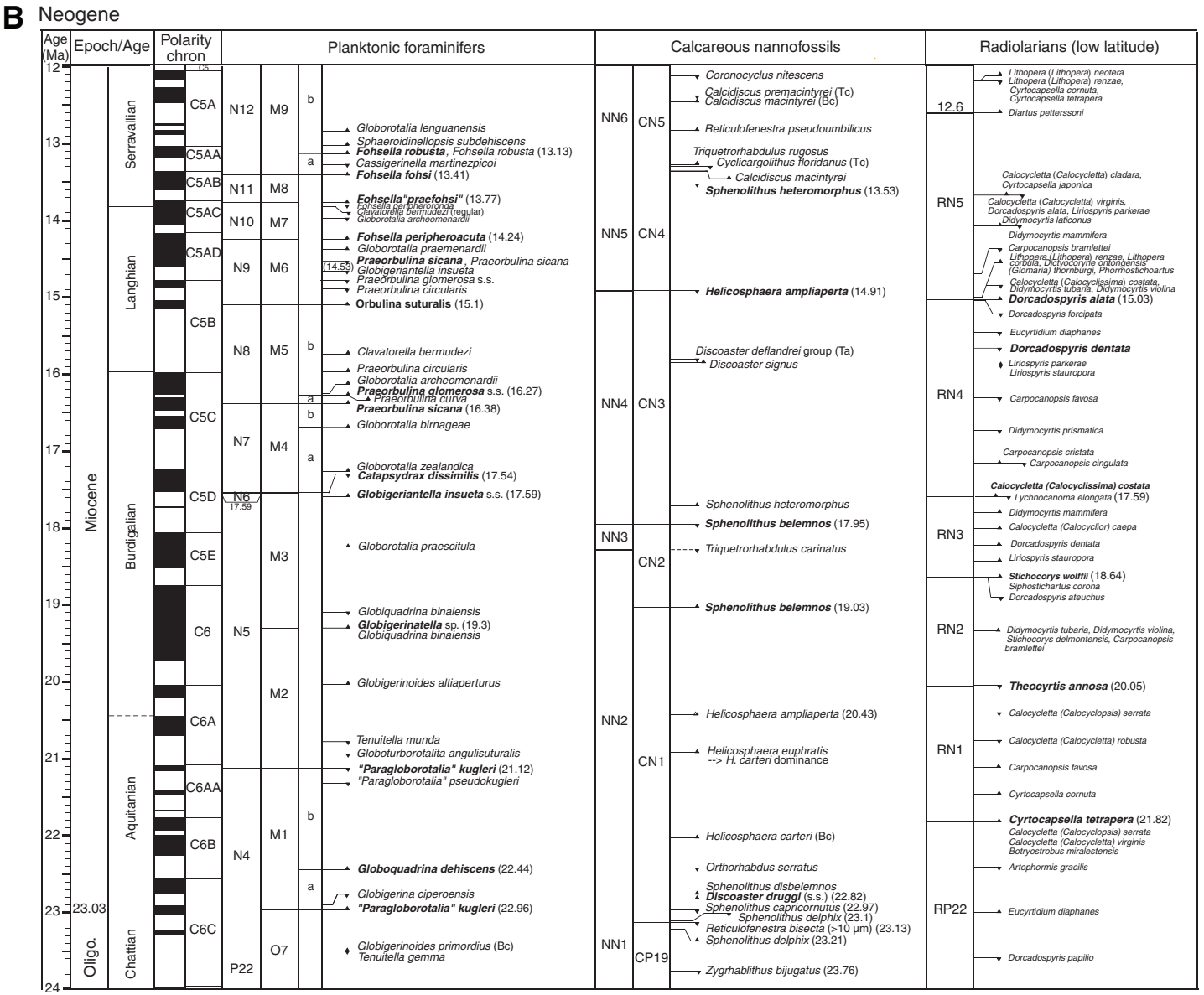

Figure F5 (continued). C. 24–44 Ma. (Continued on next page.)

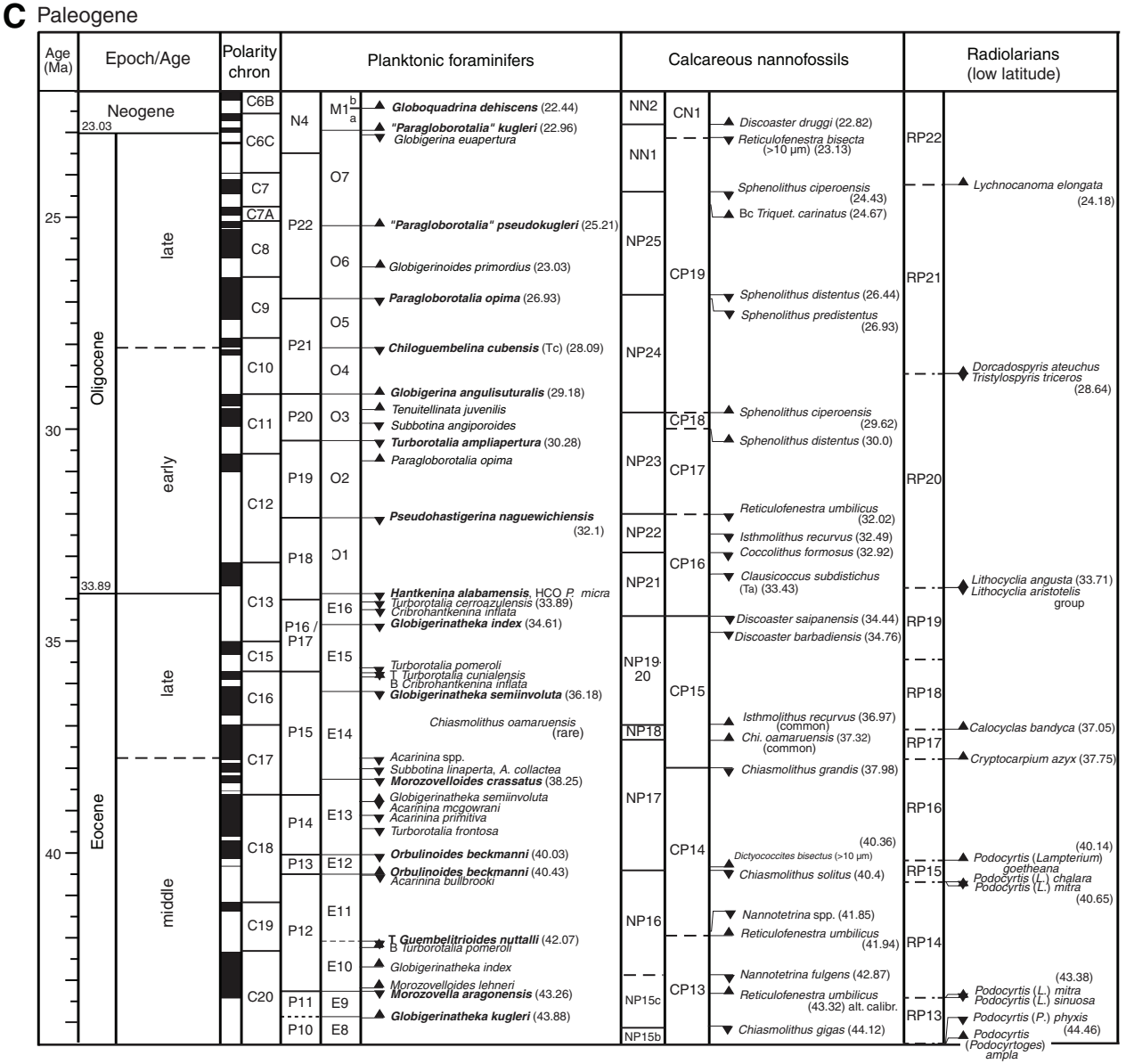

Figure F5 (continued). D. 44–67 Ma. (Continued on next page.)

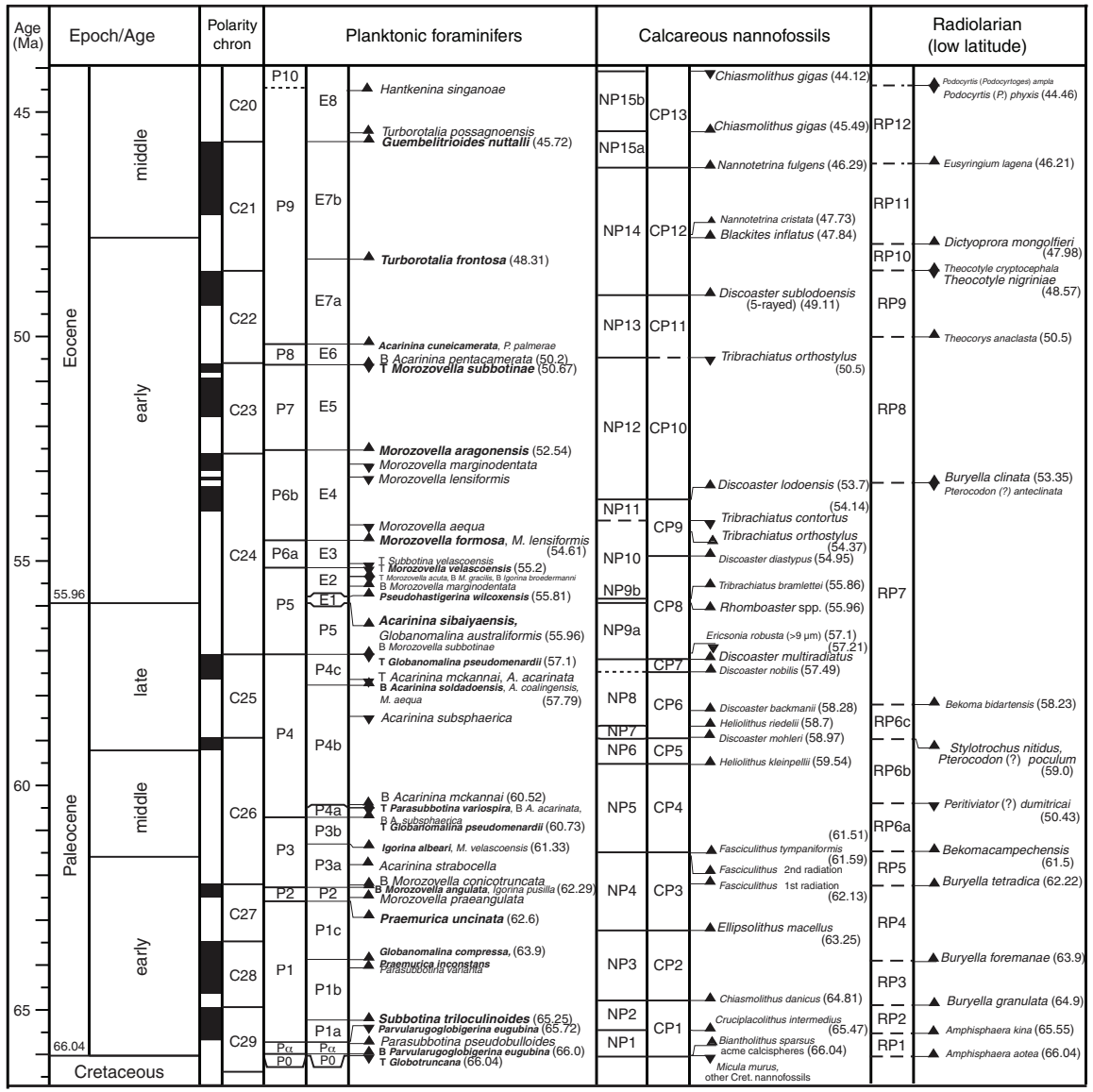

Figure F5 (continued). E. 65–75 Ma. (Continued on next page.)

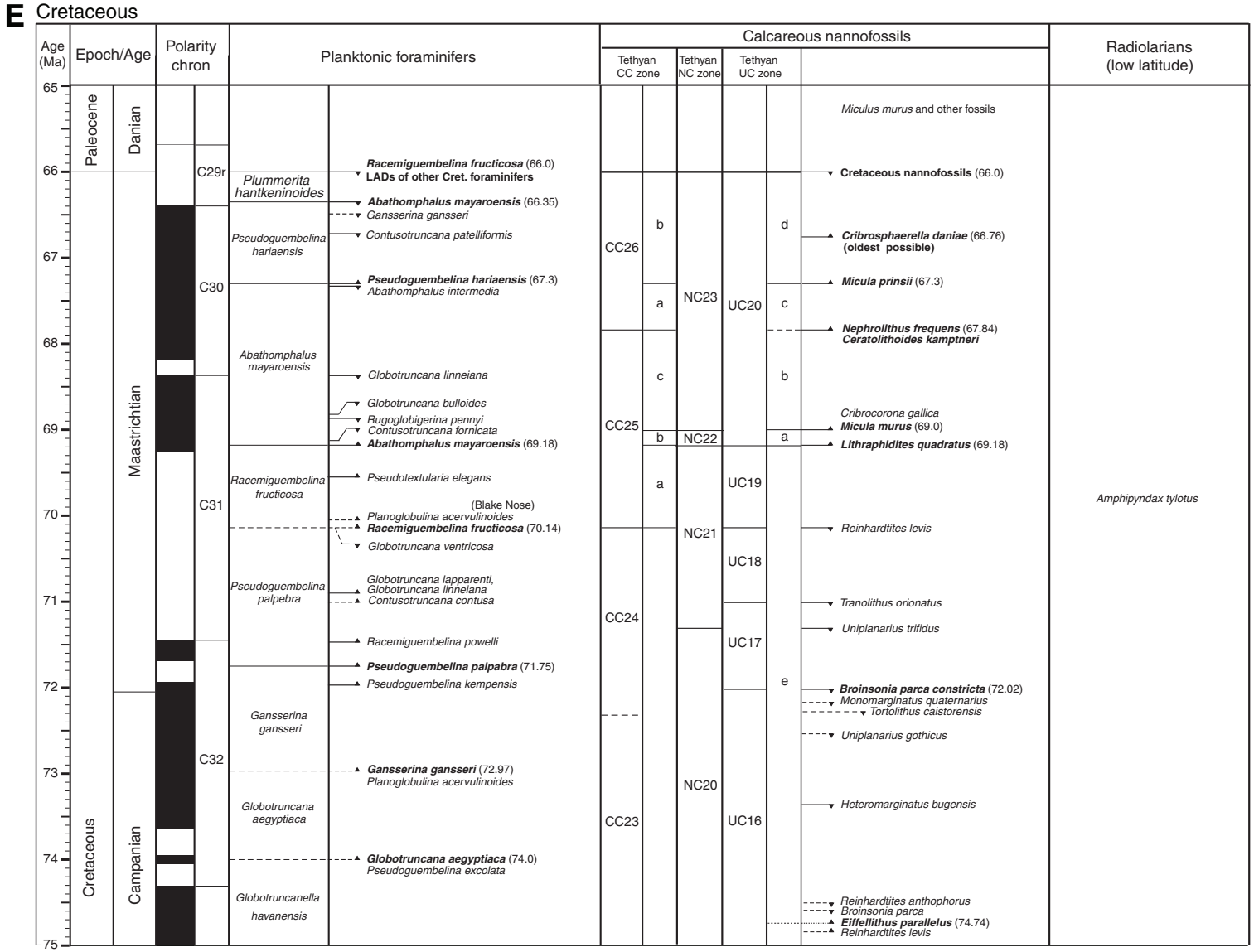

Figure F5 (continued). F. 75–85 Ma.

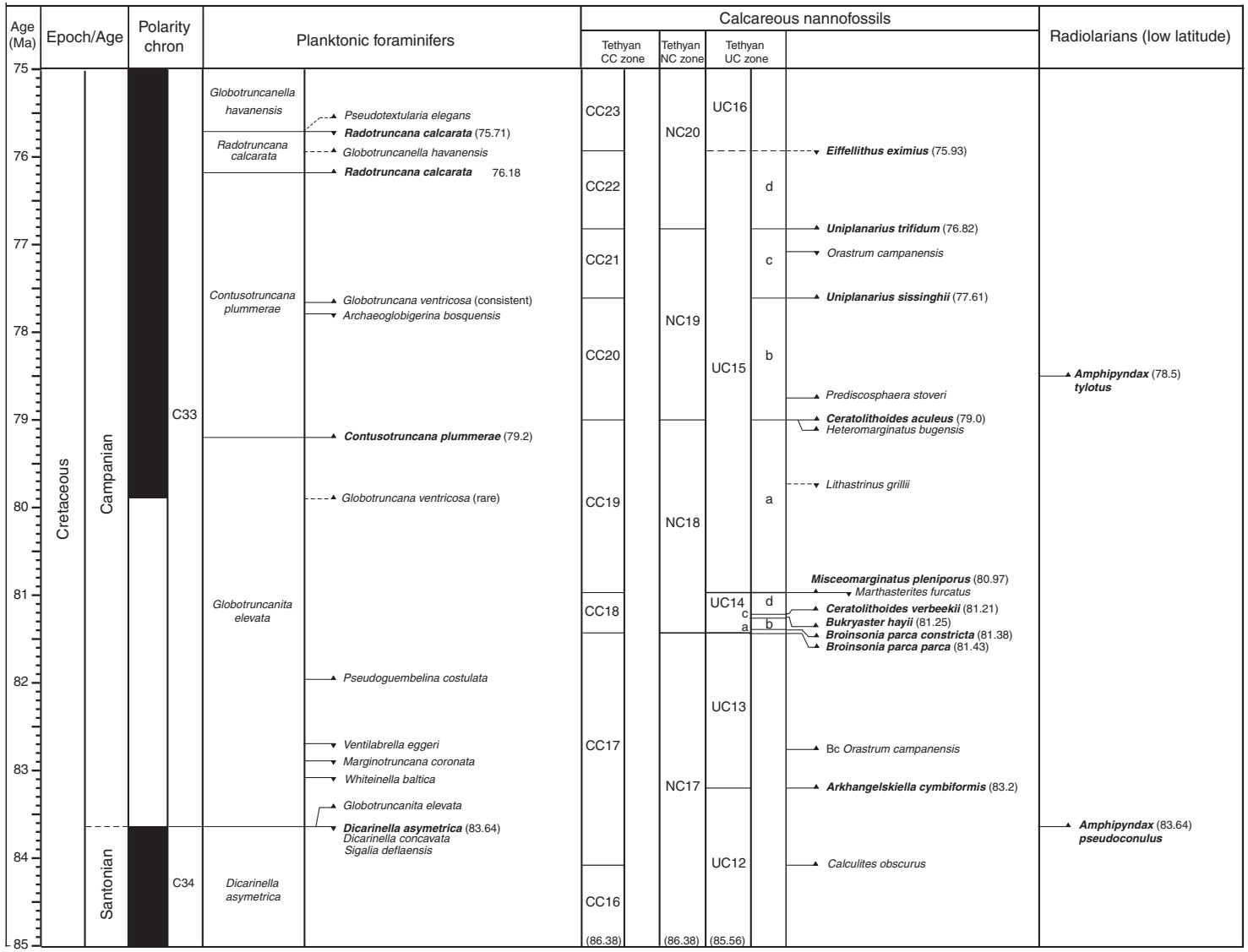

Figure F6. A. Diagram of coordinate systems used for the archive- and working section halves of cores. **B.** Natsuhara-Giken sampling cubes (7 cm^3 volume) with sample coordinate system used during Expedition 342. Hatched arrow is parallel to the "up" arrow on the sample cube and points in the –*z*-axis sample direction. **C.** Coordinate system used for the superconducting rock magnetometer onboard the R/V *JOIDES Resolution*.

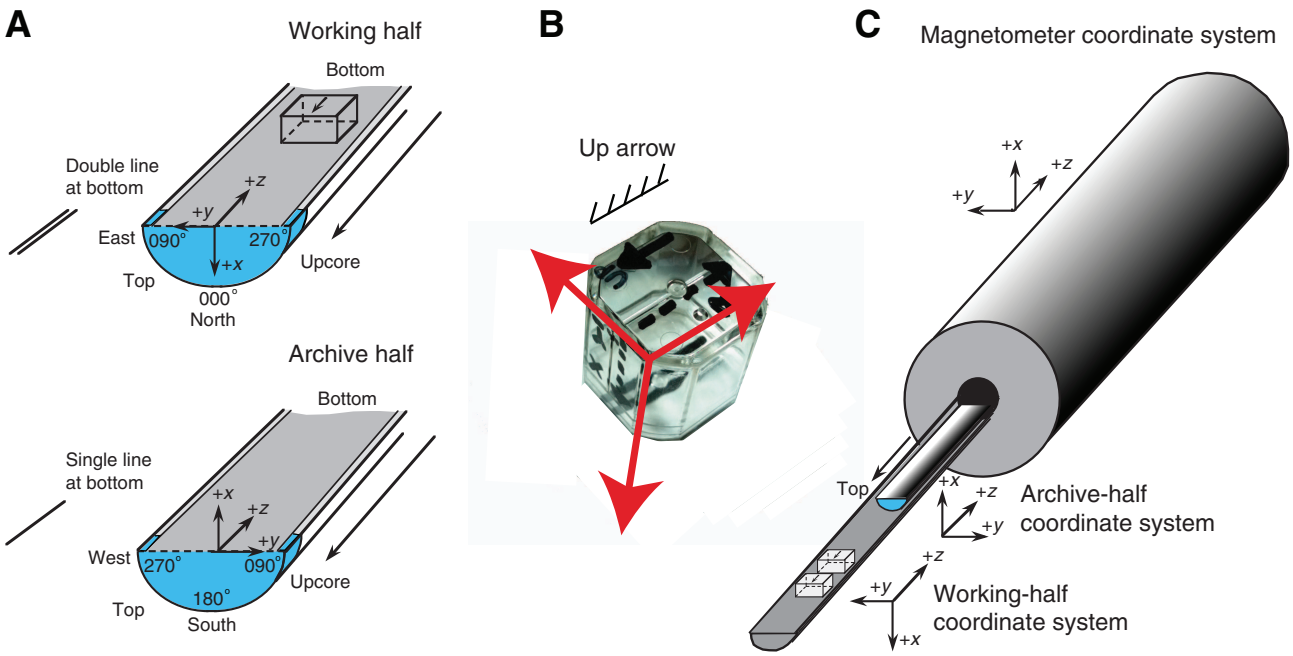

Figure F7. Photograph of the position of discrete samples in the "automatic holder" of the JR-6A magnetometer, Expedition 342.

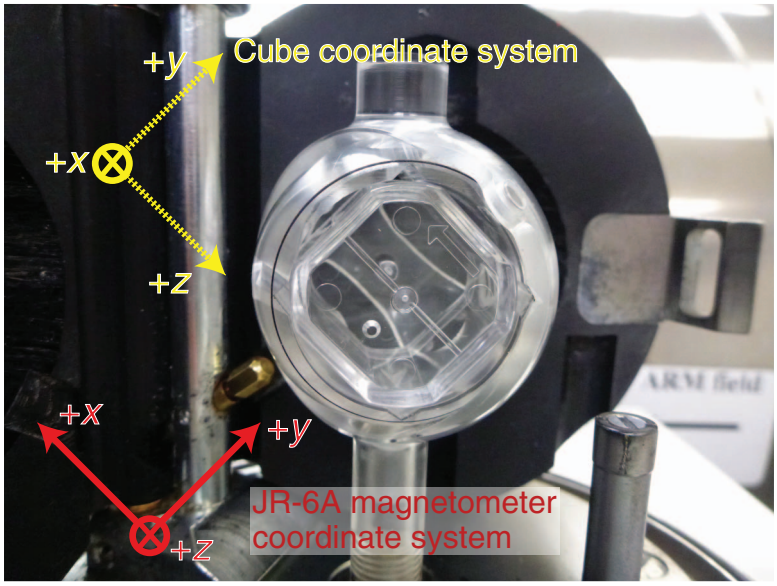

Figure F8. Interpretation of anisotropy of magnetic susceptibility data, Expedition 342. The top, colored balloons illustrate, from left to right, isotropic, oblate, prolate, and triaxial ellipsoids. **A–D.** Example data sets plotted as eigenvector directions from individual samples on equal-area projections. Squares = directions associated with the maximum eigenvalues, triangles = directions associated with intermediate eigenvalues, circles = directions associated with minimum eigenvalues. **E–H.** Bootstrapped eigenvectors from A–D, respectively. Adapted from Tauxe (2010).

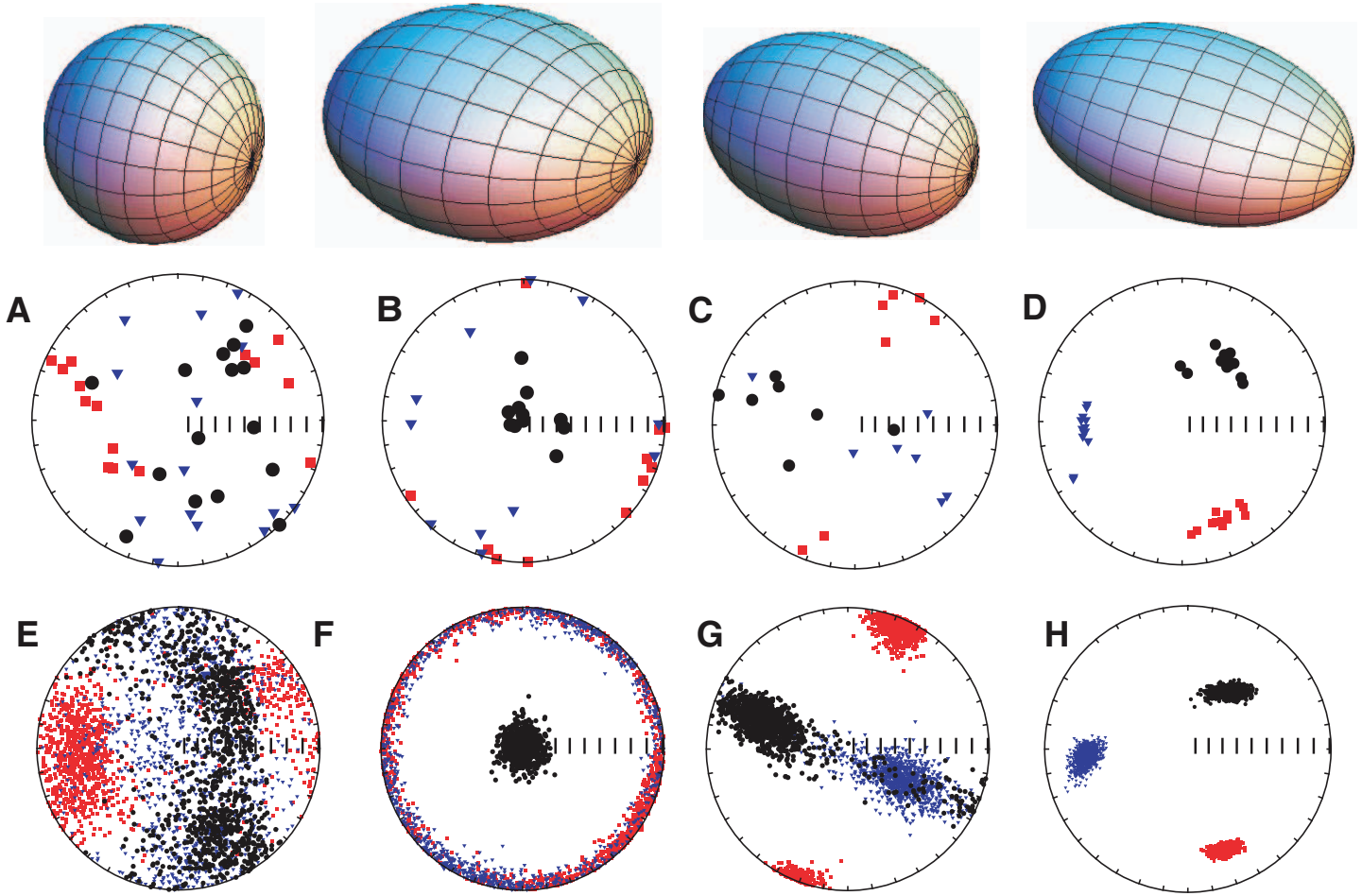

Figure F9. Plot of results of decarbonation experiment on 10 sediment samples from Site U1404 showing difference of total organic carbon (TOC_{DIFF}) and decarbonated total carbon (TC) vs. original inorganic carbon (IC).

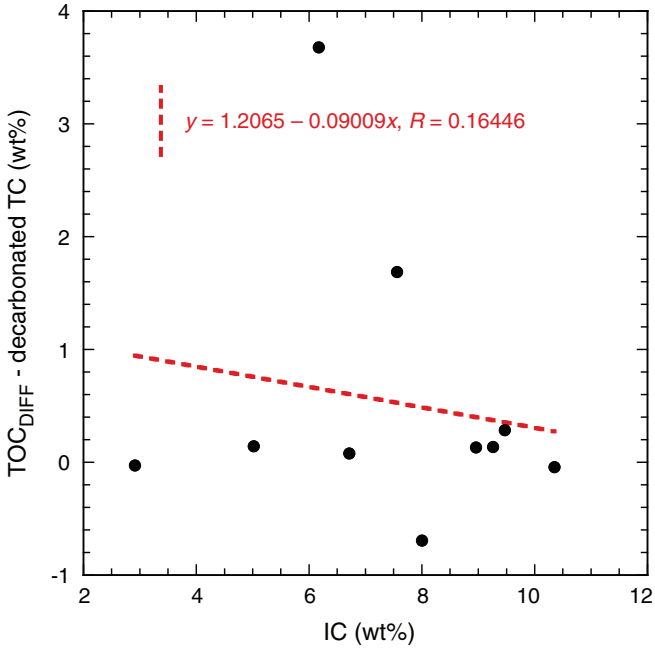

Table T1. Age estimates of calcareous nannofossil datum events, Expedition 342. (Continued on next two pages.)

Zone/ Subzone base	Species event	GTS2012 age (Ma)	Calibration reference	Expedition 320 age (Ma)	Calibration reference
NN21	B *Emiliania huxleyi*	0.29	Gradstein et al., 2012	0.29	Lourens et al., 2004
NN20	T *Pseudoemiliania lacunosa*	0.44	Gradstein et al., 2012	0.44	Lourens et al., 2004
	Tc *Reticulofenestra asanoi*	0.91	Gradstein et al., 2012	0.91	Lourens et al., 2004
	Br *Gephyrocapsa* (>4 µm)	1.04	Gradstein et al., 2012	1.01	Lourens et al., 2004
	Bc *Reticulofenestra asanoi*	1.14	Gradstein et al., 2012	1.14	Lourens et al., 2004
	T *Gephyrocapsa* (>5.5 µm)	1.24	Gradstein et al., 2012	1.26	Lourens et al., 2004
	T *Helicosphaera sellii*	1.26	Gradstein et al., 2012	1.34	Lourens et al., 2004
	B *Gephyrocapsa* (>5.5 µm)	1.62	Gradstein et al., 2012	1.56	Lourens et al., 2004
	T *Calcidiscus macintyrei*	1.60	Gradstein et al., 2012	1.61	Lourens et al., 2004
	B *Gephyrocapsa* (>4 µm)	1.73	Gradstein et al., 2012	1.69	Lourens et al., 2004
NN19	T *Discoaster brouweri*	1.93	Gradstein et al., 2012	1.93	Lourens et al., 2004
	Bc *Discoaster triradiatus*	1.95	Gradstein et al., 2012	2.14	Lourens et al., 2004
NN18	T *Discoaster pentaradiatus*	2.39	Gradstein et al., 2012	2.39	Lourens et al., 2004
NN17	T *Discoaster surculus*	2.49	Gradstein et al., 2012	2.49	Lourens et al., 2004
	Pliocene/Pleistocene boundary	2.59	Gradstein et al., 2012	NA	
	T *Discoaster tamalis*	2.80	Gradstein et al., 2012	2.8	Lourens et al., 2004
	T *Sphenolithus* spp.	3.54	Gradstein et al., 2012	3.54	Lourens et al., 2004
NN16	T *Reticulofenestra pseudoumbilicus*	3.70	Gradstein et al., 2012	3.7	Lourens et al., 2004
NN15	T *Amaurolithus*	3.92	Gradstein et al., 2012		
NN14	Bc *Discoaster asymmetricus*	4.13	Gradstein et al., 2012		
	T *Ceratolithus acutus*	5.04	Gradstein et al., 2012	5.04	Lourens et al., 2004
NN13	B *Ceratolithus rugosus*	5.12	Gradstein et al., 2012	5.05	Lourens et al., 2004
	T *Triquetrorhabdulus rugosus*	5.28	Gradstein et al., 2012	5.28	Lourens et al., 2004
	Miocene/Pliocene boundary	5.33	Gradstein et al., 2012	5.33	Lourens et al., 2004
	B *Ceratolithus larrymayeri*	5.34	Gradstein et al., 2012	5.34	Lourens et al., 2004
	B *Ceratolithus acutus*	5.35	Gradstein et al., 2012	5.35	Lourens et al., 2004
NN12	T *Discoaster quinqueramus*	5.59	Gradstein et al., 2012	5.58	Lourens et al., 2004
	Tc *Nicklithus amplificus*	5.94	Gradstein et al., 2012	5.98	Lourens et al., 2004
	X *Nicklithus amplificus/Triquetrorhabdulus rugosus*	6.79	Gradstein et al., 2012	6.79	Lourens et al., 2004
	B *Nicklithus amplificus*	6.91	Gradstein et al., 2012	6.91	Lourens et al., 2004
	B *Amaurolithus* spp.	7.42	Gradstein et al., 2012	7.36	Lourens et al., 2004
NN11	B *Discoaster berggrenii*	8.29	Gradstein et al., 2012	8.29	Lourens et al., 2004
	T *Catinaster calyculus*	9.67	Gradstein et al., 2012	9.67	Lourens et al., 2004
NN10	T *Discoaster hamatus*	9.53	Gradstein et al., 2012	9.69	Lourens et al., 2004
	T *Catinaster coalitus*	9.69	Gradstein et al., 2012	9.69	Lourens et al., 2004
NN9	B *Discoaster hamatus*	10.55	Gradstein et al., 2012	10.55	Lourens et al., 2004
	T *Coccolithus miopelagicus*	10.97	Gradstein et al., 2012	10.6	Raffi et al., 2005
	B *Catinaster calyculus*	10.79	Gradstein et al., 2012	10.76	Lourens et al., 2004
NN8	B *Catinaster coalitus*	10.89	Gradstein et al., 2012	10.89	Lourens et al., 2004
	Tc *Discoaster kugleri*	11.58	Gradstein et al., 2012	11.58	Lourens et al., 2004
NN7	Bc *Discoaster kugleri*	11.90	Gradstein et al., 2012	11.86	Lourens et al., 2004
	T *Coronocyclus nitescens*	12.12	Gradstein et al., 2012	12.12	Lourens et al., 2004
	T *Calcidiscus premacintyrei*	12.38	Gradstein et al., 2012	12.45	Lourens et al., 2004
	Tc *Cyclicargolithus floridanus*	11.85	Gradstein et al., 2012	13.33	Lourens et al., 2004
NN6	T *Sphenolithus heteromorphus*	13.53	Gradstein et al., 2012	13.53	Lourens et al., 2004
NN5	T *Helicosphaera ampliaperta*	14.91	Gradstein et al., 2012	14.91	Lourens et al., 2004
	Tc *Discoaster deflandrei*	15.80	Gradstein et al., 2012	15.66	Raffi et al., 2005
	B *Discoaster petaliformis**	15.85	Gradstein et al., 2012	15.7	Raffi et al., 2005
	Bc *Sphenolithus heteromorphus*	17.71	Gradstein et al., 2012	17.71	Lourens et al., 2004
NN4	Tc *Sphenolithus belemnos*	17.95	Gradstein et al., 2012	17.95	Lourens et al., 2004
NN3	T *Triquetrorhabdulus carinatus*	18.28	Gradstein et al., 2012	18.28	Lourens et al., 2004
	B *Sphenolithus belemnos*	19.03	Gradstein et al., 2012	19.03	Lourens et al., 2004
	B *Helicosphaera ampliaperta*	20.43	Gradstein et al., 2012	20.43	Lourens et al., 2004
	X *Helicosphaera euphratis/H. carteri*	20.92	Gradstein et al., 2012	20.92	Lourens et al., 2004
	Tc *Triquetrorhabdulus carinatus*		Gradstein et al., 2012	22.09	Raffi et al., 2005
	B *Sphenolithus disbelemnos*	22.76	Gradstein et al., 2012	22.76	Lourens et al., 2004
NN2	B *Discoaster druggii*	22.82	Gradstein et al., 2012		
	Oligocene/Miocene boundary	23.03	Gradstein et al., 2012	23.03	Lourens et al., 2004
	T *Sphenolithus delphix*	23.11	Gradstein et al., 2012	23.1	Lourens et al., 2004
	B *Sphenolithus delphix*	23.21	Gradstein et al., 2012	23.2	Lourens et al., 2004
NN1	T *Sphenolithus ciperoensis*	24.43	Gradstein et al., 2012	24.4	Blaj et al., 2009
	X *Triquetrorhabdulus longus/Triquetrorhabdulus carinatus*	24.67	Gradstein et al., 2012	24.7	Blaj et al., 2009
	Tc *Cyclicargolithus abisectus*	24.67	Gradstein et al., 2012	24.7	Lyle et al., 2002
NP25	T *Sphenolithus distentus*	26.84	Gradstein et al., 2012	26.8	Blaj et al., 2009
	T *Sphenolithus predistentus*	26.93	Gradstein et al., 2012	26.9	Blaj et al., 2009
	T *Sphenolithus pseudoradians*	28.73	Gradstein et al., 2012	28.8	Berggren et al., 1995

Table T1 (continued). (Continued on next page.)

Zone/ Subzone base	Species event	GTS2012 age (Ma)	Calibration reference	Expedition 320 age (Ma)	Calibration reference
NP24	B *Sphenolithus ciperoensis*	29.62	Gradstein et al., 2012	27.1	Blaj et al., 2009
	B *Sphenolithus distentus*	30.00	Gradstein et al., 2012	30.0	Blaj et al., 2009
NP23	T *Reticulofenestra umbilicus* (>14 µm)	32.02	Gradstein et al., 2012	32.0	Blaj et al., 2009
	T *Isthmolithus recurvus*	32.49	Gradstein et al., 2012	32.5	Villa et al., 2008
NP22	T *Coccolithus formosus*	32.92	Gradstein et al., 2012	32.9	Blaj et al., 2009
	Ta *Clausicoccus subdistichus*	33.43	Gradstein et al., 2012	NA	
	Eocene/Oligocene boundary	33.89	Gradstein et al., 2012	33.8	Pälike et al., 2006
NP21	T *Discoaster saipanensis*	34.44	Gradstein et al., 2012	34.4	Blaj et al., 2009
	T *Discoaster barbadiensis*	34.76	Gradstein et al., 2012	34.8	Blaj et al., 2009
	T *Reticulofenestra reticulata*	35.40	Gradstein et al., 2012	35.2	Backman, 1987
NP19/20	B *Isthmolithus recurvus*	36.97	Gradstein et al., 2012	36.6	Backman, 1986
NP18	Bc *Chiasmolithus oamaruensis*	37.32	Gradstein et al., 2012	37.0	Berggren et al., 1995
	T *Chiasmolithus grandis*	37.98	Gradstein et al., 2012	37.1	Backman, 1987
	B *Dictyococcites bisectus* (>10 µm)†	40.36	Gradstein et al., 2012	38.0	Berggren et al., 1995
NP17	T *Chiasmolithus solitus*	40.40	Gradstein et al., 2012	40.4	Berggren et al., 1995
	B *Reticulofenestra reticulata*	41.66	Gradstein et al., 2012	42.0	Berggren et al., 1995
	T *Nannotetrina* spp.	41.85	Gradstein et al., 2012	42.3	Backman, 1987
	B *Reticulofenestra umbilicus* (>14 µm)	41.94	Gradstein et al., 2012	42.5	Backman, 1987
NP16	T *Nannotetrina fulgens*	42.87	Gradstein et al., 2012	43.4	Backman, 1986
NP15c	T *Chiasmolithus gigas*	44.12	Gradstein et al., 2012	44.0	Backman, 1986
	B *Sphenolithus furcatolithoides*		Gradstein et al., 2012	45.8	Jovane et al., 2007
NP15b	B *Chiasmolithus gigas*	45.49	Gradstein et al., 2012	46.1	Agnini et al., 2006
NP15a	B *Nannotetrina fulgens*	46.29	Gradstein et al., 2012	46.8	Agnini et al., 2006
	B *Nannotetrina cristata*	47.73	Gradstein et al., 2012	48.0	Agnini et al., 2006
	T *Discoaster lodoensis*	47.41	Gradstein et al., 2012	48.4	Agnini et al., 2006
	B *Blackites inflatus*	47.84	Gradstein et al., 2012	NA	
NP14	B *Discoaster sublodoensis* (5 rayed)	49.11	Gradstein et al., 2012	49.5	Agnini et al., 2006
	B *Dictyococcites/Reticulofenestra*	50.50	Gradstein et al., 2012	50.7	Agnini et al., 2006
NP13	T *Tribrachiatus orthostylus*	50.50	Gradstein et al., 2012	50.7	Agnini et al., 2006
	B *Girgisia gammation*		Gradstein et al., 2012	52.8	Agnini et al., 2007
NP12	B *Discoaster lodoensis*	53.70	Gradstein et al., 2012	53.1	Agnini et al., 2007
NP11	T *Tribrachiatus contortus*	54.17	Gradstein et al., 2012	53.5	Agnini et al., 2007
	B *Sphenolithus radians*	54.17	Gradstein et al., 2012	53.5	Agnini et al., 2007
	B *Tribrachiatus orthostylus*	54.37	Gradstein et al., 2012	53.7	Agnini et al., 2007
	B *Discoaster diastypus*	54.95	Gradstein et al., 2012	54.1	Agnini et al., 2007
	T *Fasciculithus* spp.	55.64	Gradstein et al., 2012	54.7	Agnini et al., 2007
NP10	B *Rhomboaster bramlettei*	55.86	Gradstein et al., 2012	55.0	Agnini et al., 2007
	B *Rhomboaster* spp.	55.96	Gradstein et al., 2012	55.0	Agnini et al., 2007
	Paleocene/Eocene boundary	55.96	Gradstein et al., 2012	55.0	Berggren et al., 1995
	Fasciculithus div. decline	56	Gradstein et al., 2012		
	T *Ericsonia robusta* >9 µm‡	57.1	Gradstein et al., 2012	55.9	Agnini et al., 2007
	T *Fasciculithus alanii*	56	Dallanave et al. 2012		
NP9	B *Discoaster multiradiatus*	57.21	Gradstein et al., 2012	56.0	Agnini et al., 2007
	Tc *Sphenolithus anarrhopus*		Dallanave et al. 2012		
	B *Ericsonia robusta* >9 µm‡	57.54	Dallanave et al. 2012		
	B *Discoaster delicatus*‡	57.45	Dallanave et al. 2012		
	B *Fasciculithus richardii*		Dallanave et al. 2012		
	B *Discoaster okadai*	57.35	Gradstein et al., 2012	56.2	Agnini et al., 2007
	B *Discoaster nobilis*	57.5	Gradstein et al., 2012	56.2**	Agnini et al., 2007
	Tc *Discoaster backmanii*‡	57.57	Dallanave et al. 2012	56.9**	Agnini et al., 2007
	B *Discoaster backmanii*‡	58.28	Dallanave et al. 2012		
NP8	B *Heliolithus riedellii*	58.7	Gradstein et al., 2012		
NP7	B *Discoaster mohleri*	58.97	Gradstein et al., 2012	57.6**	Agnini et al., 2007
	B *Fasciculithus clinatus*		Gradstein et al., 2012	57.7**	Agnini et al., 2007
NP6	B *Heliolithus kleinpellii*	59.54	Gradstein et al., 2012	58.0**	Agnini et al., 2007
	B *Sphenolithus anarrhopus*‡	59.4	Dallanave et al. 2012	58.1**	Agnini et al., 2007
	B *Heliolithus cantabriae*	59.60	Gradstein et al., 2012	58.3**	Agnini et al., 2007
NP5	B *Fasciculithus tympaniformis*	61.51	Gradstein et al., 2012	59.9**	Agnini et al., 2007
	B *Fasciculithus*, second radiation	61.59	Gradstein et al., 2012		
	B *Neochiastozygus perfectus*	61.76	Gradstein et al., 2012	60.44**	Agnini et al., 2007
	B *Sphenolithus moriformis*	61.98	Gradstein et al., 2012		
	B *Chiasmolithus bidens/edentulus*	62.07	Gradstein et al., 2012		
	B *Fasciculithus*, first radiation	62.13	Gradstein et al., 2012		
	B *Toweius pertusus*		Dallanave et al. 2012		
NP4	B *Ellipsolithus macellus*	63.25	Gradstein et al., 2012		
	B *Prinsius dimorphosus*		Dallanave et al. 2012		
	B *Prinsius tenuiculus*		Dallanave et al. 2012		
NP3	B *Chiasmolithus danicus*	64.81	Gradstein et al., 2012		

Table T1 (continued).

Zone/ Subzone base	Species event	GTS2012 age (Ma)	Calibration reference	Expedition 320 age (Ma)	Calibration reference
	B *Cruciplacolithus tenuis*	65.47	Gradstein et al., 2012		
NP2	B *Cruciplacolithus intermedius*	?65.47	Gradstein et al., 2012		
	B *Cruciplacolithus primus* (3.5–5 µm)	65.76	Gradstein et al., 2012		
	B *Coccolithus pelagicus*		Dallanave et al. 2012		
	B *Neobiscutum parvulum*	65.9	Gradstein et al., 2012		
	T *Micula murus*, other Cretaceous nannofossils	66.04	Gradstein et al., 2012		
NP1	B *Biantholithus sparsus*; Ba calcispheres	66.04	Gradstein et al., 2012		
	Cretaceous/Paleogene boundary	66.04	Gradstein et al., 2012		
UC20d	B *Cribrosphaerella daniae* (oldest possible)	66.76	Gradstein et al., 2012		
UC20d	B *Micula prinsii*	67.3	Gradstein et al., 2012		
UC20c	B *Ceratolithoides kamptneri*	67.84	Gradstein et al., 2012		
UC20b	B *Nephrolithus frequens*	67.84	Gradstein et al., 2012		
UC20b	B *Micula murus*	69	Gradstein et al., 2012		
	B *Cribrocorona gallica*	69	Gradstein et al., 2012		
UC20	B *Lithraphidites quadratus*	69.18	Gradstein et al., 2012		
UC19	T *Reinhardtites levis*	70.14	Gradstein et al., 2012		
UC18	T *Tranolithus orionatus*	71.01	Gradstein et al., 2012		
UC18	T *Uniplanarius trifidus*	71.31	Gradstein et al., 2012		
UC17	T *Broinsonia parca constricta*	72.02	Gradstein et al., 2012		
	Campanian/Maastrichtian boundary	72.05	Gradstein et al., 2012		
UC16d	T *Monomarginatus quaternarius*	72.18	Gradstein et al., 2012		
UC16a	T *Reinhardtites anthophorus*	74.51	Gradstein et al., 2012		
UC16a	T *Eiffellithus eximius*	74.51	Gradstein et al., 2012		
	T *Lithastrinus grillii*	79.73	Gradstein et al., 2012		
UC14b	B *Broinsonia parca constricta*	81.38	Gradstein et al., 2012		
UC13	B *Arkhangelskiella cymbiformis*	83.2	Gradstein et al., 2012		
	Santonian/Campanian boundary	83.64	Gradstein et al., 2012		
UC12	T *Lithastrinus septenarius*	85.56	Gradstein et al., 2012		
	Coniacian /Santonian boundary	88.26	Gradstein et al., 2012		
UC11	B *Lithastrinus grillii*	86.5	Gradstein et al., 2012		
UC10	B *Micula stauropora*	89.77	Gradstein et al., 2012		
	Turonian/Coniacian boundary	89.77	Gradstein et al., 2012		
UC9	B *Lithastrinus septenarius* sensu lato	91.78	Gradstein et al., 2012		
UC8	B *Eiffellithus eximius*	92.99	Gradstein et al., 2012		
UC7	B *Quadrum gartneri*	93.55	Gradstein et al., 2012		
UC6b	B *Eprolithus moratus*	93.73	Gradstein et al., 2012		
	Cenomanian/Turonian boundary	93.9	Gradstein et al., 2012		
UC6a	T *Helenea chiastia*	93.9	Gradstein et al., 2012		
UC5	B *Lithraphidites acutus*	94.39	Gradstein et al., 2012		
UC3e	T *Corollithion kennedyi*	94.64	Gradstein et al., 2012		
UC3a	B *Lithraphidites acutus*	96.16	Gradstein et al., 2012		
UC1a	B *Corollithion kennedyi*	100.45	Gradstein et al., 2012		
	Albian/Cenomanian boundary	100.5	Gradstein et al., 2012		
UC0b	T *Hayesites*	100.84	Gradstein et al., 2012		
UC0a	B *Eiffellithus turriseiffelii*	103.13	Gradstein et al., 2012		

* = *Discoaster signus* in Raffi et al. (2006), † = from Fornaciari et al. (2010) recalibrated to Gradstein et al. (2012) timescale (GTS2012), ‡ = from Agnini et al. (2007) recalibrated to GTS2012. ** = age given by Agnini et al. (2007) using the Cande and Kent (1995) timescale. *Chiasmolithus danicus* is *Chiasmolithus edwardsii* of some authors. Dallanave et al. (2012) recalibrated to GTS2012. B = bottom, T = top, Tc = top common, Br = bottom rare, Bc = bottom common, X = abundance crossover. Ta = top of acme. NA = not available.

Table T2. Age estimates of planktonic foraminifer datum events, Expedition 342. (Continued on next five pages.)

Zone/Subzone base	Species event	GTS2012 age (Ma)	Calibration reference	GTS2004 age (Ma)	Calibration reference	Cande and Kent (1995) age (Ma)	Calibration reference
	T *Globorotalia flexuosa*	0.07	Gradstein et al., 2012	0.07	Wade et al., 2011	0.07	Wade et al., 2011
	B *Globigerinella calida*	0.22	Gradstein et al., 2012	0.22	Wade et al., 2011	0.22	Wade et al., 2011
	B *Globorotalia flexuosa*	0.40	Gradstein et al., 2012	0.40	Wade et al., 2011	0.40	Wade et al., 2011
	B *Globorotalia hirsuta*	0.45	Gradstein et al., 2012	0.45	Wade et al., 2011	0.45	Wade et al., 2011
PT1b	T *Globorotalia tosaensis*	0.61	Gradstein et al., 2012	0.61	Lourens et al., 2004	0.61	Wade et al., 2011
	B *Globorotalia hessi*	0.75	Gradstein et al., 2012	0.75	Wade et al., 2011	0.75	Wade et al., 2011
	X random to dextral in *Pulleniatina*	0.8	Gradstein et al., 2012			0.80	Wade et al., 2011
	T *Globoturborotalita obliquus*	1.3	Gradstein et al., 2012	1.30	Lourens et al., 2004	1.30	Wade et al., 2011
	T *Globoturborotalita apertura*	1.64	Gradstein et al., 2012			1.63	Wade et al., 2011
	T *Neogloboquadrina acostaensis*	1.58	Gradstein et al., 2012				
	T *Globoturborotalita apertura*	1.64	Gradstein et al., 2012	1.64	Lourens et al., 2004		
PT1a	T *Globigerinoides fistulosus*	1.88	Gradstein et al., 2012	1.88	Lourens et al., 2004	1.88	Wade et al., 2011
	B *Globorotalia truncatulinoides*	1.93	Gradstein et al., 2012	1.93	Lourens et al., 2004	1.93	Wade et al., 2011
	T *Globigerinoides extremus*	1.98	Gradstein et al., 2012	1.98	Lourens et al., 2004	1.99	Wade et al., 2011
	B *Pulleniatina finalis*	2.04	Gradstein et al., 2012	2.04	Lourens et al., 2004	2.05	Wade et al., 2011
	T *Globorotalia exilis* (Atl.)	2.09	Gradstein et al., 2012	2.09	Lourens et al., 2004	2.10	Wade et al., 2011
	B *Pulleniatina* (reappearance) (Atl.)	2.26	Gradstein et al., 2012	2.26	Lourens et al., 2004	2.26	Wade et al., 2011
	T *Globorotalia pertenuis*	2.3	Gradstein et al., 2012	2.30	Lourens et al., 2004	2.30	Wade et al., 2011
	T *Globoturborotalita woodi*	2.3	Gradstein et al., 2012	2.30	Lourens et al., 2004	2.30	Wade et al., 2011
PL6	T *Globorotalia miocenica* (Atl.)*	2.39	Gradstein et al., 2012	2.39	Lourens et al., 2004	2.39	Wade et al., 2011
	T *Globorotalia limbata* (Atl.)	2.39	Gradstein et al., 2012	2.39	Lourens et al., 2004	2.39	Wade et al., 2011
	Pliocene/Pleistocene boundary	2.59	Gradstein et al., 2012	1.81	Aguirre and Pasini, 1985	1.80	Cande and Kent, 1995
	T *Globorotalia pertenuis*	2.3	Gradstein et al., 2012	2.60	Wade et al., 2011	2.60	Wade et al., 2011
	T *Globoturborotalita decoraperta*	2.75	Gradstein et al., 2012	2.75	Lourens et al., 2004	2.75	Wade et al., 2011
	T *Globorotalia multicamerata*	2.98	Gradstein et al., 2012	2.98	Lourens et al., 2004	2.99	Wade et al., 2011
PL5	T *Dentoglobigerina altispira* (Atl.)*	3.13	Gradstein et al., 2012	3.13	Lourens et al., 2004	3.13	Wade et al., 2011
PL4	T *Sphaeroidinellopsis seminulina* (Atl.)*	3.16	Gradstein et al., 2012	3.16	Lourens et al., 2004	3.16	Wade et al., 2011
	T *Globorotalia cf. crassula* (N. Atl.)*	3.29	Gradstein et al., 2012				
	B *Globigerinoides fistulosus*	3.33	Gradstein et al., 2012	3.33	Wade et al., 2011	3.33	Wade et al., 2011
	B *Globorotalia tosaensis*	3.35	Gradstein et al., 2012	3.35	Wade et al., 2011	3.35	Wade et al., 2011
	T *Pulleniatina* (disappearance) (Atl.)*	3.41	Gradstein et al., 2012	3.41	Lourens et al., 2004	3.41	Wade et al., 2011
	B *Globorotalia pertenuis*	3.52	Gradstein et al., 2012	3.52	Lourens et al., 2004	3.51	Wade et al., 2011
	B *Globorotalia miocenica* (Atl.)*	3.77	Gradstein et al., 2012	3.77	Lourens et al., 2004	3.76	Wade et al., 2011
	T *Globorotalia plesiotumida*	3.77	Gradstein et al., 2012	3.77	Lourens et al., 2004	3.76	Wade et al., 2011
PL3	T *Globorotalia margaritae*	3.85	Gradstein et al., 2012	3.85	Lourens et al., 2004	3.84	Wade et al., 2011
	X *Pulleniatina* coiling sinistral to dextral	4.08	Gradstein et al., 2012	4.08	Lourens et al., 2004	4.07	Wade et al., 2011
	B *Globorotalia crassaformis* sensu lato	4.31	Gradstein et al., 2012	4.31	Lourens et al., 2004	4.30	Wade et al., 2011
PL2	T *Globoturborotalita nepenthes*	4.37	Gradstein et al., 2012	4.37	Lourens et al., 2004	4.36	Wade et al., 2011
	B *Goblorotalia exilis*	4.45	Gradstein et al., 2012	4.45	Lourens et al., 2004	4.44	Wade et al., 2011
	T *Sphaeroidinellopsis kochi*	4.53	Gradstein et al., 2012	4.53	Lourens et al., 2004	4.52	Wade et al., 2011
	T *Globorotalia cibaoensis*	4.6	Gradstein et al., 2012	4.61	Wade et al., 2011	4.60	Wade et al., 2011
	T *Globigerinoides seiglei*	4.72	Gradstein et al., 2012				
	Pliocene/Miocene boundary	5.33	Gradstein et al., 2012	5.33	Lourens et al., 2004	5.33	Wade et al., 2011
	B *Sphaeroidinella dehiscens* sensu lato	5.53	Gradstein et al., 2012	5.53	Lourens et al., 2004	5.48	Wade et al., 2011
PL1	B *Globorotalia tumida* (Atl.)*	5.72	Gradstein et al., 2012	5.72	Lourens et al., 2004	5.63	Wade et al., 2011
	B *Turborotalita humilis*	5.81	Gradstein et al., 2012	5.81	Lourens et al., 2004	5.71	Wade et al., 2011
	T *Globoquadrina dehiscens*	5.92	Gradstein et al., 2012	5.92	Wade et al., 2011	5.80	Wade et al., 2011
	B *Globorotalia margaritae*	6.08	Gradstein et al., 2012	6.08	Lourens et al., 2004	5.95	Wade et al., 2011
	B *Globigerinoides conglobatus*	6.2	Gradstein et al., 2012	6.20	Lourens et al., 2004	6.08	Wade et al., 2011

Table T2 (continued). (Continued on next page.)

Zone/Subzone base	Species event	GTS2012 age (Ma)	Calibration reference	GTS2004 age (Ma)	Calibration reference	Cande and Kent (1995) age (Ma)	Calibration reference
	X *Neogloboquadrina acostaensis* coiling sinistral to dextral	6.37	Gradstein et al., 2012	6.34	Wade et al., 2011	6.20	Wade et al., 2011
	T *Globorotalia miotumida (conomiozea),* temperate*	6.52	Gradstein et al., 2012				
	B *Pulleniatina primalis*	6.6	Gradstein et al., 2012	6.6	Wade et al., 2011	6.40	Wade et al., 2011
	X *Neogloboquadrina acostaensis* coiling dextral to sinistral	6.77	Gradstein et al., 2012	6.77	Wade et al., 2011	6.60	Wade et al., 2011
	X *Neogloboquadrina atlantica* coiling dextral to sinistral	6.99	Gradstein et al., 2012	6.99	Wade et al., 2011	6.80	Wade et al., 2011
	B *Globorotalia miotumida (conomiozea),* temperate*	7.89	Gradstein et al., 2012				
	B *Candeina nitida*	8.43	Gradstein et al., 2012				
	B *Neogloboquadrina humerosa,* temperate*	8.56	Gradstein et al., 2012	8.56	Wade et al., 2011	8.50	Wade et al., 2011
M13b	B *Globorotalia plesiotumida*	8.58	Gradstein et al., 2012	8.58	Lourens et al., 2004	8.52	Wade et al., 2011
	B *Globigerinoides extremus*	8.93	Gradstein et al., 2012	8.93	Lourens et al., 2004	8.86	Wade et al., 2011
	T *Globorotalia lenguaensis* (Atl.)*	8.97	Gradstein et al., 2012	6.13	Wade et al., 2011	6.00	Wade et al., 2011
	B *Globorotalia cibaoensis*	9.44	Gradstein et al., 2012	9.44	Lourens et al., 2004	9.34	Wade et al., 2011
	B *Globorotalia juanai*	9.69	Gradstein et al., 2012	9.69	Lourens et al., 2004	9.62	Wade et al., 2011
M13a	B *Neogloboquadrina acostaensis*, (sub)tropical*	9.83	Gradstein et al., 2012	9.83	Lourens et al., 2004	9.79	Wade et al., 2011
	T *Globorotalia challengeri*	9.99	Gradstein et al., 2012				
M12	T *Paragloborotalia mayeri/siakensis*, (sub)tropical*	10.46	Gradstein et al., 2012	10.46	Lourens et al., 2004	10.35	Wade et al., 2011
	B *Neogloboquadrina acostaensis,* temperate*	10.57	Gradstein et al., 2012				
	B *Globorotalia limbata*	10.64	Gradstein et al., 2012	10.64	Lourens et al., 2004	10.66	Wade et al., 2011
	T *Cassigerinella chipolensis*	10.89	Gradstein et al., 2012	10.89	Lourens et al., 2004	10.84	Wade et al., 2011
	B *Globoturborotalita apertura*	11.18	Gradstein et al., 2012	11.18	Lourens et al., 2004	11.12	Wade et al., 2011
	B *Globorotalia challengeri*	11.22	Gradstein et al., 2012				
	B regular *Globigerinoides obliquus*	11.25	Gradstein et al., 2012				
	T *Paragloborotalia mayeri/siakensis*, temperate*	11.4	Gradstein et al., 2012				
	B *Globoturborotalita decoraperta*	11.49	Gradstein et al., 2012	11.49	Lourens et al., 2004	11.42	Wade et al., 2011
	T *Globigerinoides subquadratus*	11.54	Gradstein et al., 2012	11.54	Lourens et al., 2004	11.46	Wade et al., 2011
M11	B *Globoturborotalita nepenthes*	11.63	Gradstein et al., 2012	11.63	Lourens et al., 2004	11.55	Wade et al., 2011
M10	T *Fohsella fohsi, Fohsella plexus*	11.79	Gradstein et al., 2012	11.79	Lourens et al., 2004	11.71	Wade et al., 2011
	T *Globorotalia praescitula*		Gradstein et al., 2012			11.90	Wade et al., 2011
	T *Clavatorella bermudezi*	12	Gradstein et al., 2012				
	B *Globorotalia lenguanensis*	12.84	Gradstein et al., 2012	12.84	Lourens et al., 2004	12.89	Wade et al., 2011
	B *Sphaeroidinellopsis subdehiscens*	13.02	Gradstein et al., 2012	13.02	Lourens et al., 2004	13.00	Wade et al., 2011
M9b	B *Fohsella robusta*	13.13	Gradstein et al., 2012	13.13	Lourens et al., 2004	13.09	Wade et al., 2011
	T *Cassigerinella martinezpicoi*	13.27	Gradstein et al., 2012	13.27	Lourens et al., 2004	13.22	Wade et al., 2011
M9a	B *Fohsella fohsi*	13.41	Gradstein et al., 2012	13.41	Lourens et al., 2004	13.34	Wade et al., 2011
	B *Neogloboquadrina nympha*	13.4855	Gradstein et al., 2012				
	T *Globorotalia praescitula* (S. Atl.)*	13.73	Gradstein et al., 2012				
M8	B *Fohsella praefohsi*	13.77	Gradstein et al., 2012	13.77	Lourens et al., 2004	13.74	Wade et al., 2011
	T *Fohsella peripheroronda*	13.8	Gradstein et al., 2012	13.80	Lourens et al., 2004	13.77	Wade et al., 2011
	T regular *Clavatorella bermudezi*	13.82	Gradstein et al., 2012	13.82	Lourens et al., 2004	13.79	Wade et al., 2011
	T *Globorotalia archeomenardii*	13.87	Gradstein et al., 2012	13.87	Lourens et al., 2004	13.84	Wade et al., 2011
M7	B *Fohsella peripheroacuta*	14.24	Gradstein et al., 2012	14.24	Lourens et al., 2004	14.23	Wade et al., 2011
	B *Globorotalia praemenardii*	14.38	Gradstein et al., 2012	14.38	Lourens et al., 2004	14.39	Wade et al., 2011
	T *Praeorbulina sicana*	14.53	Gradstein et al., 2012	14.53	Lourens et al., 2004	14.56	Wade et al., 2011
	T *Globigeriantella insueta*	14.66	Gradstein et al., 2012	14.66	Lourens et al., 2004	14.69	Wade et al., 2011
	T *Praeorbulina glomerosa* sensu stricto	14.775	Gradstein et al., 2012				
	T *Praeorbulina circularis*	14.89	Gradstein et al., 2012				
M6	B *Orbulina suturalis*	15.1	Gradstein et al., 2012	15.10	Wade et al., 2011	15.10	Wade et al., 2011
	B *Clavatorella bermudezi*	15.73	Gradstein et al., 2012	15.73	Wade et al., 2011	15.76	Wade et al., 2011

Table T2 (continued). (Continued on next page.)

Zone/Subzone base	Species event	GTS2012 age (Ma)	Calibration reference	GTS2004 age (Ma)	Calibration reference	Cande and Kent (1995) age (Ma)	Calibration reference
	B *Praeorbulina circularis*	15.96	Gradstein et al., 2012	15.96	Wade et al., 2011	16.00	Wade et al., 2011
	B *Globigerinoides diminutus*	16.0622	Gradstein et al., 2012				
	B *Globorotalia archeomenardii*	16.26	Gradstein et al., 2012	16.26	Lourens et al., 2004	16.29	Wade et al., 2011
M5b	B *Praeorbulina glomerosa* sensu stricto	16.27	Gradstein et al., 2012	16.27	Lourens et al., 2004	16.29	Wade et al., 2011
	B *Praeorbulina curva*	16.28	Gradstein et al., 2012	16.28	Wade et al., 2011	16.30	Wade et al., 2011
M5a/M4b	B *Praeorbulina sicana*	16.38	Gradstein et al., 2012	16.38	Wade et al., 2011	16.40	Wade et al., 2011
	T *Globorotalia incognita*	16.3875	Gradstein et al., 2012				
M4b	B *Fohsella birnageae*	16.69	Gradstein et al., 2012	16.69	Wade et al., 2011	16.70	Wade et al., 2011
	B *Globorotalia miozea*	16.7032	Gradstein et al., 2012				
	B *Globorotalia zealandica*	17.26	Gradstein et al., 2012	17.26	Wade et al., 2011	17.30	Wade et al., 2011
	T *Globorotalia semivera*	17.26	Gradstein et al., 2012				
M4a	T *Catapsydrax dissimilis*	17.54	Gradstein et al., 2012	17.54	Lourens et al., 2004	17.62	Wade et al., 2011
	B *Globigeriantella insueta* sensu stricto	17.59	Gradstein et al., 2012	17.59	Lourens et al., 2004	17.69	Wade et al., 2011
	T *Globoquadrina dehiscens* forma *spinosa* (S. Atl.)*	17.6066	Gradstein et al., 2012				
	B *Globorotalia praescitula*	18.26	Gradstein et al., 2012	18.26	Wade et al., 2011	18.50	Wade et al., 2011
	T *Globiquadrina binaiensis*	19.09	Gradstein et al., 2012	19.09	Lourens et al., 2004	19.43	Wade et al., 2011
M3	B *Globigerinatella* sp.	19.3	Gradstein et al., 2012	19.30	Lourens et al., 2004	19.66	Wade et al., 2011
	B *Globiquadrina binaiensis*	19.3	Gradstein et al., 2012				
	B *Globigerinoides altiaperturus*	20.03	Gradstein et al., 2012	20.03	Wade et al., 2011	20.50	Wade et al., 2011
	T *Tenuitella munda*	20.7838	Gradstein et al., 2012	20.78	Wade et al., 2011	21.40	Wade et al., 2011
	B *Globorotalia incognita*	20.9334	Gradstein et al., 2012				
	T *Globoturborotalita angulisuturalis*	20.94088	Gradstein et al., 2012	20.94	Wade et al., 2011	21.60	Wade et al., 2011
M2	T *Paragloborotalia kugleri*	21.12	Gradstein et al., 2012	21.12	Lourens et al., 2004	21.81	Wade et al., 2011
	T *Paragloborotalia pseudokugleri*	21.31	Gradstein et al., 2012	21.31	Lourens et al., 2004	22.04	Wade et al., 2011
	B *Globoquadrina dehiscens* forma *spinosa*	21.443	Gradstein et al., 2012			23.20	Wade et al., 2011
	T *Dentoglobigerina globularis*	21.9752	Gradstein et al., 2012				
M1b	B *Globoquadrina dehiscens*	22.44	Gradstein et al., 2012	22.44	Wade et al., 2011		
	T *Globigerina ciperoensis*	22.9	Gradstein et al., 2012	22.90	Lourens et al., 2004	23.68	Wade et al., 2011
	B *Globigerinoides trilobus* sensu lato	22.96	Gradstein et al., 2012	22.96	Lourens et al., 2004	23.73	Wade et al., 2011
M1a	B *Paragloborotalia kugleri*	22.96	Gradstein et al., 2012	22.96	Lourens et al., 2004	23.73	Wade et al., 2011
	Miocene/Oligocene boundary	23.03	Gradstein et al., 2012	23.03	Lourens et al., 2004	23.80	Berggren et al., 1995
	T *Globigerina euapertura*	23.03	Gradstein et al., 2012				
	T *Tenuitella gemma*	23.4951	Gradstein et al., 2012	23.60	Wade et al., 2011	24.30	Wade et al., 2011
	B common *Globigerinoides primordius*	23.4951	Gradstein et al., 2012	23.60	Wade et al., 2011	24.30	Wade et al., 2011
O7	B *Paragloborotalia pseudokugleri*	25.2145	Gradstein et al., 2012	25.40	Wade et al., 2011	25.90	Wade et al., 2011
	B *Globigerinoides primordius*	26.1169	Gradstein et al., 2012	26.30	Wade et al., 2011	26.70	Wade et al., 2011
O6	T *Paragloborotalia opima* sensu stricto	26.93	Gradstein et al., 2012	27.30	Wade et al., 2011	27.50	Wade et al., 2011
O5	T common *Chiloguembelina cubensis*	28.087	Gradstein et al., 2012	28.30	Wade et al., 2011	28.40	Wade et al., 2011
O4	B *Globigerina angulisuturalis*	29.183	Gradstein et al., 2012	29.50	Wade et al., 2011	29.40	Wade et al., 2011
	B *Tenuitellinata juvenilis*	29.502	Gradstein et al., 2012				
	T *Subbotina angiporoides*	29.8371	Gradstein et al., 2012	30.10	Wade et al., 2011	30.00	Wade et al., 2011
O3	T *Turborotalia ampliapertura*	30.2805	Gradstein et al., 2012	30.40	Wade et al., 2011	30.30	Wade et al., 2011
	B *Paragloborotalia opima*	30.7239	Gradstein et al., 2012	30.80	Wade et al., 2011	30.60	Wade et al., 2011
O2	T *Pseudohastigerina naguewichiensis*	32.0955	Gradstein et al., 2012	32.20	Wade et al., 2011	32.00	Wade et al., 2011
O1	B *Cassigerinella chipolensis*	33.88889451	Gradstein et al., 2012				
O1	**Oligocene/Eocene boundary**	33.89	Gradstein et al., 2012	33.70	Berggren et al., 1995	33.70	Berggren et al., 1995
	T *Hantkenina* spp., *Hantkenina alabamensis*	33.88889451	Gradstein et al., 2012	33.90	Wade et al., 2011	33.70	Wade et al., 2011
	T common *Pseudohastigerina micra*	33.88889451	Gradstein et al., 2012	33.90	Wade et al., 2011	33.70	Wade et al., 2011
	T *Turborotalia cerroazulensis*	34.03	Gradstein et al., 2012	34.00	Wade et al., 2011	33.80	Wade et al., 2011

Table T2 (continued). (Continued on next page.)

Zone/Subzone base	Species event	GTS2012 age (Ma)	Calibration reference	GTS2004 age (Ma)	Calibration reference	Cande and Kent (1995) age (Ma)	Calibration reference
	T *Cribrohantkenina inflata*	34.22	Gradstein et al., 2012				
E16	T *Globigerinatheka index*	34.61	Gradstein et al., 2012	34.50	Wade et al., 2011	34.30	Wade et al., 2011
	T *Turborotalia pomeroli*	35.66	Gradstein et al., 2012				
	B *Turborotalia cunialensis*	35.71	Gradstein et al., 2012	35.40	Wade et al., 2011	35.30	Wade et al., 2011
	B *Cribrohantkenina inflata*	35.87	Gradstein et al., 2012				
E15	T *Globigerinatheka semiinvoluta*	36.18	Gradstein et al., 2012	35.80	Wade et al., 2011	35.80	Wade et al., 2011
	T *Acarinina* spp.	37.75	Gradstein et al., 2012				
	T *Subbotina linaperta*	37.96	Gradstein et al., 2012				
	T *Acarinina collactea*	37.96	Gradstein et al., 2012				
E14	T *Morozovelloides crassatus*	38.25	Gradstein et al., 2012	37.70	Wade et al., 2011	38.00	Wade et al., 2011
	B *Globigerinatheka semiinvoluta*	38.62	Gradstein et al., 2012	37.70	Wade et al., 2011	38.00	Wade et al., 2011
	T *Acarinina mcgowrani*	38.62	Gradstein et al., 2012	37.70	Wade et al., 2011	38.00	Wade et al., 2011
	T *Planorotalites* spp.	38.62	Gradstein et al., 2012				
	T *Acarinina primitiva*	39.12	Gradstein et al., 2012				
	T *Turborotalia frontosa*	39.42	Gradstein et al., 2012	38.80	Wade et al., 2011	39.30	Wade et al., 2011
E13	T *Orbulinoides beckmanni*	40.03	Gradstein et al., 2012	39.40	Wade et al., 2011	40.00	Wade et al., 2011
E12	B *Orbulinoides beckmanni*	40.49	Gradstein et al., 2012	39.80	Wade et al., 2011	40.50	Wade et al., 2011
	T *Acarinina bullbrooki*	40.49	Gradstein et al., 2012	39.80	Wade et al., 2011	40.50	Wade et al., 2011
E11	T *Guembelitrioides nuttalli*	(42.07)	Gradstein et al., 2012	(41.40)	Wade et al., 2011	(42.30)	Wade et al., 2011
	B *Turborotalia pomeroli*	42.21	Gradstein et al., 2012	41.50	Wade et al., 2011	42.40	Wade et al., 2011
	B *Globigerinatheka index*	42.64	Gradstein et al., 2012	41.90	Wade et al., 2011	42.90	Wade et al., 2011
	B *Morozovelloides lehneri*	43.15	Gradstein et al., 2012	42.50	Wade et al., 2011	43.50	Wade et al., 2011
E10	T *Morozovella aragonensis*	43.26	Gradstein et al., 2012	42.60	Wade et al., 2011	43.60	Wade et al., 2011
E9	B *Globigerinatheka kugleri*	(43.88)	Gradstein et al., 2012	(43.40)	Wade et al., 2011	(44.40)	Wade et al., 2011
	B *Hantkenina singanoae*	(44.49)	Gradstein et al., 2012	43.50	Wade et al., 2011	44.50	Wade et al., 2011
	B *Turborotalia possagnoensis*	45.49	Gradstein et al., 2012				
E8	B *Guembelitrioides nuttalli*	(45.72)	Gradstein et al., 2012	45.50	Wade et al., 2011	46.40	Wade et al., 2011
E7b	B *Turborotalia frontosa*	48.31	Gradstein et al., 2012	48.60	Wade et al., 2011	49.00	Wade et al., 2011
E7a	B *Acarinina cuneicamerata*	50.2	Gradstein et al., 2012	50.30	Wade et al., 2011	50.40	Wade et al., 2011
	B *Planorotalites palmerae*	50.2	Gradstein et al., 2012	50.30	Wade et al., 2011	50.40	Wade et al., 2011
E6	T *Morozovella subbotinae*	50.67	Gradstein et al., 2012	50.80	Wade et al., 2011	50.80	Wade et al., 2011
	B *Acarinina pentacamerata*	50.67	Gradstein et al., 2012				
E5	B *Morozovella aragonensis*	52.54	Gradstein et al., 2012	52.30	Wade et al., 2011	52.30	Wade et al., 2011
	T *Morozovella marginodentata*	52.85	Gradstein et al., 2012	52.80	Wade et al., 2011	52.50	Wade et al., 2011
	T *Morozovella lensiformis*	53.14	Gradstein et al., 2012	53.10	Wade et al., 2011	52.70	Wade et al., 2011
	T *Morozovella aequa*	54.2	Gradstein et al., 2012	54.00	Wade et al., 2011	53.60	Wade et al., 2011
E4	B *Morozovella formosa*	54.61	Gradstein et al., 2012	54.40	Wade et al., 2011	54.00	Wade et al., 2011
	B *Morozovella lensiformis*	54.61	Gradstein et al., 2012	54.40	Wade et al., 2011	54.00	Wade et al., 2011
	T *Subbotina velascoensis*	55.07	Gradstein et al., 2012				
E3	T *Morozovella velascoensis*	(55.20)	Gradstein et al., 2012	54.90	Wade et al., 2011	54.50	Wade et al., 2011
	T *Morozovella acuta*	55.39	Gradstein et al., 2012	55.10	Wade et al., 2011	54.70	Wade et al., 2011
	B *Morozovella gracilis*	55.39	Gradstein et al., 2012	55.10	Wade et al., 2011	54.70	Wade et al., 2011
	B *Igorina broedermanni*	55.39	Gradstein et al., 2012	55.10	Wade et al., 2011	54.70	Wade et al., 2011
	B *Morozovella marginodentata*	55.54	Gradstein et al., 2012	55.20	Wade et al., 2011	54.80	Wade et al., 2011
E2	B *Pseudohastigerina wilcoxensis*	55.80944	Gradstein et al., 2012	55.70	Wade et al., 2011	55.40	Wade et al., 2011
	B *Globanomalina australiformis*	55.95944	Gradstein et al., 2012	55.80	Wade et al., 2011	55.50	Wade et al., 2011
E1	B *Acarinina sibaiyaensis*	55.95944	Gradstein et al., 2012	55.80	Wade et al., 2011	55.50	Wade et al., 2011
	Eocene/Paleocene boundary	55.96	Gradstein et al., 2012	55.80	Wade et al., 2011	55.50	Ouda and Aubry, 2003
P5	T *Globanomalina pseudomenardii*	57.101	Gradstein et al., 2012	56.70	Wade et al., 2011	55.90	Wade et al., 2011
	B *Morozovella subbotinae*	57.101	Gradstein et al., 2012	56.70	Wade et al., 2011	55.90	Wade et al., 2011

Table T2 (continued). (Continued on next page.)

Zone/Subzone base	Species event	GTS2012 age (Ma)	Calibration reference	GTS2004 age (Ma)	Calibration reference	Cande and Kent (1995) age (Ma)	Calibration reference
	T *Acarinina mckannai*	57.656	Gradstein et al., 2012	57.10	Wade et al., 2011	56.30	Wade et al., 2011
	T *Acarinina acarinata*	57.656	Gradstein et al., 2012	57.10	Wade et al., 2011	56.30	Wade et al., 2011
P4c	B *Acarinina soldadoensis*	57.7863	Gradstein et al., 2012	57.30	Wade et al., 2011	56.50	Wade et al., 2011
	B *Acarinina coalingensis*	57.7863	Gradstein et al., 2012	57.30	Wade et al., 2011	56.50	Wade et al., 2011
	B *Morozovella aequa*	57.7863	Gradstein et al., 2012	57.30	Wade et al., 2011	56.50	Wade et al., 2011
	T *Acarinina subsphaerica*	58.4378	Gradstein et al., 2012	57.90	Wade et al., 2011	57.10	Wade et al., 2011
	B *Acarinina mckannai*	60.4306	Gradstein et al., 2012	59.90	Wade et al., 2011	59.10	Wade et al., 2011
P4b	T *Parasubbotina variospira*	60.52012	Gradstein et al., 2012	60.00	Wade et al., 2011	59.20	Wade et al., 2011
	B *Acarinina acarinata*	60.52	Gradstein et al., 2012	60.00	Wade et al., 2011	59.20	Wade et al., 2011
	B *Acarinina subsphaerica*	60.52	Gradstein et al., 2012	60.00	Wade et al., 2011	59.20	Wade et al., 2011
P4a	B *Globanomalina pseudomenardii*	60.73	Gradstein et al., 2012	60.20	Wade et al., 2011	59.40	Wade et al., 2011
P3b	B *Igorina albeari*	61.33	Gradstein et al., 2012	60.80	Wade et al., 2011	60.00	Wade et al., 2011
	B *Morozovella velascoensis*	61.33	Gradstein et al., 2012	60.80	Wade et al., 2011	60.00	Wade et al., 2011
	B *Acarinina strabocella*	61.77	Gradstein et al., 2012				
	B *Morozovella conicotruncata*	62.22	Gradstein et al., 2012	61.70	Wade et al., 2011	60.90	Wade et al., 2011
P3a	B *Morozovella angulata*	62.29	Gradstein et al., 2012	61.70	Wade et al., 2011	61.00	Wade et al., 2011
	B *Igorina pusilla*	62.29	Gradstein et al., 2012	61.70	Wade et al., 2011	61.00	Wade et al., 2011
	B *Morozovella praeangulata*	62.46	Gradstein et al., 2012	61.90	Wade et al., 2011	61.20	Wade et al., 2011
	B *Globanomalima imitata*		Gradstein et al., 2012	(62.00)	Wade et al., 2011	(61.30)	Wade et al., 2011
P2	B *Praemurica uncinata*	62.60	Gradstein et al., 2012	62.10	Wade et al., 2011	61.40	Wade et al., 2011
P1c	B *Globanomalina compressa*	63.90	Gradstein et al., 2012	63.50	Wade et al., 2011	62.90	Wade et al., 2011
	B *Praemurica inconstans*	63.90	Gradstein et al., 2012	63.50	Wade et al., 2011	62.90	Wade et al., 2011
	B *Parasubbotina varianta*	64.02	Gradstein et al., 2012	63.60	Wade et al., 2011	63.00	Wade et al., 2011
P1b	B *Subbotina triloculinoides*	65.25	Gradstein et al., 2012	64.70	Wade et al., 2011	64.30	Wade et al., 2011
P1a	T *Parvularugoglobigerina eugubina*	65.72	Gradstein et al., 2012	65.20	Wade et al., 2011	64.80	Wade et al., 2011
	B *Parasubbotina pseudobulloides*	65.76	Gradstein et al., 2012				
	B *Parvularugoglobigerina extensa*	65.94	Gradstein et al., 2012	65.40	Wade et al., 2011	64.90	Wade et al., 2011
Pα	B *Parvularugoglobigerina eugubina*	66.00	Gradstein et al., 2012	65.46	Wade et al., 2011	64.97	Wade et al., 2011
	Cretaceous/Paleogene boundary	66.04	Gradstein et al., 2012	65.5	Wade et al., 2011		
P0	T *Globotruncana* spp., *Racemiguembelina fructicosa*; tops of other Cretaceous foraminifers	66.04	Gradstein et al., 2012	65.5	Wade et al., 2011	65	Wade et al., 2011
Plummerita hantkeninoides	T *Abathomphalus mayaroensis*	66.35	Gradstein et al., 2012				
	T *Gansserina gansseri*	(66.49)	Gradstein et al., 2012				
	T *Contusotruncana patelliformis*	66.72	Gradstein et al., 2012				
Plummerita hariaensis	B *Pseudoguembelina hariaensis*	67.3	Gradstein et al., 2012				
	T *Abathomphalus intermedia*	67.33	Gradstein et al., 2012				
	T *Globotruncana linneiana*	68.37	Gradstein et al., 2012				
	T *Globotruncana bulloides*	68.82	Gradstein et al., 2012				
	T *Rugoglobigerina pennyi*	68.86	Gradstein et al., 2012				
	T *Contusotruncana fornicata*	69.13	Gradstein et al., 2012				
Abathomphalus mayaroensis	B *Abathomphalus mayaroensis*	69.18	Gradstein et al., 2012				
	B *Pseudotextularia elegans*	69.55	Gradstein et al., 2012				
	B *Planoglobulina acervulinoides*	(70.05)	Gradstein et al., 2012				
Racemiguembelina fructicosa	B *Racemiguembelina fructicosa*	(70.14)	Gradstein et al., 2012				
	T *Globotruncana ventricosa*	(70.14)	Gradstein et al., 2012				
	B *Globotruncana lapparenti, Globotruncana linneiana*	70.90	Gradstein et al., 2012				
	B *Contusotruncana contusa*	(71.01)	Gradstein et al., 2012				
	B *Racemiguembelina powelli*	71.47	Gradstein et al., 2012				
Pseudoguembelina palpebra	B *Pseudoguembelina palpebra*	71.75	Gradstein et al., 2012				

Table T2 (continued).

Zone/Subzone base	Species event	GTS2012 age (Ma)	Calibration reference	GTS2004 age (Ma)	Calibration reference	Cande and Kent (1995) age (Ma)	Calibration reference
	B *Pseudoguembelina kempensis*	71.97	Gradstein et al., 2012				
	Maastrichtian/Campanian boundary	72.05	Gradstein et al., 2012				
Gansserina gansseri	B *Gansserina gansseri*	(72.97)	Gradstein et al., 2012				
	B *Planoglobulina acervulinoides*	(72.97)	Gradstein et al., 2012				
Globotruncana aegyptiaca	B *Globotruncana aegyptiaca*	(74.00)	Gradstein et al., 2012				
	B *Pseudoguembelina excolata*	(74.00)	Gradstein et al., 2012				
Globotruncanella havanensis	T *Radotruncana calcarata*	75.71	Gradstein et al., 2012				
	B *Pseudotextularia elegans*	(75.71)	Gradstein et al., 2012				
	B *Globotruncanella havanensis*	(75.94)	Gradstein et al., 2012				
Radotruncana calcarata	B *Radotruncana calcarata*	76.18	Gradstein et al., 2012				
	B *Globotruncana ventricosa* (consistent)	77.66	Gradstein et al., 2012				
	T *Archaeoglobigerina bosquensis*	77.79	Gradstein et al., 2012				
Contusotruncana plummerae	B *Contusotruncana plummerae*	(79.20)	Gradstein et al., 2012				
	B *Globotruncana ventricosa* (rare)	(79.90)	Gradstein et al., 2012				
	B *Pseudoguembelina costulata*	81.96	Gradstein et al., 2012				
	T *Ventilabrella eggeri*	82.71	Gradstein et al., 2012				
	T *Marginotruncana coronata*	82.89	Gradstein et al., 2012				
	T *Whiteinella baltica*	83.08	Gradstein et al., 2012				
Globotruncanita elevata	B *Globotruncanita elevata*	83.64	Gradstein et al., 2012				
	Campanian/Santonian boundary	(83.64)	Gradstein et al., 2012				

* = regional calibration age only. Calibration ages in parentheses are uncertain. GTS2012 = geomagnetic timescale of Gradstein et al. (2012), GTS2004 = geomagnetic timescale of Gradstein et al. (2004). T = top, B = bottom, X = coiling direction change, Atl. = Atlantic, N. Atl. = North Atlantic, S. Atl. = South Atlantic.

Table T3. Age estimates of radiolarian datum events, Expedition 342. (Continued on next eight pages.)

Zone/ Subzone base	Species event	GTS2012 age (Ma)	Calibration reference	Expedition 320 age (Ma)	Calibration reference	GTS2004 age (Ma)	Calibration reference	Cande and Kent (1995) age (Ma)	Calibration reference	Datum reference
RN17	B *Buccinosphaera invaginata*	0.18	Gradstein et al., 2012	0.18	Lourens et al., 2004	0.18	Gradstein et al., 2004	0.18	Berggren et al., 1995	Sanfilippo and Nigrini, 1998
RN16	T *Stylatractus universus*	0.44	Gradstein et al., 2012	0.44	Lourens et al., 2004	0.44	Gradstein et al., 2004	0.42	Berggren et al., 1995	Sanfilippo and Nigrini, 1998
RN15	B *Collosphaera tuberosa*	0.59	Gradstein et al., 2012	0.59	Lourens et al., 2004	0.59	Gradstein et al., 2004	0.61	Berggren et al., 1995	Sanfilippo and Nigrini, 1998
RN14	T *Anthocyrtidium angulare*	1.21	Gradstein et al., 2012	1.21	Lourens et al., 2004	1.21	Gradstein et al., 2004	1.12	Berggren et al., 1995	Sanfilippo and Nigrini, 1998
RN13	T *Pterocanium prismatium*	2.04	Gradstein et al., 2012	2.08	Lourens et al., 2004	2.08	Gradstein et al., 2004	1.74	Berggren et al., 1995	Sanfilippo and Nigrini, 1998
	Pliocene/Pleistocene boundary	2.59	Gradstein et al., 2012	2.59	Lourens et al., 2004	1.81	Gradstein et al., 2004	1.81	Berggren et al., 1995	
	T *Anthocyrtidium jenghisi*	2.74	Gradstein et al., 2012	2.79	Lourens et al., 2004	2.79	Gradstein et al., 2004	2.40	Berggren et al., 1995	Sanfilippo and Nigrini, 1998
RN12	T *Stichocorys peregrina*	2.87	Gradstein et al., 2012	2.90	Lourens et al., 2004	2.90	Gradstein et al., 2004	2.74	Berggren et al., 1995	Sanfilippo and Nigrini, 1998
	T *Phormostichoartus fistula*	3.49	Gradstein et al., 2012	3.96	Lourens et al., 2004	3.96	Gradstein et al., 2004	3.42	Berggren et al., 1995	Sanfilippo and Nigrini, 1998
RN11	T *Phormostichoartus doliolum*	3.89	Gradstein et al., 2012	4.03	Lourens et al., 2004	4.03	Gradstein et al., 2004	3.87	Berggren et al., 1995	Sanfilippo and Nigrini, 1998
RN10	T *Didymocyrtis penultima*	4.24	Gradstein et al., 2012	4.26	Lourens et al., 2004	4.26	Gradstein et al., 2004	4.19	Berggren et al., 1995	Sanfilippo and Nigrini, 1998
	Miocene/Pliocene boundary	5.33	Gradstein et al., 2012	5.33	Lourens et al., 2004	5.33	Gradstein et al., 2004	5.32	Berggren et al., 1995	
RN09	X *Stichocorys delmontensis/ Stichocorys peregrina*	7.78	Gradstein et al., 2012	7.75	Lourens et al., 2004	7.75	Gradstein et al., 2004	6.71	Berggren et al., 1995	Sanfilippo and Nigrini, 1998
RN08	T *Diartus hughesi*	8.39	Gradstein et al., 2012	8.39	Lourens et al., 2004	8.39	Gradstein et al., 2004	7.70	Berggren et al., 1995	Sanfilippo and Nigrini, 1998
RN07	X *Diartus petterssoni/ Diartus hughesi*	8.84	Gradstein et al., 2012	8.76	Lourens et al., 2004	8.76	Gradstein et al., 2004	8.77	Berggren et al., 1995	Sanfilippo and Nigrini, 1998
	X *Didymocyrtis antepenultima/ Didymocyrtis laticonus*	8.84	Gradstein et al., 2012							Gradstein et al., 2012
	T *Stichocorys wolffii*	8.87	Gradstein et al., 2012							Lazarus et al., 1995
	B *Phormostichoartus doliolum*	8.87	Gradstein et al., 2012							Lazarus et al., 1995
	T *Cyrtocapsella japonica*	9.86	Gradstein et al., 2012							Lazarus et al., 1995
	T *Carpocanopsis cristata*	10.68	Gradstein et al., 2012							Lazarus et al., 1995
	T *Cyrtocapsella cornuta*	12.19	Gradstein et al., 2012							Lazarus et al., 1995
	T *Cyrtocapsella tetrapera*	12.19	Gradstein et al., 2012							Lazarus et al., 1995
	T *Dorcadospyris alata*	12.50	Gradstein et al., 2012					11.84	Nigrini et al., 2006	Nigrini et al., 2006
RN06	B *Diartus petterssoni*	12.60	Gradstein et al., 2012	12.11	Lourens et al., 2004	12.11	Gradstein et al., 2004	12.43	Nigrini et al., 2006	Nigrini et al., 2006
	T *Calocycletta virginis*	13.67	Gradstein et al., 2012					12.59		Sanfilippo and Nigrini, 1998
	T *Acrocubus octopylus*	15.00	Provisional					13.32	Nigrini et al., 2006	Nigrini et al., 2006
	T *Calocycletta costata*	15.00	Gradstein et al., 2012					13.32	Nigrini et al., 2006	Nigrini et al., 2006
	T *Eucyrtidium diaphanes*	15.46	Gradstein et al., 2012					14.27	Nigrini et al., 2006	Nigrini et al., 2006
	T *Dorcadospyris dentata*	15.66	Gradstein et al., 2012					14.51	Nigrini et al., 2006	Nigrini et al., 2006
	T *Didymocyrtis tubaria/ Didymocyrtis violina*	15.00	Gradstein et al., 2012					14.69	Nigrini et al., 2006	Nigrini et al., 2006
	T *Dorcadospyris forcipata*	15.03	Gradstein et al., 2012					14.84	Nigrini et al., 2006	Nigrini et al., 2006
RN05	X *Dorcadospyris dentata/ Dorcadospyris alata*	15.03	Gradstein et al., 2012	14.78	Lourens et al., 2004	14.78	Gradstein et al., 2004	15.03	Nigrini et al., 2006	Nigrini et al., 2006
	B *Liriospyris parkerae*	15.50	Provisional					15.16	Nigrini et al., 2006	Nigrini et al., 2006

Table T3 (continued). (Continued on next page.)

Zone/ Subzone base	Species event	GTS2012 age (Ma)	Calibration reference	Expedition 320 age (Ma)	Calibration reference	GTS2004 age (Ma)	Calibration reference	Cande and Kent (1995) age (Ma)	Calibration reference	Datum reference
	B *Cyrtocapsella japonica*	13.67	Gradstein et al., 2012					15.40	Nigrini et al., 2006	Nigrini et al., 2006
	B *Dorcadospyris alata*	15.50	Provisional					15.47	Nigrini et al., 2006	Nigrini et al., 2006
	T *Carpocanopsis cingulata*	17.16	Gradstein et al., 2012					15.77	Nigrini et al., 2006	Nigrini et al., 2006
	T *Lychnocanoma elongata*	17.59	Gradstein et al., 2013					15.93	Nigrini et al., 2006	Nigrini et al., 2006
	T *Didymocyrtis prismatica*	16.73	Gradstein et al., 2012					15.96	Nigrini et al., 2006	Nigrini et al., 2006
	B *Didymocyrtis laticonus*	14.07	Gradstein et al., 2012					16.06	Nigrini et al., 2006	Nigrini et al., 2006
	B *Acrocubus octopylus* (upper)	16.50	Provisional					16.15	Nigrini et al., 2006	Nigrini et al., 2006
	B *Carpocanopsis cristata*	17.16	Gradstein et al., 2012					16.22	Nigrini et al., 2006	Nigrini et al., 2006
	B *Lithopera renzae*	17.40	Provisional					17.30	Nigrini et al., 2006	Nigrini et al., 2006
RN04	B *Calocycletta costata*	17.59	Gradstein et al., 2012	17.49	Lourens et al., 2004	17.49	Gradstein et al., 2004	17.69	Nigrini et al., 2006	Nigrini et al., 2006
	B *Dorcadospyris dentata*	18.22	Gradstein et al., 2012					17.84	Nigrini et al., 2006	Nigrini et al., 2006
	B *Liriospyris stauropora*	18.43	Gradstein et al., 2012					17.84	Nigrini et al., 2006	Nigrini et al., 2006
	T *Dorcadospyris scambos*	18.50	Provisional					18.64	Nigrini et al., 2006	Nigrini et al., 2006
	B *Siphostichartus corona*	18.64	Gradstein et al., 2012							Nigrini et al., 2006
	T *Dorcadospyris ateuchus*	18.64	Gradstein et al., 2012					18.80	Nigrini et al., 2006	Nigrini et al., 2006
RN03	B *Stichocorys wolffii*	18.64	Gradstein et al., 2012	18.57	Lourens et al., 2004	18.57	Gradstein et al., 2004	18.90	Nigrini et al., 2006	Nigrini et al., 2006
	B *Didymocyrtis mammifera*	19.00	Provisional					18.92	Nigrini et al., 2006	Nigrini et al., 2006
	B *Dorcadospyris forcipata*	19.00	Provisional					19.07	Nigrini et al., 2006	Nigrini et al., 2006
	T *Dorcadospyris simplex*	19.00	Provisional					19.22	Nigrini et al., 2006	Nigrini et al., 2006
	B *Didymocyrtis violina*	19.34	Gradstein et al., 2012					19.98	Nigrini et al., 2006	Nigrini et al., 2006
	T *Dorcadospyris praeforcipata*	19.34	Provisional					19.98	Nigrini et al., 2006	Nigrini et al., 2006
	B *Didymocyrtis tubaria*	19.34	Gradstein et al., 2012					20.15	Nigrini et al., 2006	Nigrini et al., 2006
	B *Dorcadospyris simplex* s.s.	19.34	Provisional					20.52	Nigrini et al., 2006	Nigrini et al., 2006
	B *Lophocyrtis pegetrum*	19.34	Provisional					21.14	Nigrini et al., 2006	Nigrini et al., 2006
	B *Stichocorys delmontensis*	19.34	Gradstein et al., 2012	20.60	Lourens et al., 2004	?		21.14	Nigrini et al., 2006	Nigrini et al., 2006
	B *Carpocanopsis bramlettei*	19.34	Gradstein et al., 2012					21.54	Nigrini et al., 2006	Nigrini et al., 2006
RN02	T *Theocyrtis annosa*	20.05	Gradstein et al., 2012	21.30	Kamikuri et al., 2012	21.38	Gradstein et al., 2004	21.57	Nigrini et al., 2006	Kamikuri et al., 2012
	T *Calocycletta serrata*	20.40	Gradstein et al., 2012							Sanfilippo and Nigrini, 1998
	T *Calocycletta robusta*	20.76	Gradstein et al., 2012							Sanfilippo and Nigrini, 1998
	B *Carpocanopsis favosa*	21.11	Gradstein et al., 2012							Sanfilippo and Nigrini, 1998
	B *Cyrtocapsella cornuta*	21.46	Gradstein et al., 2012	22.40	Kamikuri et al., 2012			22.57	Nigrini et al., 2006	Kamikuri et al., 2012
	B *Botryostrobus miralestensis*	21.82	Gradstein et al., 2012							Sanfilippo and Nigrini, 1998
	B *Calocycletta virginis*	21.82	Gradstein et al., 2012					21.60	Nigrini et al., 2006	Sanfilippo and Nigrini, 1998
	B *Lophocyrtis leptetrum*	21.82	Provisional	21.80	Kamikuri et al., 2012			21.73	Nigrini et al., 2006	Kamikuri et al., 2012
	T *Eucyrtidium mitodes*	21.82	Provisional	22.20	Kamikuri et al., 2012			22.32	Nigrini et al., 2006	Kamikuri et al., 2012
	B *Calocycletta serrata*	21.82	Gradstein et al., 2012	21.30	Kamikuri et al., 2012	?		22.37	Nigrini et al., 2006	Kamikuri et al., 2012
RN01	B *Cyrtocapsella tetrapera*	21.82	Gradstein et al., 2012	22.40	Kamikuri et al., 2012	22.35	Gradstein et al., 2004	22.65	Nigrini et al., 2006	Kamikuri et al., 2012
	T *Artophormis gracilis*	22.41	Gradstein et al., 2012	22.80	Kamikuri et al., 2012	22.62	Gradstein et al., 2004	22.70	Nigrini et al., 2006	Kamikuri et al., 2012
RP22b	B *Eucyrtidium diaphanes*	23.00	Gradstein et al., 2012	23.80	Kamikuri et al., 2012	22.95	Gradstein et al., 2004	22.91	Nigrini et al., 2006	Kamikuri et al., 2012
	B *Didymocyrtis bassani*	23.00	Provisional					23.05	Nigrini et al., 2006	Nigrini et al., 2006
	T *Dorcadospyris riedeli*	23.00	Provisional					23.18	Nigrini et al., 2006	Nigrini et al., 2006
	Oligocene/Miocene boundary	23.03	Gradstein et al., 2012	23.03	Lourens et al., 2004	23.03	Gradstein et al., 2004	23.80	Berggren et al., 1995	Sanfilippo and Nigrini, 1998
	T *Dorcadospyris cyclacantha*	23.20	Provisional	23.20	Kamikuri et al., 2012			23.15	Nigrini et al., 2006	Kamikuri et al., 2012
	B *Dorcadospyris cyclacantha*	23.20	Provisional	23.80	Kamikuri et al., 2012			23.42	Nigrini et al., 2006	Kamikuri et al., 2012

Table T3 (continued). (Continued on next page.)

Zone/ Subzone base	Species event	GTS2012 age (Ma)	Calibration reference	Expedition 320 age (Ma)	Calibration reference	GTS2004 age (Ma)	Calibration reference	Cande and Kent (1995) age (Ma)	Calibration reference	Datum reference
	T *Dorcadospyris papilio*	23.59	Gradstein et al., 2012	23.31	Pälike et al., 2006	23.64	Gradstein et al., 2004	23.59	Nigrini et al., 2006	Nigrini et al., 2006
	T *Liriospyris longicornuta*	23.80	Provisional	23.90	Kamikuri et al., 2012					Kamikuri et al., 2012
	T *Lychnocanoma apodora*	23.80	Provisional	24.70	Kamikuri et al., 2012					Kamikuri et al., 2012
	B *Carpocanopsis cingulata*	24.18	Gradstein et al., 2012	25.20	Pälike et al., 2006	23.90	Gradstein et al., 2004	24.63	Nigrini et al., 2006	Nigrini et al., 2006
RP22a	B *Lychnocanoma elongata*	24.18	Gradstein et al., 2012	25.20	Kamikuri et al., 2012	23.90	Gradstein et al., 2004	24.89	Nigrini et al., 2006	Kamikuri et al., 2012
	T *Lychnocanoma trifolium*	25.07	Gradstein et al., 2012	?		24.88	Gradstein et al., 2004	?	Nigrini et al., 2006	Nigrini et al., 2006
	B *Liriospyris longicornuta*			25.90	Kamikuri et al., 2012					Kamikuri et al., 2012
	B *Dorcadospyris papilio*	26.86	Gradstein et al., 2012	25.55	Pälike et al., 2006	26.83	Gradstein et al., 2004	26.07	Nigrini et al., 2006	Nigrini et al., 2006
	B *Calocycletta robusta*	25.97	Gradstein et al., 2012	26.10	Kamikuri et al., 2012	25.85	Gradstein et al., 2004	25.49	Nigrini et al., 2006	Kamikuri et al., 2012
	B *Acrocubus octopylus* (lower)	26.20	Provisional	26.30	Kamikuri et al., 2012					Kamikuri et al., 2012
RP21b	B *Lychnocanoma apodora*	26.50	Provisional	26.60	Kamikuri et al., 2012					Kamikuri et al., 2012
	T *Eucyrtidium plesiodiaphanes*	27.30	Provisional	27.30	Kamikuri et al., 2012					Kamikuri et al., 2012
	T *Lithocyclia angusta*	27.75	Gradstein et al., 2012	27.70	Kamikuri et al., 2012	27.80	Gradstein et al., 2004	28.02	Nigrini et al., 2006	Kamikuri et al., 2012
	T *Theocyrtis setanios*	28.15	Provisional	28.10	Kamikuri et al., 2012					Kamikuri et al., 2012
	B *Theocyrtis annosa*	29.10	Gradstein et al., 2012	29.00	Kamikuri et al., 2012	29.16	Gradstein et al., 2004			Kamikuri et al., 2012
RP21a	X *Tristylospyris triceros/ Dorcadospyris ateuchus*	28.64	Gradstein et al., 2012	29.10	Pälike et al., 2006	28.77	Gradstein et al., 2004	29.14	Nigrini et al., 2006	Nigrini et al., 2006
	T *Lithocyclia crux*	29.56	Gradstein et al., 2012	30.13	Pälike et al., 2006	29.54	Gradstein et al., 2004			Sanfilippo and Nigrini, 1998
	B *Eucyrtidium mitodes*	30.00	Provisional	30.30	Kamikuri et al., 2012					Kamikuri et al., 2012
	B *Lychnocanoma trifolium*	30.02	Gradstein et al., 2012	?		29.93	Gradstein et al., 2004			Sanfilippo and Nigrini, 1998
	T *Dorcadospyris pseudopapilio*	30.48	Gradstein et al., 2012	30.84	Pälike et al., 2006	30.31	Gradstein et al., 2004			Sanfilippo and Nigrini, 1998
	B *Didymocyrtis prismatica*	30.48	Gradstein et al., 2012	29.85↑	Pälike et al., 2006	30.31	Gradstein et al., 2004			Sanfilippo and Nigrini, 1998
	T *Centrobotrys petrushevskayae*	30.94	Gradstein et al., 2012	?		30.70	Gradstein et al., 2004			Sanfilippo and Nigrini, 1998
	B *Centrobotrys thermophila*	30.94	Gradstein et al., 2012	?		30.70	Gradstein et al., 2004			Sanfilippo and Nigrini, 1998
	B *Lychnodictyum audax*	31.40	Gradstein et al., 2012	30.96	Pälike et al., 2006	31.08	Gradstein et al., 2004			Sanfilippo and Nigrini, 1998
	B *Centrobotrys petrushevskayae*	31.86	Gradstein et al., 2012	30.91	Pälike et al., 2006	31.47	Gradstein et al., 2004			Sanfilippo and Nigrini, 1998
	T *Centrobotrys gravida*	31.86	Gradstein et al., 2012	30.91	Pälike et al., 2006	31.47	Gradstein et al., 2004			Sanfilippo and Nigrini, 1998
	B *Dorcadospyris pseudopapilio*	31.86	Gradstein et al., 2012	31.00	Pälike et al., 2006	31.47	Gradstein et al., 2004			Sanfilippo and Nigrini, 1998
	B *Theocyrtis setanios*	31.10	Provisional	31.00	Kamikuri et al., 2012					Kamikuri et al., 2012
	T *Dorcadospyris spinosa*	31.10	Provisional	31.00	Kamikuri et al., 2012					Kamikuri et al., 2012
	B *Dorcadospyris circulus*	31.10	Provisional	31.10	Kamikuri et al., 2012					Kamikuri et al., 2012
RP20c	B *Eucyrtidium plesiodiaphanes*	31.30	Provisional	31.20	Kamikuri et al., 2012					Kamikuri et al., 2012
	T *Theocyrtis tuberosa*	31.30	Provisional	31.20	Kamikuri et al., 2012	?	Gradstein et al., 2004			Kamikuri et al., 2012
	B *Artophormis gracilis*	32.32	Gradstein et al., 2012	?		31.85	Gradstein et al., 2004			Sanfilippo and Nigrini, 1998
	T *Artophormis barbadensis*	32.32	Gradstein et al., 2012	?		31.85	Gradstein et al., 2004			Sanfilippo and Nigrini, 1998
	B *Lithocyclia crux*	32.32	Gradstein et al., 2012	31.01	Pälike et al., 2006	31.85	Gradstein et al., 2004			Sanfilippo and Nigrini, 1998
	B *Dorcadospyris spinosa*	32.78	Provisional	32.40	Kamikuri et al., 2012					Kamikuri et al., 2012
	T *Centrobotrys gravida*	32.78	Gradstein et al., 2012	32.40	Kamikuri et al., 2012	32.24	Gradstein et al., 2004			Kamikuri et al., 2012
	B *Centrobotrys gravida*	32.80	Provisional	33.00	Kamikuri et al., 2012					Kamikuri et al., 2012

Table T3 (continued). (Continued on next page.)

Zone/ Subzone base	Species event	GTS2012 age (Ma)	Calibration reference	Expedition 320 age (Ma)	Calibration reference	GTS2004 age (Ma)	Calibration reference	Cande and Kent (1995) age (Ma)	Calibration reference	Datum reference
	B *Dorcadospyris pseudopapilio*	32.80	Provisional	33.00	Kamikuri et al., 2012					Kamikuri et al., 2012
RP20b	B *Theocyrtis tuberosa*	32.80	Provisional	33.00↑	Kamikuri et al., 2012					Kamikuri et al., 2012
	T *Dictyoprora pirum*	33.24	Gradstein et al., 2012	?		32.62	Gradstein et al., 2004			Sanfilippo and Nigrini, 1998
	B *Phormostichoartus fistula*	33.24	Gradstein et al., 2012	?		32.62	Gradstein et al., 2004			Sanfilippo and Nigrini, 1998
	B *Lophocyrtis oberhaensliae*	33.89	Provisional	33.80	Kamikuri et al., 2012					Kamikuri et al., 2012
RP20a	X *Lithocyclia aristotelis* gr./ *Lithocyclia angusta*	33.89	Gradstein et al., 2012	33.80	Kamikuri et al., 2012	33.01	Gradstein et al., 2004	32.80	Berggren et al., 1995	Kamikuri et al., 2012
	Eocene/Oligocene boundary	33.89	Gradstein et al., 2012	33.80	Pälike et al., 2006	33.90	Gradstein et al., 2004	33.70	Berggren et al., 1995	Sanfilippo and Nigrini, 1998
	T *Calocycletta anekathen*	33.89	Provisional	33.80	Kamikuri et al., 2012					Kamikuri et al., 2012
	T *Cryptocarpium ornatum*	33.89	Gradstein et al., 2012	33.80	Kamikuri et al., 2012	33.01	Gradstein et al., 2004	32.80	Berggren et al., 1995	Kamikuri et al., 2012
	T *Dictyoprora mongolferi*	33.89	Gradstein et al., 2012	33.80	Kamikuri et al., 2012	33.01	Gradstein et al., 2004	32.80	Berggren et al., 1995	Kamikuri et al., 2012
	T *Lychnocanoma amphitrite*	33.89	Gradstein et al., 2012	33.80	Kamikuri et al., 2012	33.01	Gradstein et al., 2004	32.80	Berggren et al., 1995	Kamikuri et al., 2012
	T *Dictyoprora armadillo*	34.13	Gradstein et al., 2012	?		33.51	Gradstein et al., 2004			Sanfilippo and Nigrini, 1998
	T *Lophocyrtis jacchia*	34.55	Gradstein et al., 2012	?		34.01	Gradstein et al., 2004			Sanfilippo and Nigrini, 1998
	B *Lithocyclia angusta*	34.90	Provisional	34.80	Kamikuri et al., 2012					Kamikuri et al., 2012
	T *Calocyclas turris*	34.97	Gradstein et al., 2012	34.83	Pälike et al., 2006	34.50	Gradstein et al., 2004			Sanfilippo and Nigrini, 1998
	B *Lophocyrtis milowi*	34.97	Provisional	34.90	Kamikuri et al., 2012					Kamikuri et al., 2012
	T *Thyrsocyrtis bromia*	34.97	Gradstein et al., 2012	35.18	Pälike et al., 2006	34.50	Gradstein et al., 2004			Sanfilippo and Nigrini, 1998
	T *Eusyringium fistuligerum*	36.39	Gradstein et al., 2012	35.20	Kamikuri et al., 2012	35.80	Gradstein et al., 2004			Kamikuri et al., 2012
	T *Calocyclas bandyca*	35.40	Gradstein et al., 2012	35.20	Kamikuri et al., 2012	35.00	Gradstein et al., 2004	34.90	Berggren et al., 1995	Kamikuri et al., 2012
	T *Cryptocarpium azyx*	34.97	Gradstein et al., 2012	35.30	Kamikuri et al., 2012	34.50	Gradstein et al., 2004			Kamikuri et al., 2012
	T *Calocyclas hispida*	35.40	Gradstein et al., 2012	35.30	Pälike et al., 2006	35.00	Gradstein et al., 2004	34.90	Berggren et al., 1995	Sanfilippo and Nigrini, 1998
	T *Lychnocanoma bellum*	35.40	Gradstein et al., 2012	35.30	Pälike et al., 2006	35.00	Gradstein et al., 2004	34.90	Berggren et al., 1995	Sanfilippo and Nigrini, 1998
	T *Podocyrtis papalis*	35.40	Gradstein et al., 2012	35.30	Pälike et al., 2006	35.00	Gradstein et al., 2004	34.90	Berggren et al., 1995	Sanfilippo and Nigrini, 1998
	T *Thyrsocyrtis rhizodon*	34.97	Gradstein et al., 2012	35.4↓	Pälike et al., 2006	34.50	Gradstein et al., 2004			Sanfilippo and Nigrini, 1998
RP19	B *Lophocyrtis hadra*	35.40	Gradstein et al., 2012	35.40	Kamikuri et al., 2012					Kamikuri et al., 2012
	T *Thyrsocyrtis tetracantha**	35.40	Gradstein et al., 2012	35.40	Kamikuri et al., 2012	35.00	Gradstein et al., 2004	34.90	Berggren et al., 1995	Kamikuri et al., 2012
	T *Thyrsocyrtis lochites**	35.40	Gradstein et al., 2012	35.40	Kamikuri et al., 2012	35.00	Gradstein et al., 2004	34.90	Berggren et al., 1995	Kamikuri et al., 2012
	T *Thyrsocyrtis triacantha*	35.73	Gradstein et al., 2012	35.51	Pälike et al., 2006	35.27	Gradstein et al., 2004			Sanfilippo and Nigrini, 1998
	T *Podocyrtis goetheana*	36.72	Gradstein et al., 2012	?	Pälike et al., 2006	36.06	Gradstein et al., 2004			Sanfilippo and Nigrini, 1998
	B *Lophocyrtis jacchia*	37.00	Provisional	36.80	Kamikuri et al., 2012					Kamikuri et al., 2012
	B *Calocycletta anekathen*	37.05	Gradstein et al., 2012	36.90	Kamikuri et al., 2012					Kamikuri et al., 2012
RP18	B *Calocyclas bandyca*	37.05	Gradstein et al., 2012	36.90	Kamikuri et al., 2012	36.32	Gradstein et al., 2004	36.40	Berggren et al., 1995	Kamikuri et al., 2012
	T *Podocyrtis chalara*	37.22	Gradstein et al., 2012	?	Pälike et al., 2006	36.60	Gradstein et al., 2004			Sanfilippo and Nigrini, 1998
	B *Calocyclas turris*	37.58	Gradstein et al., 2012	?	Pälike et al., 2006	37.15	Gradstein et al., 2004			Sanfilippo and Nigrini, 1998
	T *Calocyclas hispida*	37.58	Gradstein et al., 2012	?	Pälike et al., 2006	37.58	Gradstein et al., 2004			Sanfilippo and Nigrini, 1998

Table T3 (continued). (Continued on next page.)

Zone/ Subzone base	Species event	GTS2012 age (Ma)	Calibration reference	Expedition 320 age (Ma)	Calibration reference	GTS2004 age (Ma)	Calibration reference	Cande and Kent (1995) age (Ma)	Calibration reference	Datum reference
	B *Lychnocanoma amphitrite*	37.40	Gradstein et al., 2012	36.60	Kamikuri et al., 2012	36.87	Gradstein et al., 2004			Kamikuri et al., 2012
	T *Spongatractus pachystylus*	37.75	Provisional	37.90	Pälike et al., 2006	37.58	Gradstein et al., 2004			Sanfilippo and Nigrini, 1998
RP17	B *Cryptocarpium azyx*	37.75	Gradstein et al., 2012	38.00	Kamikuri et al., 2012	37.43	Gradstein et al., 2004	37.70	Berggren et al., 1995	Kamikuri et al., 2012
	T *Calocycloma ampulla*	38.00	Provisional	38.20	Kamikuri et al., 2012					Kamikuri et al., 2012
	T *Anthocyrtoma* spp.	38.20	Provisional	38.40	Kamikuri et al., 2012					Kamikuri et al., 2012
	B *Thyrsocyrtis bromia*	38.55	Gradstein et al., 2012	38.50	Kamikuri et al., 2012	37.73	Gradstein et al., 2004			Kamikuri et al., 2012
	T *Theocotylissa ficus*	38.95	Gradstein et al., 2012	?	Pälike et al., 2006	37.88	Gradstein et al., 2004			Sanfilippo and Nigrini, 1998
	T *Dorcadospyris anastasis*	38.95	Provisional	38.50	Kamikuri et al., 2012					Kamikuri et al., 2012
	B *Thyrsocyrtis tetracantha*	38.95	Gradstein et al., 2012	38.50	Kamikuri et al., 2012	37.88	Gradstein et al., 2004			Kamikuri et al., 2012
	B *Lithocyclia aristotelis* gr.	38.95	Provisional	39.30	Kamikuri et al., 2012	38.19	Gradstein et al., 2004	38.80	Berggren et al., 1995	Kamikuri et al., 2012
	T *Lithochytris vespertilio*	38.95	Provisional	39.60	Kamikuri et al., 2012					Kamikuri et al., 2012
	B *Dictyoprora pirum*	38.95	Gradstein et al., 2012	39.65	Pälike et al., 2006	37.88	Gradstein et al., 2004			Kamikuri et al., 2012
	B *Dictyoprora armadillo*	39.75	Gradstein et al., 2012	39.65↑	Pälike et al., 2006	38.19	Gradstein et al., 2004			Sanfilippo and Nigrini, 1998
	B *Dorcadospyris anastasis*	40.14	Provisional	39.90	Kamikuri et al., 2012					Kamikuri et al., 2012
RP16	B *Podocyrtis goetheana*	40.14	Gradstein et al., 2012	39.90	Kamikuri et al., 2012	38.34	Gradstein et al., 2004	38.80	Berggren et al., 1995	Kamikuri et al., 2012
	T *Sethochytris triconiscus*	40.50	Gradstein et al., 2012	40.10	Kamikuri et al., 2012	38.04	Gradstein et al., 2004			Kamikuri et al., 2012
	T *Lophocyrtis biaurita*	40.50	Provisional	40.80	Kamikuri et al., 2012					Kamikuri et al., 2012
RP15	X *Podocyrtis mitra/ Podocyrtis chalara*	40.65	Gradstein et al., 2012	41.40	Kamikuri et al., 2012	38.93	Gradstein et al., 2004	39.50	Berggren et al., 1995	Kamikuri et al., 2012
	T *Podocyrtis trachodes*	40.65	Gradstein et al., 2012	41.50	Kamikuri et al., 2012	38.64	Gradstein et al., 2004			Kamikuri et al., 2012
	T *Phormocyrtis striata striata*	40.65	Gradstein et al., 2012	47.9↓	Kamikuri et al., 2012	38.93	Gradstein et al., 2004	39.50	Berggren et al., 1995	Kamikuri et al., 2012
	B *Tristylospyris triceros*	40.65	Gradstein et al., 2012	40.70	Berggren et al., 1995	38.93	Gradstein et al., 2004	39.50	Berggren et al., 1995	Sanfilippo and Nigrini, 1998
	B *Cryptocarpium ornatum*	41.33	Gradstein et al., 2012	41.80	Kamikuri et al., 2012	39.66	Gradstein et al., 2004			Kamikuri et al., 2012
	T *Podocyrtis ampla*	42.01	Gradstein et al., 2012	41.67↑	Berggren et al., 1995	40.39	Gradstein et al., 2004			Sanfilippo and Nigrini, 1998
	B *Zealithapium mitra*	42.30	Provisional	41.90	Kamikuri et al., 2012					Kamikuri et al., 2012
	T *Zealithapium anoectum*	42.50	Provisional	42.10	Kamikuri et al., 2012					Kamikuri et al., 2012
	B *Sethochytris triconiscus*	42.69	Gradstein et al., 2012	42.20	Kamikuri et al., 2012	41.11	Gradstein et al., 2004			Kamikuri et al., 2012
	T *Eusyringium lagena*	42.69	Gradstein et al., 2012	42.30	Kamikuri et al., 2012	41.11	Gradstein et al., 2004			Kamikuri et al., 2012
	T *Podocyrtis fasciolata*	42.69	Gradstein et al., 2012	?		41.11	Gradstein et al., 2004			Sanfilippo and Nigrini, 1998
	T *Podocyrtis helenae*	42.69	Gradstein et al., 2012	44.15	Berggren et al., 1995	41.11	Gradstein et al., 2004			Sanfilippo and Nigrini, 1998
	B *Thyrsocyrtis lochites*	42.69	Gradstein et al., 2012	?		41.11	Gradstein et al., 2004			Sanfilippo and Nigrini, 1998
	B *Artophormis barbadensis*	42.69	Gradstein et al., 2012	?		41.11	Gradstein et al., 2004			Sanfilippo and Nigrini, 1998
	B *Podocyrtis helenae*	43.38	Provisional	43.70	Kamikuri et al., 2012	43.18	Gradstein et al., 2004			Kamikuri et al., 2012
RP14	X *Podocyrtis sinuosa/ Podocyrtis mitra*	43.38	Gradstein et al., 2012	43.70	Berggren et al., 1995	41.84	Gradstein et al., 2004	42.80	Berggren et al., 1995	Sanfilippo and Nigrini, 1998
	T *Calocyclas trichopa*	43.38	Provisional	43.70	Kamikuri et al., 2012					Kamikuri et al., 2012
	B *Podocyrtis fasciolata*	43.50	Provisional	43.90	Kamikuri et al., 2012					Kamikuri et al., 2012
	B *Podocyrtis trachodes*	43.59	Gradstein et al., 2012	43.22↑	Berggren et al., 1995	42.17	Gradstein et al., 2004			Sanfilippo and Nigrini, 1998
	T *Podocyrtis dorus*	43.81	Gradstein et al., 2012	?		42.51	Gradstein et al., 2004			Sanfilippo and Nigrini, 1998
	X *Eusyringium lagena/ Eusyringium fistuligerum*	44.03	Gradstein et al., 2012	?		42.85	Gradstein et al., 2004			Sanfilippo and Nigrini, 1998

Table T3 (continued). (Continued on next page.)

Zone/ Subzone base	Species event	GTS2012 age (Ma)	Calibration reference	Expedition 320 age (Ma)	Calibration reference	GTS2004 age (Ma)	Calibration reference	Cande and Kent (1995) age (Ma)	Calibration reference	Datum reference
	B *Podocyrtis fasciolata*	44.25	Gradstein et al., 2012	43.87	Berggren et al., 1995	43.18	Gradstein et al., 2004			Sanfilippo and Nigrini, 1998
	B *Eusyringium fistuligerum*	44.46	Sanfilippo and Blome, 2001	44.30	Kamikuri et al., 2012	44.60	Gradstein et al., 2004			Kamikuri et al., 2012
	B *Calocyclas trichopa*	44.46	Provisional	44.40	Kamikuri et al., 2012					Kamikuri et al., 2012
RP13	X *Podocyrtis phyxis/ Podocyrtis ampla*	44.46	Gradstein et al., 2012	44.60	Kamikuri et al., 2012	43.52	Gradstein et al., 2004	44.50	Berggren et al., 1995	Kamikuri et al., 2012
	T *Theocorys plesioanaclasta*	44.46	Provisional	44.70	Kamikuri et al., 2012					Kamikuri et al., 2012
	T *Theocotyle venezuelensis*	44.46	Gradstein et al., 2012	44.77	Berggren et al., 1995	43.52	Gradstein et al., 2004	44.50	Berggren et al., 1995	Sanfilippo and Nigrini, 1998
	T *Podocyrtis diamesa*	45.63	Gradstein et al., 2012	44.44↑	Berggren et al., 1995	45.68	Gradstein et al., 2004			Sanfilippo and Nigrini, 1998
	T *Theocotyle nigriniae*	45.63	Gradstein et al., 2012	?		45.68	Gradstein et al., 2004			Sanfilippo and Nigrini, 1998
	T *Periphaena tripyramis triangula*	45.63	Provisional	45.30	Kamikuri et al., 2012					Kamikuri et al., 2012
	T *Theocotyle conica*	45.63	Gradstein et al., 2012	45.32	Berggren et al., 1995	45.68	Gradstein et al., 2004			Sanfilippo and Nigrini, 1998
	T *Lamptonium fabaeforme constrictum*	45.63	Gradstein et al., 2012	45.62	Berggren et al., 1995	45.68	Gradstein et al., 2004			Sanfilippo and Nigrini, 1998
	T *Thyrsocyrtis robusta*	45.63	Gradstein et al., 2012	46.16	Berggren et al., 1995	45.68	Gradstein et al., 2004			Sanfilippo and Nigrini, 1998
	T *Thyrsocyrtis hirsuta*	45.63	Gradstein et al., 2012	46.19	Berggren et al., 1995	45.68	Gradstein et al., 2004			Sanfilippo and Nigrini, 1998
	B *Podocyrtis phyxis*	45.63	Gradstein et al., 2012	46.44	Berggren et al., 1995	45.68	Gradstein et al., 2004			Sanfilippo and Nigrini, 1998
	T *Lamptonium fabaeforme chaunothorax*	45.63	Gradstein et al., 2012	46.61	Berggren et al., 1995	45.68	Gradstein et al., 2004			Sanfilippo and Nigrini, 1998
	B *Calocycloma ampulla*	46.21	Provisional	45.70	Kamikuri et al., 2012					Kamikuri et al., 2012
	B *Lychnocanoma bajunensis*	46.21	Provisional	45.70	Kamikuri et al., 2012					Kamikuri et al., 2012
	B *Rhopalocanium ornatum*	46.21	Provisional	45.70	Kamikuri et al., 2012					Kamikuri et al., 2012
	X *Thyrsocyrtis tensa/ Thyrsocyrtis triacantha*	46.21	Gradstein et al., 2012	45.70	Berggren et al., 1995	46.76	Gradstein et al., 2004	47.50	Berggren et al., 1995	Sanfilippo and Nigrini, 1998
RP12	B *Eusyringium lagena*	46.21	Gradstein et al., 2012	45.70	Kamikuri et al., 2012	46.76	Gradstein et al., 2004	47.50	Berggren et al., 1995	Kamikuri et al., 2012
	T *Calocycloma castum*	46.21	Provisional	45.70	Kamikuri et al., 2012	47.94	Gradstein et al., 2004	48.50	Berggren et al., 1995	Kamikuri et al., 2012
	T *Lamptonium fabaeforme fabaeforme*	46.80	Gradstein et al., 2012	45.88↑	Berggren et al., 1995	47.16	Gradstein et al., 2004			Sanfilippo and Nigrini, 1998
	T *Theocorys anaclasta*	49.00	Provisional	46.40	Kamikuri et al., 2012	45.68	Gradstein et al., 2004			Kamikuri et al., 2012
	B *Theocorys anaclasta*	50.05	Gradstein et al., 2012	47.40	Kamikuri et al., 2012	50.14	Gradstein et al., 2004	50.30	Berggren et al., 1995	Kamikuri et al., 2012
	B *Podocyrtis dorus*	46.80	Gradstein et al., 2012	?		47.16	Gradstein et al., 2004			Sanfilippo and Nigrini, 1998
	X *Theocotyle cryptocephala/ Theocotyle conica*	47.39	Gradstein et al., 2012	49.74↓	Berggren et al., 1995	47.55	Gradstein et al., 2004			Sanfilippo and Nigrini, 1998
	B *Zealithapium plegmacantha*	47.90	Provisional	47.80	Kamikuri et al., 2012					Kamikuri et al., 2012
	T *Buryella clinata*	47.90	Provisional	47.80	Berggren et al., 1995	48.60	Gradstein et al., 2004	49.00	Berggren et al., 1995	Sanfilippo and Nigrini, 1998
RP11	B *Dictyoprora mongolfieri*	47.98	Gradstein et al., 2012	47.90	Kamikuri et al., 2012	47.94	Gradstein et al., 2004	48.50	Berggren et al., 1995	Kamikuri et al., 2012
	T *Lithochytris archaea*	47.98	Provisional	47.90	Kamikuri et al., 2012					Kamikuri et al., 2012
	T *Podocyrtis acalles*	48.13	Gradstein et al., 2012	?		48.11	Gradstein et al., 2004			Sanfilippo and Nigrini, 1998
	B *Podocyrtis sinuosa*	48.13	Gradstein et al., 2012	?		48.11	Gradstein et al., 2004			Sanfilippo and Nigrini, 1998

Table T3 (continued). (Continued on next page.)

Zone/ Subzone base	Species event	GTS2012 age (Ma)	Calibration reference	Expedition 320 age (Ma)	Calibration reference	GTS2004 age (Ma)	Calibration reference	Cande and Kent (1995) age (Ma)	Calibration reference	Datum reference
	B *Thyrsocyrtis robusta*	48.27	Gradstein et al., 2012	?		48.27	Gradstein et al., 2004			Sanfilippo and Nigrini, 1998
	B *Theocotyle venezuelensis*	48.42	Gradstein et al., 2012	?		48.44	Gradstein et al., 2004			Sanfilippo and Nigrini, 1998
	B *Lithochytris vespertilio*	48.57	Gradstein et al., 2012	49.00	Kamikuri et al., 2012					Kamikuri et al., 2012
	B *Lithocyclia ocellus* gr.	48.57	Gradstein et al., 2012	49.00	Kamikuri et al., 2012					Kamikuri et al., 2012
RP10	X *Theocotyle nigriniae/ heocotyle cryptocephala*	48.57	Gradstein et al., 2012	49.00	Berggren et al., 1995	48.60	Gradstein et al., 2004	49.00	Berggren et al., 1995	Sanfilippo and Nigrini, 1998
	X *Spongatractus balbis/ Spongatractus pachystylus*	48.86	Gradstein et al., 2012	49.74*	Berggren et al., 1995	48.91	Gradstein et al., 2004			Sanfilippo and Nigrini, 1998
	T *Lamptonium sanfilippoae*	49.16	Gradstein et al., 2012	49.74*	Berggren et al., 1995	49.22	Gradstein et al., 2004			Sanfilippo and Nigrini, 1998
	B *Thyrsocyrtis rhizodon*	49.46	Gradstein et al., 2012	49.74*	Berggren et al., 1995	49.53	Gradstein et al., 2004			Sanfilippo and Nigrini, 1998
	B *Podocyrtis diamesa*	49.75	Gradstein et al., 2012	49.74*	Berggren et al., 1995	49.83	Gradstein et al., 2004			Sanfilippo and Nigrini, 1998
	B *Dictyophimus craticula*	50.05	Provisional	49.90	Kamikuri et al., 2012					Kamikuri et al., 2012
	B *Periphaena tripyramis triangula*	50.05	Provisional	49.90	Kamikuri et al., 2012					Kamikuri et al., 2012
RP9	B *Theocorys plesioanaclasta*	50.05	Gradstein et al., 2012	49.90	Berggren et al., 1995	50.14	Gradstein et al., 2004	50.30	Berggren et al., 1995	Kamikuri et al., 2012
	B *Podocyrtis acalles*	50.05	Gradstein et al., 2012	50*	Berggren et al., 1995	50.14	Gradstein et al., 2004	50.30	Berggren et al., 1995	Sanfilippo and Nigrini, 1998
	B *Lychnocanoma bellum*	50.05	Gradstein et al., 2012	50*	Berggren et al., 1995	50.14	Gradstein et al., 2004	50.30	Berggren et al., 1995	Sanfilippo and Nigrini, 1998
	B *Lamptonium fabaeforme constrictum*	50.05	Gradstein et al., 2012	50*	Berggren et al., 1995	50.14	Gradstein et al., 2004	50.30	Berggren et al., 1995	Sanfilippo and Nigrini, 1998
	X *Phormocyrtis striata exquisita/P. striata striata*	50.05	Gradstein et al., 2012	50*	Berggren et al., 1995	50.14	Gradstein et al., 2004	50.30	Berggren et al., 1995	Sanfilippo and Nigrini, 1998
	T *Phormocyrtis cubensis*	50.05	Gradstein et al., 2012	50*	Berggren et al., 1995	50.14	Gradstein et al., 2004	50.30	Berggren et al., 1995	Sanfilippo and Nigrini, 1998
	T *Phormocyrts turgida*	50.87	Sanfilippo and Blome, 2001							Sanfilippo and Nigrini, 1998
	T *Bekoma bidartensis*	50.87	Gradstein et al., 2012			50.91	Gradstein et al., 2004			Sanfilippo and Nigrini, 1998
	T *Buryella tetradica*	50.87	Gradstein et al., 2012			50.91	Gradstein et al., 2004			Sanfilippo and Nigrini, 1998
	T *Pterocodon*(?) *ampla*	50.87	Gradstein et al., 2012			50.91	Gradstein et al., 2004			Sanfilippo and Nigrini, 1998
	T *Thyrsocyrtis tarsipes*	50.87	Gradstein et al., 2012			50.91	Gradstein et al., 2004			Sanfilippo and Nigrini, 1998
	T *Theocotylissa alpha* (RP9?)	51.70	Gradstein et al., 2012			51.69	Gradstein et al., 2004			Sanfilippo and Nigrini, 1998
	B *Thyrsocyrtis tensa*	51.70	Gradstein et al., 2012			51.69	Gradstein et al., 2004			Sanfilippo and Nigrini, 1998
	B *Theocotylissa ficus*	51.70	Gradstein et al., 2012			51.69	Gradstein et al., 2004			Sanfilippo and Nigrini, 1998
	B *Calocyclas hispida*	52.52	Gradstein et al., 2012			52.46	Gradstein et al., 2004			Sanfilippo and Nigrini, 1998
RP8	X *Pterocodon*(?) *anteclinata/ Buryella clinata*	53.35	Gradstein et al., 2012	52.9*	Berggren et al., 1995	53.23	Gradstein et al., 2004	52.85	Berggren et al., 1995	Sanfilippo and Nigrini, 1998
	B *Spongatractus balbis*	53.35	Gradstein et al., 2012	52.9*	Berggren et al., 1995	53.23	Gradstein et al., 2004	52.85	Berggren et al., 1995	Sanfilippo and Nigrini, 1998

Table T3 (continued). (Continued on next page.)

Zone/ Subzone base	Species event	GTS2012 age (Ma)	Calibration reference	Expedition 320 age (Ma)	Calibration reference	GTS2004 age (Ma)	Calibration reference	Cande and Kent (1995) age (Ma)	Calibration reference	Datum reference
	B *Lamptonium sanfilippoae*	53.35	Gradstein et al., 2012	52.9*	Berggren et al., 1995	53.23	Gradstein et al., 2004	52.85	Berggren et al., 1995	Sanfilippo and Nigrini, 1998
	B *Theocotyle nigriniae*	53.35	Gradstein et al., 2012	52.9*	Berggren et al., 1995	53.23	Gradstein et al., 2004	52.85	Berggren et al., 1995	Sanfilippo and Nigrini, 1998
	B *Thyrsocyrtis hirsuta*	53.35	Gradstein et al., 2012	52.9*	Berggren et al., 1995	53.23	Gradstein et al., 2004	52.85	Berggren et al., 1995	Sanfilippo and Nigrini, 1998
	B *Theocotylissa alpha*	54.04	Gradstein et al., 2012			53.87	Gradstein et al., 2004			Sanfilippo and Nigrini, 1998
	B *Lamptonium fabaeforme chaunothorax*	54.74	Gradstein et al., 2012			54.51	Gradstein et al., 2004			Sanfilippo and Nigrini, 1998
	B *Calocycloma castum*	55.40	Sanfilippo and Blome, 2001			55.79	Sanfilippo and Blome, 2001			Sanfilippo and Nigrini, 1998
	B *Lophocyrtis jacchia*	55.44	Gradstein et al., 2012			55.15	Gradstein et al., 2004			Sanfilippo and Nigrini, 1998
	B *Pterocodon*(?) *anteclinata*	55.44	Sanfilippo and Blome, 2001			55.15	Sanfilippo and Blome, 2001			Sanfilippo and Nigrini, 1998
	T *Stylosphaera goruna*	55.50	Sanfilippo and Blome, 2001			55.20	Sanfilippo and Blome, 2001			Sanfilippo and Nigrini, 1998
	X *Lamptonium pennatum*/ *Lamptonium fabaeforme fabaeforme* (ET)	55.90	Sanfilippo and Blome, 2001			55.79	Gradstein et al., 2004			Sanfilippo and Nigrini, 1998
	B *Theocorys phyzella*	55.90	Sanfilippo and Blome, 2001			55.79	Sanfilippo and Blome, 2001			Sanfilippo and Nigrini, 1998
	B *Phormocyrtis turgida*	55.96	Sanfilippo and Blome, 2001			55.80	Sanfilippo and Blome, 2001			Sanfilippo and Nigrini, 1998
	Paleocene/Eocene boundary	55.96	Gradstein et al., 2012	55.00	Berggren et al., 1995	55.80	Gradstein et al., 2004	55.50	Berggren et al., 1995	Sanfilippo and Nigrini, 1998
	B *Lamptonium fabaeforme fabaeforme*	56.14	Gradstein et al., 2013			56.00	Sanfilippo and Blome, 2001			Sanfilippo and Nigrini, 1998
	B *Amphicraspedum prolixum*	56.14	Sanfilippo and Blome, 2001			56.00	Sanfilippo and Blome, 2001			Sanfilippo and Nigrini, 1998
	T *Bekoma campechensis*	57.53	Gradstein et al., 2012			57.07	Gradstein et al., 2004			Sanfilippo and Nigrini, 1998
RP7	X *Bekoma campechensis*/ *Bekoma bidartensis*	58.23	Gradstein et al., 2012			57.71	Gradstein et al., 2004			Nishimura, 1992
	B *Podocyrtis papalis* (early form)	58.50	Provisional			56.43	Sanfilippo and Blome, 2001			Nishimura, 1992
	B *Phormocyrtis cubensis*	58.61	Gradstein et al., 2012			58.07	Gradstein et al., 2004			Sanfilippo and Nigrini, 1998
RP6c	B *Stylotrochus nitidus* or *Pterocodon*? *poculum*	59.00	Gradstein et al., 2012			58.43	Gradstein et al., 2004			Sanfilippo and Nigrini, 1998
	T *Buryella pentadica*	59.71	Gradstein et al., 2012			59.21	Gradstein et al., 2004	56.90	Berggren et al., 1995	Sanfilippo and Nigrini, 1998
RP6b	T *Peritiviator*? *dumitricai*	60.40	Gradstein et al., 2012			59.99	Gradstein et al., 2004	57.80	Berggren et al., 1995	Sanfilippo and Nigrini, 1998
	B *Pterocodon*(?) *ampla*	60.97	Gradstein et al., 2012			60.47	Gradstein et al., 2004	59.20	Berggren et al., 1995	Sanfilippo and Nigrini, 1998
RP6a	B *Bekoma campechensis*	61.50	Gradstein et al., 2012			60.95	Gradstein et al., 2004	60.20	Berggren et al., 1995	Sanfilippo and Nigrini, 1998
RP5	B *Buryella tetradica*	62.20	Gradstein et al., 2012			61.65	Gradstein et al., 2004	60.90	Berggren et al., 1995	Hollis, 2002
	B *Amphisphaera coronata*	63.00	Hollis, 2002			62.50	Hollis, 2002	61.90	Hollis, 2002	Hollis, 2002
RP4	B *Buryella foremanae*	63.90	Gradstein et al., 2012			63.38	Gradstein et al., 2004	62.80	Berggren et al., 1995	Hollis, 2002

Table T3 (continued).

Zone/ Subzone base	Species event	GTS2012 age (Ma)	Calibration reference	Expedition 320 age (Ma)	Calibration reference	GTS2004 age (Ma)	Calibration reference	Cande and Kent (1995) age (Ma)	Calibration reference	Datum reference
RP3	B *Buryella granulata*	64.90	Gradstein et al., 2012			64.37	Gradstein et al., 2004	63.90	Berggren et al., 1995	Hollis, 1997
RP2	B *Amphisphaera kina*	65.55	Gradstein et al., 2012			64.99	Gradstein et al., 2004	64.60	Berggren et al., 1995	Sanfilippo and Nigrini, 1998
RP1	B *Amphisphaera aotea*	66.04	Gradstein et al., 2012			65.50	Gradstein et al., 2004	65.00	Berggren et al., 1995	Sanfilippo and Nigrini, 1998
	Cretaceous/Paleogene boundary	66.04	Gradstein et al., 2012		Berggren et al., 1995	65.50	Gradstein et al., 2004	65.00	Berggren et al., 1995	Berggren et al., 1995
	B *Orbiculiforma renillaeformis*	72.00	Gradstein et al., 2012				Gradstein et al., 2004			Pessagno, 1976
	Campanian/Maastrichtian boundary	72.05	Gradstein et al., 2012				Gradstein et al., 2004			
RK9	B *Amphipyndax tylotus*	75.00	Gradstein et al., 2012				Gradstein et al., 2004			Sanfilippo and Riedel, 1985

* = event poorly constrained near base of hole. GTS2012 = geomagnetic timescale of Gradstein et al. (2012), GTS2004 = geomagnetic timescale of Gradstein et al. (2004). B = bottom, T = top, X = faunal crossover (>50% descendent). Provisional ages based on Kamikuri et al. (2012). ↑ = recorded earlier than indicated by Gradstein et al. (2012). ↓ = recorded later than indicated by Gradstein et al. (2012).

Table T4. Taxonomic list for calcareous nannofossil datums, Expedition 342. (Continued on next page.)

Biantholithus sparsus Bramlette and Martini, 1964
Broinsonia parca constricta Hattner et al., 1980
Calcidiscus macintyrei (Bukry and Bramlette, 1969) Loeblich and Tappan, 1978
Calcidiscus premacintyrei Theodoridis, 1984
Catinaster calyculus Martini and Bramlette, 1963
Catinaster coalitus Martini and Bramlette, 1963
Ceratolithoides kamptneri Bramlette and Martini, 1964
Ceratolithus acutus Gartner and Bukry, 1974
Ceratolithus larrymayeri Backman and Raffi, 1998
Ceratolithus rugosus Bukry and Bramlette, 1968
Chiasmolithus bidens (Bramlette and Sullivan, 1961) Hay and Mohler, 1967
Chiasmolithus danicus (Brotzen, 1959) Hay and Mohler, 1967
Chiasmolithus edentulus van Heck and Prins, 1987
Chiasmolithus gigas (Bramlette and Sullivan, 1961) Radomski, 1968
Chiasmolithus grandis (Bramlette and Riedel, 1954) Radomski, 1968
Chiasmolithus oamaruensis (Deflandre, 1954) Hay et al., 1966
Chiasmolithus solitus (Bramlette and Sullivan, 1961) Locker, 1968
Coccolithus formosus (Kamptner, 1963) Wise, 1973
Coccolithus miopelagicus Bukry, 1971
Coccolithus pelagicus (Wallich, 1877) Schiller, 1930
Coronocyclus nitescens (Kamptner, 1963) Bramlette and Wilcoxon, 1967
Cribrocorona gallica (Stradner, 1963) Perch-Nielsen, 1973
Cribrosphaerella daniae Perch-Nielsen, 1973
Cruciplacolithus intermedius van Heck and Prins, 1987
Cruciplacolithus primus Perch-Nielsen, 1977
Cruciplacolithus tenuis (Stradner, 1961) Hay and Mohler in Hay et al., 1967
Cyclicargolithus floridanus (Roth and Hay in Hay et al., 1967) Bukry, 1971
Dictyococcites bisectus (Hay et al., 1966) Bukry and Percival, 1971
Discoaster backmanii Agnini et al., 2008
Discoaster barbadiensis Tan, 1927
Discoaster berggrenii Bukry, 1971
Discoaster brouweri Tan, 1927, emend. Bramlette and Riedel, 1954
Discoaster deflandrei Bramlette and Riedel, 1954
Discoaster delicatus Bramlette and Sullivan, 1961
Discoaster diastypus Bramlette and Sullivan, 1961
Discoaster hamatus Martini and Bramlette, 1963
Discoaster kugleri Martini and Bramlette, 1963
Discoaster lodoensis Bramlette and Riedel, 1954
Discoaster mohleri Bramlette and Percival, 1971
Discoaster multiradiatus Bramlette and Riedel, 1954
Discoaster nobilis Martini, 1961
Discoaster okadai Bukry, 1981
Discoaster pentaradiatus Tan, 1927
Discoaster quinqueramus Gartner, 1969
Discoaster saipanensis Bramlette and Riedel, 1954
Discoaster sublodoensis Bramlette and Sullivan, 1961
Discoaster surculus Martini and Bramlette, 1963
Discoaster tamalis Kamptner, 1967
Discoaster triradiatus Tan, 1927
Eiffellithus eximius (Stover, 1966) Perch-Nielsen, 1968
Ellipsolithus macellus (Bramlette and Sullivan, 1961) Sullivan, 1964
Emiliania huxleyi (Lohmann, 1902) Hay and Mohler in Hay et al., 1967
Ericsonia robusta (Bramlette and Sullivan, 1961) Edwards and Perch-Nielsen, 1975
Fasciculithus alanii Perch-Nielsen, 1971
Fasciculithus clinatus Bukry, 1971
Fasciculithus richardii Perch-Nielsen, 1971
Fasciculithus tympaniformis Hay and Mohler in Hay et al., 1967
Girgisia gammation (Bramlette and Sullivan, 1961) Varol, 1989
Helicosphaera ampliaperta Bramlette and Wilcoxon, 1967
Helicosphaera euphratis Haq, 1966
Helicosphaera sellii (Bukry and Bramlette 1969) Jafar and Martini, 1975
Heliolithus cantabriae Perch-Nielsen, 1971
Heliolithus kleinpellii Sullivan, 1964
Isthmolithus recurvus Deflandre in Deflandre and Fert, 1954
Lithraphidites quadratus Bramlette and Martini, 1964
Micula murus (Martini, 1961) Bukry, 1973
Micula prinsii Perch-Nielsen, 1979
Monomarginatus quaternarius Wind and Wise in Wise and Wind, 1977
Nannotetrina cristata (Martini, 1958) Perch-Nielsen, 1971

Table T4 (continued).

Nannotetrina fulgens (Stradner, 1960) Achuthan and Stradner, 1969
Neobiscutum parvulum (Romein, 1979) Varol, 1989
Neochiastozygus perfectus Perch-Nielsen, 1981
Nephrolithus frequens Górka, 1957
Nicklithus amplificus (Bukry and Percival, 1971) Raffi et al., 1998
Prinsius dimorphosus (Perch-Nielsen, 1969) Perch-Nielsen, 1977
Prinsius tenuiculus (Okada and Thierstein, 1979) Perch-Nielsen, 1981
Pseudoemiliania lacunosa (Kamptner, 1963) Gartner, 1969
Reinhardtites anthophorus (Deflandre, 1959) Perch-Nielsen, 1968
Reinhardtites levis Prins and Sissingh in Sissingh, 1977
Reticulofenestra asanoi Sato and Takayama, 1992
Reticulofenestra pseudoumbilicus (Gartner, 1967) Gartner, 1969
Reticulofenestra reticulata (Gartner and Smith, 1967) Roth and Thierstein, 1972
Reticulofenestra umbilicus (Levin, 1965) Martini and Ritzkowski, 1968
Rhomboaster bramlettei (Brönimann and Stradner, 1960) Bybell and Self-Trail, 1995
Sphenolithus anarrhopus Bukry and Bramlette, 1969
Sphenolithus belemnos Bramlette and Wilcoxon, 1967
Sphenolithus ciperoensis Bramlette and Wilcoxon, 1967
Sphenolithus delphix Bukry, 1973
Sphenolithus disbelemnos Fornaciari and Rio, 1996
Sphenolithus distentus (Martini, 1965) Bramlette and Wilcoxon, 1967
Sphenolithus furcatolithoides Locker, 1967
Sphenolithus heteromorphosus Deflandre, 1953
Sphenolithus moriformis (Brönimann and Stradner, 1960) Bramlette and Wilcoxon, 1967
Sphenolithus predistentus Bramlette and Wilcoxon, 1967
Sphenolithus radians Deflandre in Grassé 1952
Toweius pertusus (Sullivan, 1965) Romein, 1979
Tranolithus orionatus (Reinhardt, 1966a) Reinhardt, 1966b
Tribrachiatus contortus (Stradner, 1958) Bukry, 1972
Tribrachiatus orthostylus Shamrai, 1963
Triquetrorhabdulus carinatus Martini, 1965
Triquetrorhabdulus rugosus Bramlette and Wilcoxon, 1967
Uniplanarius trifidus (Stradner in Stradner and Papp, 1961) Hattner and Wise, 1980

Table T5. Taxonomic species list for planktonic foraminifer datums. Expedition 342. (Continued on next three pages.)

Abathomphalus intermedius (Bolli, 1951)
Abathomphalus mayaroensis (Bolli, 1951)
Acarinina acarinata (Subbotina, 1953)
Acarinina aspensis (Colom, 1954)
Acarinina broedermanni (Cushman and Bermudez)
Acarinina bullbrooki (Bolli)
Acarinina coalingensis (Cushman and Hanra, 1922)
Acarinina collactea (Finlay, 1939)
Acarinina cuneicamerata (Blow, 1979)
Acarinina mcgowrani Wade and Pearson, 2006
Acarinina mckannai (White, 1928)
Acarinina medizzai (Tourmarkine and Bolli, 1975)
Acarinina primitiva (Finlay, 1947)
Acarinina pseudotopilensis (Subbotina, 1953)
Acarinina quetra (Bolli, 1957)
Acarinina rohri (Bronnimann and Bermudez, 1953)
Acarinina sibaiyaensis (El Naggar, 1966)
Acarinina soldadoensis (Bronnimann, 1952)
Acarinina soldadoensis angulosa (Bolli, 1957)
Acarinina spp. (Subbotina, 1953)
Acarinina subsphaerica (Subbotina, 1947)
Acarinina topilensis (Cushman, 1925)
Acarinina wilcoxensis (Cushman and Ponton, 1932)
Archaeoglobigerina australis (Huber, 1990)
Archaeoglobigerina blowi (Pessagno, 1967)
Archaeoglobigerina bosquensis (Pessagno, 1967)
Archaeoglobigerina cretacea (d'Orbigny, 1840)
Bolliella calida (Parker, 1962)
Bolliella praeadamsi (Chaproniere, 1991)
Candeina nitida (d'Orbigny, 1839)
Cassigerinella chipolensis (Cushman and Ponton, 1932)
Cassigerinella martinezpicoi (Bermudez and Seiglie, 1967)
Catapsydrax dissimilis (Cushman and Bermudez)
Catapsydrax stainforthi Bolli, Loeblich, and Tappan, 1957
Catapsydrax unicavus Bolli, Loeblich, and Tappan, 1957
Chiloguembelina cubensis (Palmer, 1934)
Chiloguembelina martini (Pijpers, 1933 as *Textularia*)
Chiloguembelina midwayensis (Cushman, 1940)
Chiloguembelina sp. (Carter, McCave, Richter, Carter, et al., 1999)
Chiloguembelina wilcoxensis (Cushman and Ponton, 1932)
Clavatorella bermudezi (Bolli, 1957)
Clavigerinella akersi (Bolli, Loeblich, and Tappan, 1957)
Clavigerinella columbiana (Petters, 1954)
Clavigerinella eocanica (Nuttall, 1928)
Clavigerinella jarvisi (Cushman, 1930)
Contusotruncana contusa (Cushman, 1926)
Contusotruncana fornicata (Plummer, 1931)
Contusotruncana patelliformis (Gandolfi, 1955)
Contusotruncana plummerae (Gandolfi, 1955)
Cribrohantkenina inflata (Howe, 1928)
Dentoglobigerina sellii (Borsetti, 1959)
Dentoglobigerina tapuriensis (Blow and Banner, 1962)
Dicarinella asymetrica (Sigal, 1952)
Dicarinella concavata (Brotzen, 1934)
Falsotruncana maslakovae (Caron, 1981)
Fohsella birnageae (Blow, 1959)
Fohsella fohsi fohsi (Cushman and Ellisor, 1939)
Fohsella fohsi lobata (Bermudez, 1939)
Fohsella lenguaensis (Bolli, 1957)
Fohsella peripheroacuta (Blow and Banner, 1966)
Fohsella peripheroronda (Blow and Banner, 1966)
Fohsella praefohsi (Blow and Banner, 1966)
Fohsella robusta (Bolli, 1950)
Gansserina gansseri (Bolli, 1951)
Globanomalina australiformis (Jenkins, 1966)
Globanomalina compressa (Plummer, 1926)
Globanomalina imitata (Subbotina, 1953)
Globanomalina pseudomenardii (Bolli, 1957)
Globigerina ampliapertura (Bolli, 1957)
Globigerina angulisuturalis (Bolli, 1957)

Table T5 (continued). (Continued on next page.)

Globigerina decoraperta (Takayanagi and Saito, 1962)
Globigerina nepenthes (Todd, 1957)
Globigerina ouachitaensis (Howe and Wallace, 1932)
Globigerinatella insueta (Cushman and Stainforth, 1945)
Globigerinatheka index (Finlay, 1939)
Globigerinatheka kugleri (Bolli, Loeblich, and Tappan, 1957)
Globigerinatheka mexicana (Cushman, 1925)
Globigerinatheka semiinvoluta (Keijzer, 1945)
Globigerinatheka subconglobata (Shutskaya, 1958)
Globigerinatheka tropicalis (Blow and Banner, 1962)
Globigerinella calida
Globigerinelloides ultramicrus (Subbotina, 1949)
Globigerinoides altiapertura (Bolli, 1957)
Globigerinoides conglobatus (Brady, 1879)
Globigerinoides extremus (Bolli and Bermudez, 1965)
Globigerinoides fistulosus (Schubert, 1910)
Globigerinoides obliquus (Bolli, 1957)
Globigerinoides primordius (Blow and Banner, 1962)
Globigerinoides quadrilobatus (d'Orbigny, 1846)
Globigerinoides seigliei (Bermudez and Bolli, 1969)
Globoconella conoidea (Walters, 1965)
Globoconella conomiozea (Kennett, 1966)
Globoconella inflata (d'Orbigny, 1839)
Globoconella miozea (Finlay, 1939)
Globoconella praescitula (Blow, 1959)
Globoconella sphericomiozea (Walters, 1965)
Globoconella zealandica (Hornibrook, 1958)
Globoconusa daubjergensis (Bronnimann, 1953)
Globoquadrina altispira altispira (Cushman and Jarvis, 1936)
Globoquadrina baroemoenensis (LeRoy, 1939)
Globoquadrina binaiensis (Koch, 1935)
Globoquadrina dehiscens (Chapman, Parr, and Collins, 1934)
Globoquadrina globularis (Bermudez, 1961)
Globorotalia archeomenardii (Bolli, 1957)
Globorotalia crassaformis crassaformis (Galloway and Wissler, 1927)
Globorotalia exilis (Blow, 1969)
Globorotalia excelsa (Sprovieri, 1980)
Globorotalia flexuosa (Koch, 1923)
Globorotalia hessi (Bolli and Premoli Silva, 1973)
Globorotalia hirsuta
Globorotalia lenguaensis (Bolli, 1957)
Globorotalia limbata (Fornasini, 1902 as *Rotalia*)
Globorotalia menardii (Parker, Jones, and Brady, 1865)
Globorotalia merotumida (Blow and Banner, 1965)
Globorotalia miocenica (Palmer, 1945)
Globorotalia miotumida (Jenkins, 1960)
Globorotalia miozea (Finlay, 1939)
Globorotalia multicamerata (Cushman and Jarvis, 1930)
Globorotalia pertenuis (Beard, 1969)
Globorotalia plesiotumida (Blow and Banner, 1965)
Globorotalia praemenardii (Cushman and Stainforth, 1945)
Globorotalia praescitula (Blow, 1959)
Globorotalia ronda (Stainforth et al., 1975)
Globorotalia semivera (Hornibrook, 1961)
Globorotalia tosaensis (Takayanagi and Saito, 1962)
Globorotalia truncatulinoides (d'Orbigny, 1839)
Globorotalia tumida (Brady, 1877)
Globorotaloides carcoselleensis (Toumarkine and Bolli, 1975)
Globotruncana aegyptiaca (Nakkady, 1950)
Globotruncana arca (Cushman, 1926)
Globotruncana linneiana (d'Orbigny, 1839)
Globotruncana ventricosa (White, 1928)
Globotruncanella havanensis (Voorwijk, 1937)
Globotruncanita atlantica (Caron, 1972)
Globotruncanita calcarata (Cushman, 1927)
Globoturborotalita apertura
Globoturborotalita nepenthes (Todd, 1957)
Globoturborotalita obliquas
Globoturborotalita woodi (Jenkins, 1960)
Guembelitria cretacea (Cushman, 1933)
Guembelitrioides nuttali (Hamilton, 1953)

Table T5 (continued). (Continued on next page.)

Hantkenina alabamensis (Cushman, 1925)
Hantkenina mexicana (Cushman, 1925)
Hantkenina nuttalli (Toumarkine, 1981)
Hantkenina singanoae Pearson and Coxall, 2006
Hantkenina spp. (Cushman, 1925)
Hirsutella cibaoensis (Bermudez, 1949)
Hirsutella juanai (Bermudez and Bolli, 1969)
Hirsutella margaritae (Bolli and Bermudez, 1965)
Igorina albeari (Cushman and Bermudez, 1949)
Igorina broedermanni (Cushman and Bermudez, 1949)
Igorina pusilla (Bolli, 1957)
Morozovella acuta (Toulmin, 1941)
Morozovella aequa (Cushman and Renz, 1942)
Morozovella allisonensis (Kelly, Bralower, and Zachos, 1996)
Morozovella angulata (White, 1928)
Morozovella apanthesma (Loeblich and Tappan, 1957)
Morozovella aragonensis (Nuttall, 1930)
Morozovella broedermanni (Cushman and Bermudez, 1949)
Morozovella caucasica (Glaessner, 1937)
Morozovella conicotruncata (Subbotina, 1947)
Morozovella formosa (Bolli, 1957)
Morozovella gracilis (Bolli, 1957)
Morozovella lensiformis (Subbotina, 1953)
Morozovella marginodentata (Subbotina, 1953)
Morozovella praeangulata (Blow, 1979)
Morozovella praecursoria (Morozova, 1957)
Morozovella quetra (Bolli, 1957)
Morozovella spinulosa (Cushman, 1927)
Morozovella subbotinae (Morozova, 1929)
Morozovella velascoensis (Cushman, 1925)
Morozovelloides crassatus Cushman, 1925
Morozovelloides lehneri Cushman and Jaris, 1929
Muricoglobigerina senni (Beckman, 1953)
Neogloboquadrina acostaensis (Blow, 1959)
Neogloboquadrina asanoi (Maiya, Saito, and Sato, 1976)
Neogloboquadrina atlantica (Berggren, 1972)
Neogloboquadrina humerosa (Gervais, 1996)
Neogloboquadrina nympha (Jenkins, 1967)
Orbulina bilobata (d'Orbigny, 1846)
Orbulina universa (d'Orbigny, 1839)
Orbulinoides beckmanni (Saito, 1962)
Paragloborotalia kugleri (Bolli, 1957)
Paragloborotalia mayeri (Cushman and Ellisor, 1939a)
Paragloborotalia nana (Bolli, 1957)
Paragloborotalia opima (Bolli, 1957)
Paragloborotalia pseudokugleri (Blow, 1969)
Paragloborotalia siakensis (LeRoy, 1939)
Parasubbotina griffinae (Blow, 1979)
Parasubbotina variospira (Belford, 1984)
Parvularugoglobigerina eugubina (Luterbacher and Premoli Silva, 1964)
Parvularugoglobigerina extensa (Blow, 1979)
Planoglobulina acervulinoides (Egger, 1899)
Planorotalites palmerae (Cushman and Bermudez, 1937)
Planorotalites spp. (Morozova, 1957)
Praemurica inconstans (Subbotina, 1953)
Praemurica uncinata (Bolli, 1957)
Praeorbulina curva (Blow, 1956)
Praeorbulina glomerosa (Blow, 1956)
Praeorbulina sicana (de Stefani, 1952)
Pseudoglobigerinella bolivariata (Petters, 1954)
Pseudoguembelina costulata (Cushman, 1938)
Pseudoguembelina excolata (Cushman, 1938)
Pseudoguembelina hariaensis (Nederbagt, 1991)
Pseudoguembelina kempensis (Esker, 1968)
Pseudoguembelina palpebra (Bronnimann and Brown, 1953)
Pseudohastigerina micra (Cole, 1927 as *Nonion*)
Pseudohastigerina naguewichiensis (Myatliuk, 1950)
Pseudohastigerina wilcoxensis (Cushman and Ponton, 1932)
Pseudotextularia elegans (Rzehak)
Pulleniatina finalis (Banner and Blow, 1967)
Pulleniatina obliquiloculata (Parker and Jones, 1865)

Table T5 (continued).

Pulleniatina primalis (dex) (Banner and Blow, 1967)
Pulleniatina primalis (sin) (Banner and Blow, 1967)
Pulleniatina sp. (Chaproniere, 1994)
Pulleniatina spectabilis (Parker, 1965)
Racemiguembelina fructicosa (Egger, 1899)
Radotruncana calcarata (Cushman, 1927)
Rugoglobigerina hexacamerata (Bronnimann, 1952)
Rugoglobigerina rugosa (Plummer, 1926)
Sphaeroidinella dehiscens (Parker and Jones)
Sphaeroidinellopsis kochi (Caudri, 1934)
Sphaeroidinellopsis paenedehiscens (Blow, 1969)
Sphaeroidinellopsis seminulina (Schwager, 1866)
Sphaeroidinellopsis subdehiscens (Blow, 1969)
Subbotina angiporoides (Hornibrook, 1965)
Subbotina brevis (Jenkins, 1966)
Subbotina euapertura (Jenkins, 1960)
Subbotina inaequispira (Subbotina, 1953)
Subbotina linaperta (Finlay, 1939)
Subbotina lozanoi (Colom, 1954)
Subbotina triloculinoides (Plummer, 1926)
Subbotina utilisindex (Jenkins and Orr, 1973)
Subbotina velascoensis (Cushman, 1925)
Tenuitella insolita (Jenkins, 1966)
Tenuitella minutissima (Bolli, 1957)
Tenuitella munda (Jenkins, 1966)
Tenuitella pseudoedita (Subbotina, 1960)
Tenuitella reissi (Loeblich and Tappan, 1957)
Tenuitella selleyi (Li, Radford, and Banner, 1992)
Turborotalia ampliapertura (Bolli, 1957)
Turborotalia boweri (Bolli, 1957)
Turborotalia cerroazulensis (Toumarkine and Bolli, 1970)
Turborotalia cocoaensis (Cushman, 1928)
Turborotalia cunialensis (Toumarkine and Bolli, 1970)
Turborotalia frontosa Subbotina, 1953
Turborotalia griffinae (Blow, 1979)
Turborotalia pomeroli (Toumarkine and Bolli, 1970)
Turborotalia possagnoensis (Tourmarkine and Bolli, 1970)
Turborotalita humilis (Brady, 1884 as *Truncatulina*)
Ventilabrella eggeri (Cushman, 1928)
Whiteinella baltica (Douglas and Rankin, 1969)

Table T6. Taxonomic list for radiolarian datums, Expedition 342. (Continued on next two pages.)

Acrocubus octopylus Haeckel, 1887
Actinomma leptodernum (Jorgensen) 1900
Amphicraspedum murrayanum Haeckel, 1887
Amphicraspedum prolixum Sanfilippo and Riedel, 1973
Amphipyndax tylotus Foreman, 1978
Amphisphaera aotea Hollis, 1993
Amphisphaera coronata (Ehrenberg) 1873
Amphisphaera goruna (Sanfilippo and Riedel) 1973
Amphisphaera kina Hollis, 1993
Anthocyrtidium angulare Nigrini, 1971
Anthocyrtidium jenghisi Streeter, 1988
Anthocyrtoma spp. Nigrini et al., 2006
Artophormis barbadensis (Ehrenberg) 1873, 1875
Artophormis gracilis Riedel, 1959
Axoprunum pierinae group (Clark and Campbell) 1942
Bekoma bidartensis Riedel and Sanfilippo, 1971
Bekoma campechensis Foreman, 1973
Bekoma divaricata Foreman, 1973
Botryostrobus miralestensis (Campbell and Clark) 1944
Buccinosphaera invaginata Haeckel, 1887
Buryella clinata Foreman, 1973, 1975
Buryella foremanae Petrushevskaya, 1977
Buryella granulata Petrushevskaya, 1977
Buryella pentadica Foreman, 1973
Buryella tetradica Foreman, 1973
Calocyclas bandyca (Mato and Theyer) 1980
Calocyclas hispida (Ehrenberg) 1873, 1875
Calocyclas semipolita Clark and Campbell, 1942
Calocyclas trichopa (Ehrenberg) 1874
Calocyclas turris Ehrenberg, 1873, 1875
Calocycletta anekathen Sanfilippo and Nigrini in Nigrini et al., 2006
Calocycletta costata (Riedel) 1959
Calocycletta robusta Moore, 1971
Calocycletta serrata Moore, 1972
Calocycletta virginis Haeckel, 1887
Calocycloma ampulla (Ehrenberg) 1854
Calocycloma castum (Haeckel) 1887
Carpocanopsis bramlettei Riedel and Sanfilippo, 1971
Carpocanopsis cingulata Riedel and Sanfilippo, 1971
Carpocanopsis cristata (Carnevale) 1908
Carpocanopsis favosa (Haeckel, 1887)
Centrobotrys gravida Moore, 1971
Centrobotrys petrushevskayae Sanfilippo and Riedel, 1973
Centrobotrys thermophila Petrushevskaya, 1965
Clathrocyclas australis Hollis, 1997
Collosphaera tuberosa Haeckel, 1887
Cryptocarpium azyx (Sanfilippo and Riedel) 1973
Cryptocarpium ornatum (Ehrenberg) 1873, 1875
Cycladophora davisiana Ehrenberg, 1861
Cyrtocapsella cornuta Haeckel, 1887
Cyrtocapsella japonica (Nakaseko) 1963
Cyrtocapsella tetrapera (Haeckel) 1887
Diartus hughesi (Campbell and Clark) 1944
Diartus petterssoni (Riedel and Sanfilippo) 1970
Dictyophimus craticula Ehrenberg, 1874
Dictyoprora amphora group (Haeckel) 1887
Dictyoprora armadillo (Ehrenberg) 1873, 1875
Dictyoprora mongolfieri (Ehrenberg) 1854
Dictyoprora pirum (Ehrenberg) 1873, 1875
Didymocyrtis bassani Carnevale, 1908
Didymocyrtis laticonus (Riedel) 1959
Didymocyrtis mammifera (Haeckel) 1887
Didymocyrtis penultima (Riedel) 1957
Didymocyrtis prismatica (Haeckel) 1887
Didymocyrtis tubaria (Haeckel) 1887
Didymocyrtis violina (Haeckel) 1887
Dorcadospyris alata (Riedel, 1959)
Dorcadospyris anastasis Sanfilippo in Nigrini et al., 2006
Dorcadospyris ateuchus (Ehrenberg) 1873, 1875
Dorcadospyris circulus (Haeckel) 1887
Dorcadospyris cyclacantha Moore in Nigrini et al., 2006

Table T6 (continued). (Continued on next page.)

Dorcadospyris dentata Haeckel, 1887
Dorcadospyris forcipata (Haeckel) 1887
Dorcadospyris papilio (Riedel) 1959
Dorcadospyris praeforcipata Moore, 1971
Dorcadospyris pseudopapilio Moore, 1971
Dorcadospyris riedeli Moore, 1971
Dorcadospyris scambos Moore and Nigrini in Nigrini et al., 2006
Dorcadospyris simplex (Riedel) 1959
Dorcadospyris spinosa Moore, 1971
Eucyrtidium antiquum Caulet, 1991
Eucyrtidium cheni Takemura, 1992
Eucyrtidium diaphanes Sanfilippo and Riedel in Sanfilippo et al., 1973
Eucyrtidium mitodes Nigrini in Nigrini et al., 2006
Eucyrtidium plesiodiaphanes Sanfilippo in Sanfilippo and Nigrini, 1995
Eucyrtidium spinosum Takemura, 1992
Eusyringium fistuligerum (Ehrenberg) 1873, 1875
Eusyringium lagena (Ehrenberg) 1873, 1875
Heliodiscus asteriscus Haeckel, 1887
Lamptonium fabaeforme chaunothorax Riedel and Sanfilippo, 1970
Lamptonium fabaeforme constrictum Riedel and Sanfilippo, 1970
Lamptonium fabaeforme fabaeforme (Krasheninnikov) 1960
Lamptonium pennatum Foreman, 1973
Lamptonium sanfilippoae Foreman, 1973
Liriospyris longicornuta Goll, 1968
Liriospyris parkerae Riedel and Sanfilippo, 1971
Liriospyris stauropora (Haeckel) 1887
Lithelius minor group Jorgensen, 1899
Lithochytris vespertilio Ehrenberg, 1874
Lithocyclia angusta (Riedel) 1959
Lithocyclia aristotelis group (Ehrenberg) 1847
Lithocyclia crux Moore, 1971
Lithocyclia ocellus Ehrenberg, 1854
Lithomelissa(?) *hoplites* Foreman, 1968
Lithopera renzae Sanfilippo and Riedel, 1970
Lophocyrtis (*Cyclampterium*) *hadra* (Riedel and Sanfilippo) 1986
Lophocyrtis (*Cyclampterium*) *leptetrum* (Sanfilippo and Riedel) 1970
Lophocyrtis (*Cyclampterium*) *milowi* (Riedel and Sanfilippo) 1971
Lophocyrtis (*Cyclampterium*) *pegetrum* (Sanfilippo and Riedel) 1970
Lophocyrtis (*Lophocyrtis*) *jacchia* (Ehrenberg) 1873, 1875
Lophocyrtis (*Sciadiopeplus*) *oberhaensliae* Sanfilippo, 1990
Lophocyrtis biaurita (Ehrenberg) 1873, 1875
Lophocyrtis dumitricai Sanfilippo, 1990
Lophocyrtis longiventer (Chen) 1975
Lophocyrtis semipolita group Clark and Campbell, 1942
Lychnocanoma amphitrite Foreman, 1973
Lychnocanoma apodora Sanfilippo in Sanfilippo and Nigrini, 1995
Lychnocanoma auxilla Foreman, 1973
Lychnocanoma bajunensis Renz, 1984
Lychnocanoma bellum (Clark and Campbell) 1942
Lychnocanoma conica (Clark and Campbell) 1942
Lychnocanoma elongata (Vinassa de Regny) 1900
Lychnocanoma trifolium (Riedel and Sanfilippo) 1971
Lychnodictyum audax Riedel, 1953
Orbiculiforma renillaeformis (Campbell and Clark) 1944
Periphaena decora (Ehrenberg) 1873, 1875
Periphaena heliasteriscus (Clark and Campbell) 1942
Periphaena tripyramis triangula (Sutton) 1896
Peritiviator (?) *dumitricai* Nishimura, 1992
Phormocyrtis cubensis (Riedel and Sanfilippo) 1971
Phormocyrtis striata exquisita (Kozlova, in Kozlova and Gorbovetz) 1966
Phormocyrtis striata praexquisita Nishimura, 1992
Phormocyrtis striata striata Brandt in Wetzel, 1935
Phormocyrtis turgida (Krasheninnikov) 1960
Phormostichoartus doliolum (Riedel and Sanfilippo) 1971
Phormostichoartus fistula Nigrini, 1977
Podocyrtis acalles Sanfilippo and Riedel, 1992
Podocyrtis ampla Ehrenberg, 1873, 1875
Podocyrtis aphorma Riedel and Sanfilippo, 1970
Podocyrtis chalara Riedel and Sanfilippo, 1970
Podocyrtis diamesa Riedel and Sanfilippo, 1970
Podocyrtis dorus Sanfilippo and Riedel, 1973

Table T6 (continued).

Podocyrtis fasciolata (Nigrini) 1974
Podocyrtis goetheana (Haeckel) 1887
Podocyrtis helenae Nigrini, 1974
Podocyrtis mitra Ehrenberg, 1854
Podocyrtis papalis Ehrenberg, 1847
Podocyrtis phyxis (Sanfilippo and Riedel) 1973
Podocyrtis sinuosa Ehrenberg, 1873, 1875
Podocyrtis trachodes Riedel and Sanfilippo, 1970
Pterocanium prismatium Riedel, 1957
Pterocodon (?) *ampla* (Brandt) 1935
Pterocodon (?) *anteclinata* Foreman, 1975
Pterocodon (?) *poculum* Nishimura, 1992
Rhopalocanium ornatum Ehrenberg, 1847
Sethochytris bablylonis (Clark and Campbell) 1942
Sethochytris triconiscus Haeckel, 1887
Siphostichoartus corona (Haeckel) 1887
Spongatractus balbis Sanfilippo and Riedel, 1973
Spongatractus pachystylus (Ehrenberg) 1873, 1875
Stichocorys delmontensis (Campbell and Clark) 1944
Stichocorys peregrina (Riedel) 1953
Stichocorys wolffii Haeckel, 1887
Stylatractus universus Hays, 1970
Stylotrochus nitidus Sanfilippo and Riedel, 1973
Theocorys acroria Foreman, 1973
Theocorys anaclasta Riedel and Sanfilippo, 1970
Theocorys plesioanaclasta Kamikuri and Moore in Kamikuri et al., 2012
Theocorys (?) aff. *phyzella* Foreman, Sanfilippo, and Blome, 2001
Theocorys (?) *phyzella* Foreman, 1973
Theocotyle conica Foreman, 1973
Theocotyle cryptocephala (Ehrenberg) 1873, 1875
Theocotyle nigriniae Riedel and Sanfilippo, 1970
Theocotyle venezuelensis Riedel and Sanfilippo, 1970
Theocotylissa alpha Foreman, 1973
Theocotylissa ficus (Ehrenberg) 1873,1875
Theocyrtis annosa (Riedel) 1959
Theocyrtis setanios Nigrini and Sanfilippo in Nigrini et al., 2006
Theocyrtis tuberosa Riedel, 1959
Thyrsocyrtis bromia Ehrenberg, 1873, 1875
Thyrsocyrtis hirsuta (Krasheninnikov) 1960
Thyrsocyrtis lochites Sanfilippo and Riedel, 1982
Thyrsocyrtis rhizodon Ehrenberg, 1873, 1875
Thyrsocyrtis robusta Riedel and Sanfilippo, 1970
Thyrsocyrtis tarsipes Foreman, 1973
Thyrsocyrtis tensa Foreman, 1973
Thyrsocyrtis tetracantha (Ehrenberg) 1873, 1875
Thyrsocyrtis triacantha (Ehrenberg) 1873, 1875
Tristylospyris triceros (Ehrenberg) 1873, 1875
Zealithapium anoectum (Riedel and Sanfilippo) 1973
Zealithapium mitra (Ehrenberg) 1873
Zealithapium plegmacantha (Riedel and Sanfilippo) 1970
Zygocircus buetschli Haeckel, 1887

Table T7. Geomagnetic polarity timescale used during Expedition 342. (Continued on next five pages.)

Geological age	Base age (Ma)		Polarity chron	Age (Ma) Top	Age (Ma) Base	Duration (m.y.)	Remarks
Neogene							
Holocene	11.5 ka						
Pleistocene		C1	C1n (Brunhes)	0	0.781	0.781	Base of middle Pleistocene (Ionian) is base of Brunhes Chron.
late (Tarantian)	0.126		C1r.1r (Matuyama)	0.781	0.988	0.207	
middle (Ionian)	0.781		C1r.1n (Jaramillo)	0.988	1.072	0.084	
			C1r.2r	1.072	1.173	0.101	
			C1r.2n (Cobb Mountain)	1.173	1.185	0.012	Cobb Mountain cryptochron is within early part of Matuyama Chron (C1r).
			C1r.3r	1.185	1.778	0.593	
early (Calabrian)	1.806	C2	C2n (Olduvai)	1.778	1.945	0.167	Base of Calabrian is in lower part of Olduvai Chron.
			C2r.1r	1.945	2.128	0.183	
			C2r.1n (Reunion)	2.128	2.148	0.020	
			C2r.2r (Matuyama)	2.128	2.581	0.453	Base of Pleistocene is near base of Matuyama Chron.
(Gelasian)	2.588						
Pliocene		C2A	C2An.1n (Gauss)	0.000	3.032	3.032	"Gauss normal chron" (C2An) contains two reversed intervals: Kaena (2An.1r) and Mammoth (2An.2r).
			C2An.1r (Keana)	3.032	3.116	0.084	
			C2An.2n	3.116	3.207	0.091	
			C2An.2r (Mammoth)	3.207	3.330	0.123	
late (Piacenzian)	3.600		C2An.3n (Gauss)	3.330	3.596	0.266	Base of Piacenzian is base of Chron C2An.3n.
			C2Ar (Gilbert)	3.596	4.187	0.591	"Gilbert reversed chron" spans Chrons C2Ar through C3r.
		C3	C3n.1n (Cochiti)	4.187	4.300	0.113	
			C3n.1r	4.300	4.493	0.193	
			C3n.2n (Nunivak)	4.493	4.631	0.138	
			C3n.2r	4.631	4.799	0.168	
			C3n.3n (Sidufjall)	4.799	4.896	0.097	
			C3n.3r	4.896	4.997	0.101	
early (Zanclean)	5.332		C3n.4n (Thvera)	4.997	5.235	0.238	Base of Miocene is in uppermost Chron C3r.
Miocene			C3r (Gilbert)	5.235	6.033	0.798	
		C3A	C3An.1n	6.033	6.252	0.219	
			C3An.1r	6.252	6.436	0.184	
			C3An.2n	6.436	6.733	0.297	
			C3Ar	6.733	7.140	0.407	
		C3B	C3Bn	7.140	7.212	0.072	
late (Messinian)	7.246		C3Br.1r	7.212	7.251	0.039	Base of Messinian is in lowermost Chron C3Br.1r.
			C3Br.1n	7.251	7.285	0.034	
			C3Br.2r	7.285	7.454	0.169	
			C3Br.2n	7.454	7.489	0.035	
			C3Br.3r	7.489	7.528	0.039	
		C4	C4n.1n	7.528	7.642	0.114	
			C4n.1r	7.642	7.695	0.053	
			C4n.2n	7.695	8.108	0.413	

Table T7 (continued). (Continued on next page.)

Geological age	Base age (Ma)		Polarity chron	Age (Ma) Top	Age (Ma) Base	Duration (m.y.)	Remarks
			C4r.1r	8.108	8.254	0.146	
			C4r.1n	8.254	8.300	0.046	
			C4r.2r	8.300	8.771	0.471	Cryptochron C4r.2r-1 is within C4r.2r (~8.661–8.699 Ma).
		C4A	C4An	8.771	9.105	0.334	
			C4Ar.1r	9.105	9.311	0.206	
			C4Ar.1n	9.311	9.426	0.115	
			C4Ar.2r	9.426	9.647	0.221	
			C4Ar.2n	9.647	9.721	0.074	
			C4Ar.3r	9.721	9.786	0.065	
		C5	C5n.1n	9.786	9.937	0.151	
			C5n.1r	9.937	9.984	0.047	
			C5n.2n	9.984	11.056	1.072	Cryptochrons C5n.2n-1, C5n.2n-2, and C5n.2n-3.
			C5r.1r	11.056	11.146	0.090	
			C5r.1n	11.146	11.188	0.042	
			C5r.2r	11.188	11.592	0.404	Subchron C5r.2r-1 is within C5r.2r (~11.263–11.308 Ma).
(Tortonian)	11.63		C5r.2n	11.592	11.657	0.065	Base of Tortonian is near base of Chron C5r.2n.
			C5r.3r	11.657	12.049	0.392	
		C5A	C5An.1n	12.049	12.174	0.125	
			C5An.1r	12.174	12.272	0.098	
			C5An.2n	12.272	12.474	0.202	
			C5Ar.1r	12.474	12.735	0.261	
			C5Ar.1n	12.735	12.770	0.035	
			C5Ar.2r	12.770	12.829	0.059	
			C5Ar.2n	12.829	12.887	0.058	
			C5Ar.3r	12.887	13.032	0.145	
		C5AA	C5AAn	13.032	13.183	0.151	
			C5AAr	13.183	13.363	0.180	
		C5AB	C5ABn	13.363	13.608	0.245	
			C5ABr	13.608	13.739	0.131	
middle (Serravallian)	13.82	C5AC	C5ACn	13.739	14.070	0.331	Base of Serravalian is upper Chron C5ACn.
			C5ACr	14.070	14.163	0.093	
		C5AD	C5ADn	14.163	14.609	0.446	
			C5ADr	14.609	14.775	0.166	
		C5B	C5Bn.1n	14.775	14.870	0.095	
			C5Bn.1r	14.870	15.032	0.162	
			C5Bn.2n	15.032	15.160	0.128	
(Langhian)	15.97		C5Br	15.160	15.974	0.814	Base of Langhian is base of Chron C5Br.
		C5C	C5Cn.1n	15.974	16.268	0.294	
			C5Cn.1r	16.268	16.303	0.035	

Table T7 (continued). (Continued on next page.)

Geological age	Base age (Ma)		Polarity chron	Age (Ma) Top	Age (Ma) Base	Duration (m.y.)	Remarks
			C5Cn.2n	16.303	16.472	0.169	
			C5Cn.2r	16.472	16.543	0.071	
			C5Cn.3n	16.543	16.721	0.178	
			C5Cr	16.721	17.235	0.514	
		C5D	C5Dn	17.235	17.533	0.298	
			C5Dr.1r	17.533	17.717	0.184	
			C5Dr.1n	17.717	17.740	0.023	Cryptochron is in Chron C5Dr.
			C5Dr.2r	17.740	18.056	0.316	
		C5E	C5En	18.056	18.524	0.468	
			C5Er	18.524	18.748	0.224	
		C6	C6n	18.748	19.722	0.974	
			C6r	19.722	20.040	0.318	Cryptochron C6r-1.
		C6A	C6An.1n	20.040	20.213	0.173	
early (Burdigalian)	20.44		C6An.1r	20.213	20.439	0.226	Base of Burdigalian (working version) is approximately base of Chron C6An.1r (used here) or of Chron C6An.1n.
			C6An.2n	20.439	20.709	0.270	
			C6Ar	20.709	21.083	0.374	
		C6AA	C6AAn	21.083	21.159	0.076	
			C6AAr.1r	21.159	21.403	0.244	
			C6AAr.1n	21.403	21.483	0.080	
			C6AAr.2r	21.483	21.659	0.176	
			C6AAr.2n	21.659	21.688	0.029	
			C6AAr.3r	21.688	21.767	0.079	
		C6B	C6Bn.1n	21.767	21.936	0.169	
			C6Bn.1r	21.936	21.992	0.056	
			C6Bn.2n	21.992	22.268	0.276	
			C6Br	22.268	22.564	0.296	
		C6C	C6Cn.1n	22.564	22.754	0.190	
			C6Cn.1r	22.754	22.902	0.148	
(Aquitanian)	23.03		C6Cn.2n	22.902	23.030	0.128	Base of Miocene is base of Chron C6Cn.2n.
Paleogene			C6Cn.2r	23.030	23.233	0.203	
Oligocene			C6Cn.3n	23.233	23.295	0.062	
			C6Cr	23.295	23.962	0.667	
		C7	C7n.1n	23.962	24.000	0.038	
			C7n.1r	24.000	24.109	0.109	
			C7n.2n	24.109	24.474	0.365	
			C7r	24.474	24.761	0.287	Cryptochron C7r-1.
		C7A	C7An	24.761	24.984	0.223	
			C7Ar	24.984	25.099	0.115	

Table T7 (continued). (Continued on next page.)

Geological age	Base age (Ma)		Polarity chron	Age (Ma) Top	Age (Ma) Base	Duration (m.y.)	Remarks
		C8	C8n.1n	25.099	25.264	0.165	
			C8n.1r	25.264	25.304	0.040	
			C8n.2n	25.304	25.987	0.683	Cryptochron C8n.2n-1.
			C8r	25.987	26.420	0.433	
		C9	C9n	26.420	27.439	1.019	Cryptochrons C9n-1and C9n-2.
			C9r	27.439	27.859	0.420	Cryptochron C9r-1.
late (Chattian)	28.09	C10	C10n.1n	27.859	28.087	0.228	Base of Chattian (working version) is base of Chron C10n.1n. Base is potentially at ~70% up in "undifferentiated Chron C10n" in candidate GSSP in Italy (Coccioni et al., 2008), which would project as equivalent to Chron C10n.1n.4.
			C10n.1r	28.087	28.141	0.054	
			C10n.2n	28.141	28.278	0.137	
			C10r	28.278	29.183	0.905	Cryptochrons C10r-1 and C10r-2.
		C11	C11n.1n	29.183	29.477	0.294	
			C11n.1r	29.477	29.527	0.050	
			C11n.2n	29.527	29.970	0.443	
			C11r	29.970	30.591	0.621	Cryptochron C11r-1.
		C12	C12n	30.591	31.034	0.443	
			C12r	31.034	33.157	2.123	Cryptochrons C12r-1 through C12r-8.
		C13	C13n	33.157	33.705	0.548	Cryptochron C13n-1.
early (Rupelian) Cryptochrons C13r-1 through C13r-4	33.89		C13r	33.705	34.999	1.294	Base of Rupelian is at Chron C13r.86.
Eocene		C15	C15n	34.999	35.294	0.295	"C14" does not exist.
			C15r	35.294	35.706	0.411	
		C16	C16n.1n	35.706	35.892	0.186	
			C16n.1r	35.892	36.051	0.159	
			C16n.2n	36.051	36.700	0.649	
			C16r	36.700	36.969	0.269	
late (Priabonian)	37.75	C17	C17n.1n	36.969	37.753	0.784	Base of Priabonian (working version) assigned as base of Chron C17n.1n.
			C17n.1r	37.753	37.872	0.119	
			C17n.2n	37.872	38.093	0.221	
			C17n.2r	38.093	38.159	0.065	
			C17n.3n	38.159	38.333	0.174	
			C17r	38.333	38.615	0.283	
		C18	C18n.1n	38.615	39.627	1.012	Cryptochron C18n.1n-1.
			C18n.1r	39.627	39.698	0.070	
			C18n.2n	39.698	40.145	0.447	
middle (Bartonian)	41.15		C18r	40.145	41.154	1.010	Base of Bartonian (working version) assigned as base of Chron C18r.
		C19	C19n	41.154	41.390	0.235	

Table T7 (continued). (Continued on next page.)

Geological age	Base age (Ma)		Polarity chron	Age (Ma) Top	Age (Ma) Base	Duration (m.y.)	Remarks
			C19r	41.390	42.301	0.912	
		C20	C20n	42.301	43.432	1.130	
			C20r	43.432	45.724	2.292	
		C21	C21n	45.724	47.349	1.625	
(Lutetian)	47.84		C21r	47.349	48.566	1.217	Base of Lutetian is Chron C21r.6.
		C22	C22n	48.566	49.344	0.778	
			C22r	49.344	50.628	1.283	
		C23	C23n.1n	50.628	50.835	0.207	
			C23n.1r	50.835	50.961	0.126	
			C23n.2n	50.961	51.833	0.872	
			C23r	51.833	52.620	0.787	
		C24	C24n.1n	52.620	53.074	0.454	
			C24n.1r	53.074	53.199	0.125	
			C24n.2n	53.199	53.274	0.075	
			C24n.2r	53.274	53.416	0.142	
			C24n.3n	53.416	53.983	0.567	
early (Ypresian)	55.96		C24r	53.983	57.101	3.118	Base of Eocene is 1.14 m.y. after beginning of Chron C24r, or Chron C24r.37. Cryptochrons C24r-1 through C24r-11.
Paleocene		C25	C25n	57.101	57.656	0.555	
			C25r	57.656	58.959	1.303	Cryptochrons C25r-1 through C25r-5.
late (Thanetian)	59.24	C26	C26n	58.959	59.237	0.278	Base of Thanetian is base of Chron C26n.
middle (Selandian)	61.61		C26r	59.237	62.221	2.984	Base of Selandian is an isotope shift at 30. Precession cycles (0.61 m.y. if 20.5 k.y. cycles) above base of Chron C26r at GSSP. Cryptochrons C26r-1 through C26r-7.
		C27	C27n	62.221	62.517	0.296	
			C27r	62.517	63.494	0.977	
		C28	C28n	63.494	64.667	1.173	
			C28r	64.667	64.958	0.291	Cryptochron C28r-1
		C29	C29n	64.958	65.688	0.730	
early (Danian)	66.04		C29r	65.688	66.398	0.710	Mesozoic/Cenozoic boundary event is Chron C29r.5 in total Chron C29r span of 710 k.y. according to cycles (Husson et al., 2011; Thibault et al., submitted).
Cretaceous		C30	C30n	66.398	68.196	1.798	Pre-Chron 29r C-sequence ages based entirely on cycle stratigraphy because of lack of adequate radiometric age constraints. Duration of Chron C30n is 1.798 m.y. (Husson et al., 2011; Thibault et al., submitted).
			C30r	68.196	68.369	0.173	Duration of Chron C30r is 173 m.y. (Husson et al., 2011; Thibault et al., 2012).
		C31	C31n	68.369	69.269	0.900	Duration of Chron C31n is 0.9 m.y. (Husson et al., 2011).

Table T7 (continued).

Geological age	Base age (Ma)		Polarity chron	Age (Ma) Top	Age (Ma) Base	Duration (m.y.)	Remarks
			C31r	69.269	71.449	2.180	Duration of Chron C31r is 2.18 m.y. (Husson et al., 2011). Base of Chron C31r is within the lower *Baculites grandis* ammonite zone constrained by Ar/Ar ages of 70.65 ± 0.65 Ma (2σ) within that zone.
		C32	C32n.1n	71.449	71.689	0.240	Duration of Chron C32n.1n is 0.24 m.y. (Husson et al, 2011).
			C32n.1r	71.689	71.939	0.250	Duration of Chron C32n.1r assigned as 0.25 m.y. (same as GTS2004 spline fit).
Maastrichtian	72.05		C32n.2n	71.939	73.649	1.710	Base of Maastrichtian is approximately at Chron C32n.2n.9, or at 72.05 Ma from spline fit to ammonite zones. Duration of Chron C32n.1n is 1.71 m.y. (Husson et al., 2011).
			C32r.1r	73.649	73.949	0.300	Duration of Chron C32r.1r is 0.3 m.y. (Husson et al., 2011).
			C32r.1n	73.949	74.049	0.100	Duration of Chron C32r.1n is 0.1 m.y. (Husson et al., 2011).
			C32r.2r	74.049	74.309	0.260	Duration of Chron C32n.2r assigned as 0.26 m.y. (same as GTS2004 spline fit).
		C33	C33n	74.309	79.900	5.591	Base of Chron C33n constrained by Ar/Ar dates to be slightly younger than 80.08 Ma ± 0.61 m.y.; following Hicks (1995), it is extrapolated as 0.2 m.y. younger (79.9 m.y.).
Campanian	83.64		C33r	79.900	83.640	3.740	Base of Chron C33r assigned as base of Campanian as in North American ammonite zonation, with age from spline fit of the bracketing bentonites.
Santonian		C34	C34n	83.64			Chron C33r may include upper part of the English Chalk usage of Santonian.